DEVELOPMENT OF DIRECT-INVERSE 3-D METHODS

FOR APPLIED TRANSONIC AERODYNAMIC WING DESIGN AND ANALYSIS

Aerospace Engineering Department

Semiannual Progress Report

July 1, 1988 - December 31, 1988

TEXAS A&M UNIVERSITY

TAMRF Report No. 5373-89-01

February 1989

NASA Grant No. NAG-1-619

Leland A. Carlson
Professor of Aerospace Engineering
Texas A&M University
College Station, Texas 77843-3141

TEXAS ENGINEERING EXPERIMENT STATION

DEVELOPMENT OF DIRECT-INVERSE 3-D METHODS FOR APPLIED TRANSONIC AERODYNAMIC WING DESIGN AND ANALYSIS

Semiannual Progress Report

July 1, 1988 -- December 31, 1988

TAMRF Report No. 5373-89-01

February 1989

NASA Grant No. NAG-1-619

Leland A. Carlson
Professor of Aerospace Engineering
Texas A&M University
College Station, Texas 77843-3141

DEVELOPMENT OF DIRECT-INVERSE 3-D METHODS FOR APPLIED TRANSONIC AERODYNAMIC WING DESIGN AND ANALYSIS

I. Introduction

This report covers the period from July 1, 1988 thru December 31, 1988. The primary task during this period has been the comtinued development of the TAW5D transonic inverse wing design method with viscous interaction effects included.

II. Personnel

The staff associated with this project during the present reporting period have been Dr. Leland A. Carlson, Principal Investigator, and Robert R. Ratcliff, Graduate Research Assistant. The work performed during this phase of the project is primarily associated with the Master's Thesis of Mr. Ratcliff. It is anticipated that Robert will receive his degree in May 1989.

III. Research Progress

During the past six months, most of the research effort has been concentrated in the areas of program refinements, supression of divergent spanwise oscillations, and viscous studies. To a significant extent, these efforts have been summarized in an extended abstract of a paper proposed for the AIAA 7th Applied Aerodynamics Conference; and this extended abstract is included in this report as Appendix A. In addition, comments concerning these various areas are presented as follows:

A. Program Refinements --

The following improvements have been made in the TAW5D design/analysis program:

(a) A simple plotting subroutine using basic Fortran commands has been written to allow the user to view the designed section shapes as part of the output file generated by TAW5D. This addition allows the user to conduct the design process more efficiently.

(b) Close to optimum damping parameters and flow iterations between surface updates have been obtained through numerical experimentation for one design case including viscous interaction using Wing-A on the medium and fine grids. The effect on the final design of the number of iterations before the first surface update has also been studied. It has been found that as the design region is moved closer to the leading edge that more flow iterations are needed before the first surface update is performed in order to insure an accurate nose shape. Since large changes in the airfoil occur with the first surface update, a more accurate solution will speed up convergence. The results from this study will be shown in the final report.

(c) In the calculation of the quantity $(\rho hV)/(\rho hU)$ on the surface of the wing, which is intgegrated to yield the section shapes, the idea of evaluating $\rho hU(i,Ky,K)$

using the more conveient quantity ρhU(i,ky-1,k), where ky is the jth grid point lying on the wing, has been investigated. This method assumes that the flux ohU is constant in the region immediately above the wing. In order to verify this approach, a subroutine was written to calculate the flux ρhU(i,ky,k) dirrectly using finite differences. Although the numbers were slightly different from the first approach, the effect on the final design was negligible for the cases studied to date.

B. Supression of Divergent Spanwise Oscillations --

As discussed in Appendix A of this report, an annoying spanwise oscillation of the residual, and hence of the section shapes, originates at the first spanwise station from the root and propagates spanwise as a decaying oscillation. This oscillation is due in part to the compensation terms which include spanwise derivatives of the potential, and it becomes more significant as the wing aspect ratio is decreased or the sweep is increased.

As indicated in previous progress reports, considerable effort has been expended over the past year in attempts to eliminate or at least mitigate this annoying and sometimes troublesome oscillation. During the present reporting period four methods have been formulated to supress this oscillation problem. These are as follows:

(1) Specify the inverse boundary condition at every other spanwise station and linearly interpolate the inverse displacements to the stations lying in-between;

(2) Specify the inverse boundary condition at every spanwise grid station but only calculate displacments at every other station and linearly interpolate the displacements to the stations in-between;

(3) Smooth the slopes, $(\rho hV)/(\rho hU)$, in the spanwise direction in the design region before the integration of the tangency condition; and

(4) Calculate all spanwise derivatives of the potential based upon a locally smoothed potential function in the spanwise direction.

Each of these methods has certain advantages in different design situations. For instance, methods (3) and (4) give the designer the most flexibility in that the desired pressure distributions can be imposed at every spanwise grid station and the section shapes corresponding to each grid station can be calculated relatively independently of the adjacent stations. On the other hand, since the first two methods require interpolation, the section shapes determined by these methods at say odd stations are directly dependent upon the shapes at even stations. Although with these latter methods the designer loses some flexibility, a smoother distribution of section thicknesses in the spanwise direction is obtained, which in many cases may be an asset. Of course, from a designer's standpoint, method (1) is the most restrictive of the four techniques; but it yields the smoothest designs in the spanwise direction. In addition, and perhaps more importantly, method (1) converges the quickest. These methods have all been tested on medium grids, and studies are currently in progress to test them using fine grids to insure that they are independent of grid size.

C. Viscous Studies --

In previous studies when viscous pressures were used as input to an inviscidly designed wing, the resulting section shapes were "unsatisfactory" at the edges of the design regions in that there was a sudden increase in thickness corresponding to the boundary layer inherently included in the region designed with viscous pressures with the consequence that the resulting profile was not as accurately obtained as usual. In order to determine more specifically how the outboard and inboard regions of the wing, which were not being desgined, affected the design of the middle section, a study was conducted in which the entire wing was designed inviscidly using pressures obtained from a viscous analysis of the target wing, Lockheed Wing-A. The resulting wing, while being a little thicker in regions of large boundary layer thickness, had a smoothly varying thickness distribution which corresponded closely to the displacement surface of the actual wing. This study verified that the solution in the inboard and outboard direct regions of the wing had, in fact, been responsible for the shape changes at the edges of the design region in the case reported in a previous paper, where only part of the wing was designed inviscidly.

During the course of this project, there have been many instances where even a viscous analysis of a wing could not be accomplished succesfully without diverging due to large separated regions being predicted by the boundary layer solver. This phenomena frequently occurred when studying Lockheed Wings B and C, but sometimes it even occurred with Wing A. In fact, in some cases the boundary layer solver could not even be executed completely due to its inability to find an appropriate starting solution. In some cases these problems have been avoided by finding an appropriate sequence of flow field iterations and boundary layer updates or by going to a finer grid from the one currently being utilized. However, in many cases a few degrees of dihedral had to be added to the wing to allevite this premature separation problem. At the present time, it appears that this boundary layer solver problem needs further investigation.

IV. Current and Future Efforts

Obviously, the primary effort during the next reporting period will be the completion of Robert Ratcliff's thesis and the preparation of the project final report. However, depending upon the time and financial resources available, the following items may be investigated:

(1) It has been discovered that the skewness of the grid lines leaving the wing tip in the spanwise direction has a large effect on the accuracy of the sections designed in the tip region. As a consequence, some check for grid skewness or a method to minimize the effect of skewness on the final solution is needed. If time permits, appropriate sections will be added to the program.

(2) The logic necessary to design a segment of the wing which starts aft of the leading edge and terminates prior to the trailing edge is currently being studied and hopefully will be included in the final version of the code. If at all possible, test cases demonstrating this option will be shown in the final report.

(3) Since the spanwise stability problem is now better understood, the trailing edge of the designed airfoil sections may be allowed to float if the correct method to supress the spanwise oscillation is utilized. This approach would allow an additional degree of freedom in the design solution procedure and may permit the solution of "difficult" design problems. This conjecture will be tested by including logic which allows the trailing edge to "float" and performing appropriate test cases using the previously discussed spanwise oscillation suppression methods. In these tests, the accuracy of the designed sectional thickness profiles and the sectional angle of attacks will be ascertained.

(4) As mentioned in previous reports, two different methods are used in FLO30 to define the potentials at ghost points in the fuselage adjacent to the root section of the wing. One approach uses the flow tangency condition, while the other linearly extrapolates the potentials in the spanwise direction to the ghost point loction. Since these potentials are used in the inverse boundary conditions, their method of determination may have an effect on the design of the wing, especially at the root. Hopefully, resources will be available to permit the investigation of the influence of these ghost potentials.

(5) Currently, the only time the spanwise derivatives of the potential are based upon a spanwise smoothed potential function, is in the calculation of the residual immediately before the integration of the flow tangency condition or surface update. Note that this procedure is only used when the fourth method of spanwise oscillation suppression is utilized. It is planned to investigate the effect on the final design of carrying out this smoothing approach every time the residual is calculated.

V. Grant Monitor

The NASA Technical Monitor for this project is Richard L. Campbell, Applied Aerodynamics Group, Transonic Aerodynamics Branch, Applied Aerodynamics Division, NASA Langley, (I think -- I have not kept up with recent organizational changes).

APPENDIX A

A DIRECT-INVERSE TRANSONIC WING DESIGN METHOD IN CURVILINEAR COORDINATES INCLUDING VISCOUS-INTERACTION

An Extended Abstract by:

Robert R. Ratcliff and Leland A. Carlson

Aerospace Engineering Department

Texas A&M University

College Station, Texas 77843

Phone : (409) 845 - 7541

December 9, 1988

Summary

Progress in the direct-inverse wing design method in curvilinear coordinates has been made. This includes the remedying of a spanwise oscillation problem and the assessment of grid skewness, viscous interaction, and the initial airfoil section on the final design. It was found that : in response to the spanwise oscillation problem that designing at every other spanwise station produced the best results for the cases presented, a smoothly varying grid is especially needed for the accurate design at the wing tip, boundary layer displacement thicknesses must be included in a successful wing design, the design of high and medium aspect-ratio wings is possible with this code, and that the final airfoil section designed is fairly independent of the initial section.

A DIRECT-INVERSE TRANSONIC WING-DESIGN METHOD IN CURVILINEAR COORDINATES INCLUDING VISCOUS-INTERACTION

Introduction

With the advent of efficient numerical schemes that accurately model the irrotational transonic flow about complex configurations such as wing-bodies and computers with ever increasing memory capacities and computational speeds necessary to execute these schemes in a reasonable amount of time, the efficient design of wings for transonic flight is quickly becoming a reality. Although transonic potential schemes combined with integral boundary layer solvers may not perfectly model the real flow field as closely as Euler or Navier Stokes Schemes, they can significantly reduce the exhorbitant wind tunnel costs and time expenditures associated with transonic wing design.

Many methods ranging from optimization techniques[1-2] to various inverse methods have been formulated using potential solvers to design wings in transonic flight[3-9]. One such method, which has been under development at Texas A&M University for the last several years, is the direct-inverse transonic wing design method. In this method the airfoil sections making up the wing are created by specifying desired pressure distributions over all or part of the wing aft of the leading edge, solving via finite-difference or finite-volume techniques the mixed Neumann and Dirichlet boundary value problem associated with the full potential equation for compressible flow, and then integrating the flow boundary condition at each spanwise station in the design region. The pressure distributions can be selected by

Journal model is *AIAA Journal of Aircraft.*

the experienced engineer to have such desirable characteristics as mild or nonexistent shocks, a slowly increasing adverse pressure gradient, a center of pressure giving a desirable pitching moment or an efficient spanwise loading. The designer may also use wind tunnel tests of successful airfoils as an aid in picking a desirable pressure distribution.

The direct-inverse technique has been successfully used in a stretched and sheared cartesian system[6-7] and more recently in a curvilinear system. This paper presents progress in the latter. It will include a brief description of the analysis and design methods, techniques used to suppress a spanwise oscillation problem resulting from the interaction of the design method with the potential solver, and it will present a series of test cases that will reveal the lack of dependency of the design on the initial airfoil section, the importance of including viscous effects in wing design, and any constraints due to aspect ratio and sweep of the wings and grid skewness in the spanwise direction.

Background

The base Fortran program which was modified intially by Gally[9] for inverse wing design, is TAWFIVE[10]. This program not only has the capability of computing the potential field about a fairly general wing and fuselage combination but also includes a three dimensional integral boundary layer scheme to provide the necessary viscous effects, including the boundary layer displacement thickness, wake curvature and thickness.

The inviscid numerical scheme is based upon Jameson's and Caughey's conservative, finite-volume, full potential flow solver, FLO30. Computations are performed on a body-fitted, sheared, parabolic, wind-tunnel type coordinate system.

The theory behind this will be briefly discussed, but the reader is encouraged to refer to references (11-14) for a more in depth study.

FLO30 solves the compressible potential equation in conservative form written in curvilinear coordinates :

$$(\rho h U)_\xi + (\rho h V)_\eta + (\rho h W)_\zeta = 0 \tag{1}$$

where the physical velocities, u, v, w are related to the gradient of the reduced potential function, ϕ, by :

$$\begin{pmatrix} u \\ v \\ w \end{pmatrix} = \left[\mathbf{H}^T\right]^{-1} \begin{pmatrix} \phi_\xi \\ \phi_\eta \\ \phi_\zeta \end{pmatrix} + \begin{pmatrix} Cos(\alpha) \\ Sin(\alpha) \\ 0 \end{pmatrix} \tag{2}$$

and the contravariant velocities U, V, W are related to the physical velocities by :

$$\begin{pmatrix} U \\ V \\ W \end{pmatrix} = \mathbf{H}^{-1} \begin{pmatrix} u \\ v \\ w \end{pmatrix} \tag{3}$$

where $\mathbf{H}$ is the transformation matrix defined as:

$$\mathbf{H} = \begin{pmatrix} x_\xi & x_\eta & x_\zeta \\ y_\xi & y_\eta & y_\zeta \\ z_\xi & z_\eta & z_\zeta \end{pmatrix} \qquad \text{with} \qquad h = |\mathbf{H}| \tag{4}$$

The local air density normalized by the freestream density can be derived in terms of the local speed of sound using the energy equation and isentropic relations to yield :

$$\rho = \left(\frac{a}{a_\infty}\right)^5 \tag{5}$$

where the local speed of sound normalized by the freestream speed, q_∞, can be calculated in terms of the speed of sound at stagnation using :

$$a^2 = a_o^2 - \left(\frac{q}{q_\infty}\right)^2 \left(\frac{\gamma - 1}{2}\right) \tag{6}$$

In a finite-volume scheme, the discrete nature of the finite difference model is considered from the onset and its formulation is directly analagous to the method in which the original compressible continuity equation was derived. The FLO30 finite-volume scheme does this using a staggered box approach. This method used to discretize the differential equation is best explained with the aid of the 2-D cells in figure 1 and the 2-D, incompressible version of equation 1 written in cartesian coordinates :

$$(U)_X + (V)_Y = 0 \tag{7}$$

The staggered boxes make up sets of interlocking primary and secondary cells. The values of the potential function at grid points, which are located at the corners of the four primary cells shown, are used to calculate the fluxes, U and V, at the centers of each primary cell (which are also the corners of the secondary cell) in the following manner :

$$\begin{aligned} U &= \phi_X = \mu_Y \delta_X \phi \\ V &= \phi_Y = \mu_X \delta_Y \phi \end{aligned} \tag{8}$$

where μ and δ are averaging and differentiating operators respectively and are defined as :

$$\begin{aligned} \mu_X f &= \frac{1}{2}\left(f_{i+\frac{1}{2},j} + f_{i-\frac{1}{2},j}\right) \\ \delta_X f &= f_{i+\frac{1}{2},j} - f_{i-\frac{1}{2},j} \end{aligned} \tag{9}$$

where it is assumed that $\Delta X = 1$ These fluxes , U and V, calculated at each of the primary cell centers are then averaged in the Y direction and the X direction, respectively, and the net flux into the cube is obtained resulting in:

$$\mu_Y \delta_X (U) + \mu_X \delta_Y (V) = 0 \tag{10}$$

which is the discretized version of equation 7.

Jameson found that lumping the fluxes at the primary cell centers led to an uncoupling of the solution between adjacent grid points. Therefore, he added some compensation terms which basically extrapolate the fluxes from the corners of the secondary cell to a distance, ϵ, towards the midpoint of each secondary cell face. For example, given an $\epsilon = .25$ the flux, U, at the corresponding grid location $\left(i+\frac{1}{2}, j+\frac{1}{4}\right)$ is :

$$U_{i+\frac{1}{2},j+\frac{1}{4}} = U_{i+\frac{1}{2},j+\frac{1}{2}} - .25\left(\frac{\partial U}{\partial Y}\right)_{i+\frac{1}{2},j+\frac{1}{2}} \tag{11}$$

where :

$$\left(\frac{\partial U}{\partial Y}_{i+\frac{1}{2},j+\frac{1}{2}}\right) = \delta_{XY}\left(\phi\right)_{i+\frac{1}{2},j+\frac{1}{2}} \tag{12}$$

When all the fluxes are extrapolated in this manner and included in equation 10, it leads to :

$$\mu_{YY}\delta_{XX}\phi + \mu_{XX}\delta_{YY}\phi - .25\delta_{XXYY}\phi = 0 \tag{13}$$

If the same procedure is extended to a three dimensional flowfield in curvilinear coordinates, the discretized full potential equation becomes :

$$\begin{aligned}&\mu_{\eta\zeta}\delta_{\xi}\left(\rho hU + P\right) + \mu_{\zeta\xi}\delta_{\eta}\left(\rho hV + Q\right) + \mu_{\xi\eta}\delta_{\zeta}\left(\rho hW + R\right)\\ &\quad - \epsilon\left(\mu_{\zeta}\delta_{\xi\eta}Q_{\xi\eta} + \mu_{\xi}\delta_{\eta\zeta}Q_{\eta\zeta} + \mu_{\eta}\delta_{\zeta\xi}Q_{\zeta\xi} - \frac{\delta_{\xi\eta\zeta}Q_{\xi\eta\zeta}}{2}\right) = 0\end{aligned} \tag{14}$$

where the Q's are the compensation terms defined by Jameson as :

$$\begin{aligned}Q_{\xi\eta} &= \left(A_{\xi} + A_{\eta}\right)\mu_{\zeta}\delta_{\xi\eta}\phi\\ Q_{\eta\zeta} &= \left(A_{\eta} + A_{\xi}\right)\mu_{\xi}\delta_{\eta\zeta}\phi\\ Q_{\zeta\xi} &= \left(A_{\zeta} + A_{\xi}\right)\mu_{\eta}\delta_{\zeta\xi}\phi\\ Q_{\zeta\xi} &= \left(A_{\xi} + A_{\eta} + A_{\zeta}\right)\delta_{\xi\eta\zeta}\phi\end{aligned} \tag{15}$$

And, $A_{\xi}, A_{\eta}, A_{\zeta}$ are influence coefficients which compensate for the dependence of ρ on ϕ_{ξ}, ϕ_{η}, and ϕ_{ζ}. P, Q, and R are Jameson's upwinding terms which desymmetrize

the scheme in supersonic zones and exclude unreal, discontinous expansions from the solution by providing an artificial viscosity. This equation, solved via SLOR, is of course a direct statement of the conversation of mass and should tend to zero as the solution converges unless mass is being created within the secondary cell.

As mentioned earlier, a body-fitted, wind tunnel-type grid is used in FLO30 which is shown in figure 2. The grid shown is the coarsest mesh and has 40 x 6 x 8 grid points in the X, Y, and Z directions, respectively. With this grid, the wing becomes a constant Y surface, and each cylindrical looking shell is a constant Z surface. Constant X lines can be seen running spanwise on the wing at a constant chord fraction from the leading edge. Notice also, due to the conformal transformation used, that constant X lines are packed close to the leading edge of the wing. This becomes to be an attractive feature when designing airfoil sections using the direct-inverse approach. Moreover, constant Z lines are spaced evenly on the wing and will, on the finest mesh, give the designer up to 21 spanwise stations where at the pressure distributions can be specified.

The tangency boundary conditions are simply enforced by reflecting the fluxes above the surface to ghost points below the wing, fuselage or symmetry plane such that the out of plane component of the flux is zero at the surface.

Inverse Design Method

As stated earlier, in the direct-inverse method a pressure boundary condition is enforced rather than flow tangency aft of the leading edge of the sections of the wing which are to be redesigned. After Gally[9,15], the input pressure coefficient can

be written in terms of the Mach number, M, and the dynamic pressure, q, as:

$$C_p = \frac{2}{\gamma {M^2}_\infty}\left[\left[1+\frac{\gamma-1}{2}{M_\infty}^2\left(1-\frac{q^2}{{q^2}_\infty}\right)\right]^{\frac{\gamma}{\gamma-1}}-1\right] \tag{16}$$

where $q^2 = \left(u^2+v^2+w^2\right){q^2}_\infty$.

Solving for u in equation 2 and equation 16 and then equating the two results in :

$$J_{11}\phi_\xi + J_{12}\phi_\eta + J_{13}\phi_\zeta = \left[\frac{1-\frac{2}{(\gamma-1){M^2}_\infty}\left[\left(1+\frac{\gamma {M^2}_\infty C_p}{2}\right)^{\frac{\gamma-1}{\gamma}}-1\right]}{1+\left(\frac{v}{u}\right)^2+\left(\frac{w}{u}\right)^2}\right]^{\frac{1}{2}} - \cos\alpha \tag{17}$$

where $J_{i,j}$ are the elements of $\left(H^T\right)^{-1}$

A potential, $\phi_{i,j,k}$, can be found in terms of the pressure coefficient by expanding about the grid point location $\left(i+\frac{1}{2},j,k\right)$, and then using central differences in the ξ and ζ direction and second order backward differences in the normal direction, η, yielding :

$$\begin{aligned}{\phi^{n+1}}_{i,ky,k} = \frac{1}{J_{11}+\frac{3}{4}J_{12}}\Big\{ & J_{11}{\phi^n}_{i-1,ky,k} \\ & - J_{12}\Big[3{\phi^n}_{i-1,ky,k} - 4\left({\phi^n}_{i,ky-1,k}+{\phi^n}_{i-1,ky-1,k}\right) \\ & + {\phi^n}_{i,ky-2,k}+{\phi^n}_{i-1,ky-2,k}\Big]/4 \\ & - J_{13}\left({\phi^n}_{i,ky,k+1}+{\phi^n}_{i-1,ky,k+1}-{\phi^n}_{i,ky,k-1}-{\phi^n}_{i-1,ky,k-1}\right)/4 \\ & + F\left(C_{p\ i-\frac{1}{2},k}\right)\Big\}\end{aligned} \tag{18}$$

where $F\left(C_{p\ i-\frac{1}{2},k}\right)$ is the right hand side of equation 17 and $j = ky$ on the wing surface.

Since the grid is boundary conforming, the wing sections in the design region must be updated every so often by integrating the flow tangency condition written

in curvilinear coordinates:

$$\left(\frac{\partial \eta}{\partial \xi}\right)_{i,ky,k} = \frac{V}{U} - \frac{W}{U}\left(\frac{\partial \eta}{\partial \zeta}\right)_{i,ky,k} \tag{19}$$

Assuming that the spanwise terms are relatively small, this equation reduces to:

$$\left(\frac{\partial \eta}{\partial \xi}\right)_{i,ky,k} = \left(\frac{V}{U}\right)_{i,ky,k} \tag{20}$$

(This assumption was verified by solving equation 19 iteratively using constant values for the ratios of the velocities obtained at the present time level; the spanwise terms were at least two orders of magnitude smaller than the chordwise terms prior to the creation of the new grid, when of course all the derivatives of η with respect to the spanwise direction, ζ, or the chordwise direction, ξ, on the wing are zero.)

V can be obtained most accurately from the residual expression. Using the predefined averaging and differencing operators :

$$\mu_\eta \left(\rho h V\right)_{i,ky,k} = \frac{1}{2}\left(\left(\rho h V\right)_{i,ky+\frac{1}{2},k} + \left(\rho h V\right)_{i,ky-\frac{1}{2},k}\right) \tag{21}$$

$$\delta_Y \left(\rho h V\right)_{i,ky,k} = \left(\left(\rho h V\right)_{i,ky-\frac{1}{2},k} - \left(\rho h V\right)_{i,ky+\frac{1}{2},k}\right) \tag{22}$$

and combining, yields :

$$\delta_Y \left(\rho h V\right)_{i,ky,k} = 2\left(\rho h V\right)_{i,ky-\frac{1}{2},k} - 2\mu_Y \left(\rho h V\right)_{i,ky,k} \tag{23}$$

Substituting this into the residual expression, equation 14, and solving for the out of plane flux, $\rho h V$, on the wing surface yields :

$$\begin{aligned} 2\mu_{\xi\eta\zeta}\left(\rho h V\right)_{i,ky,k} = {} & \mu_{\eta\zeta}\delta_X \left(\rho h U\right)_{i,ky,k} + 2\mu_{\xi\zeta}\left(\rho h V_{i,ky-\frac{1}{2},k}\right) + \\ & \mu_{\xi\eta}\delta_Z \left(\rho h W_{i,ky,k}\right) + \textit{ compensation and upwinding terms} \end{aligned} \tag{24}$$

Now, since at convergence the flow should also be tangent to the designed surface, the tangency condition is enforced in the residual expression, equation 14, by setting :

$$(\rho hV)_{i,ky+\frac{1}{2},k} = -(\rho hV)_{i,ky-\frac{1}{2},k} \tag{25}$$

Since the resulting expression is identical to equation 24, the expression for the normal flux becomes :

$$\mu_{\xi\eta\zeta}\,(\rho hV)_{i,ky,k} = \frac{Residual}{2.0} \tag{26}$$

Note that since the residual is not zero in the design region due to the inverse boundary condition, this expression reveals that there will be an ejection of fluid from the boundary. No attempt was made to account for this addition of mass into the flowfield, since at convergence it would be negligible. Upon substitution of equation 26 into equation 20 and using the cell averaged flux ρhU on the surface this becomes :

$$\frac{\partial \eta}{\partial \xi} = \frac{Residual}{2\mu_{\xi\eta\zeta}\,(\rho hU)} \tag{27}$$

The displacements normal to the surface are obtained by integrating from the beginning of the inverse region to the trailing edge at each spanwise station using the trapezoidal rule. (Higher order integration schemes were tried but had little effect on the final answer, except on a fairly coarse grid in regions of high curvature like the cove region of a supercritical airfoil.) Assuming that the grid line leaving the wing is normal to the wing, this displacement, $\Delta\eta$, is then converted from computational to physical units by scaling it by the transformation metrics such that :

$$\Delta l = \Delta\eta\sqrt{\frac{\partial x}{\partial \xi}^2 + \frac{\partial y}{\partial \eta}^2} \tag{28}$$

After subtracting the boundary layer displacement thickness from the inverse displacements, Δl, which have been linearly interpolated to the user defined input stations, the resulting displacements are added to the initial airfoil sections yielding the new wing surface for the current time level.

Many times, the trailing edge thickness may be too large if the leading edge curvature is too small or may be 'fish-tailed' if the leading edge curvature is too large. These undesirable situations are remedied by a procedure called relofting where the designed surface is rotated about the leading edge to meet a specified trailing edge ordinate. To illustrate the previous procedures, a history of the convergence of a typical design is shown at every seven surface updates in figure 3.

Spanwise Oscillations

An annoying divergent spanwise oscillation problem has surfaced when designing a wing which required extensive relofting, especially when the initial section was thinner than the target. This led to sections which were too thick or too thin at adjacent constant Z grid stations (see figure 4). This problem was more pronounced when the sweep was increased or the aspect ratio was decreased. After many failed attempts at remedying this by reformulating the inverse boundary condition, attention was directed towards the residual and the terms composing it. The residual was broken into its components and plotted after each surface update. Sample plots for a divergent case are shown at three different time levels in figure 5. As can be seen, the compensation terms which include spanwise derivatives of ϕ at first are very small compared to the rest of the terms, but later tend to dominate and amplify the oscillation. This oscillation starts at the direct-inverse interface or, in other words, at the first spanwise station from the root in the design region and propagates

spanwise as a damped oscillation with a period of two grid spacings. Presently, it is thought that the mismatch in the potentials at the direct-inverse interface in the spanwise direction is being amplified by those compensation terms which include spanwise derivatives of the potential function. The residual is then undershot and overshot on alternating spanwise stations. This oscillation is further magnified by relofting, which creates a section that is too thin when the slopes defined in equation 27, which of course are directly proportional to the Residual, are too large and vice-versa. Since more or less fluid has to be ejected from the section thats too thin or thick respectively to give the streamline approximately corresponding to the correct target section, the potential field at each design station is taken further away from the adjacent fields by the inverse boundary condition which forces an even further undershoot or overshoot of the residual. It should be noted that this problem is not soley due to the implementation of the direct-inverse technique since this oscillation has not been observed with the ZEBRA design code, but seems to be unique to the coupling of the method with the analysis code, FLO30.

After exploring many alternatives to counter this problem, four methods have been discovered to damp out the spanwise oscillation.

A) Specify the inverse boundary condition at every other spanwise station and linearly interpolate the inverse displacements to the stations lying in between.

B) Specify the inverse boundary condition at every station, but again only calculate displacements at every other station and linearly interpolate the displacements to the stations in between.

C) Smooth the slopes, $\frac{\rho hV}{\rho hU}$, in the spanwise direction in the design region. (Note: smoothing the integrated slopes (i.e the displacements) did not suppress the oscillation, but only slowed the rate of divergence.)

D) Calculate all spanwise derivatives of the potential based upon a smoothed potential function in the spanwise direction as follows :

$$(\phi_\zeta)_{i,j,k+\frac{1}{2}} = \frac{(\phi_{i,j,k+2} - \phi_{i,j,k} + \phi_{i,j,k+1} - \phi_{i,j,k-1})}{4.0} \tag{29}$$

Preliminary results are shown in figures 6-9 for the four different approaches. All four were designed inviscidly on a medium grid (60x12x16) using Lockheed Wing-A at an angle of attack of two degrees and a Mach number of .8. A NACA 0012 section was used as the initial section in the entire design region which stretched from 30-70% semispan and began 5% aft of the leading edge and extended to the trailing edge. Using the RMS of the error between the target sectiona and the section designed as a measure of goodness, the technique A and D produced the best results for this case in the interior as well as at the edges of the design region, while for the same number of flowfield iterations, the technique C produced the most unsatisfactory results when compared to the target sections. The effect of each approach on the Residual can be seen by refering to figures 10-13. The smoothing approaches work well when designing in the interior of the wing, but they do not give satisfactory results at the root and tip of the wing where smoothing the quickly varying potential functions leads to large errors in the residual.

Spanwise Grid Skewness

Recently it was discovered, quite inadvertently, that the skewness of the constant X grid lines leaving the tip of the wing (See figure 14) had a dramatic effect on the design of the sections near the wing tip. If the grid was significantly skewed it was impossible to obtain the correct airfoil shapes in the tip region as can be seen in figure 15. This is thought to be due to the large errors associated with

a skewed grid which are revealed in the pressure distributions (figure 16). These errors in the solution seem to have caused the shock location to move further aft. Although the skeweness of the grid was quite extreme in this case, these results affirm the need for smoothly varying grids in wing design, at least in the spanwise direction.

Boundary Layer and Wake Effects

It was of interest to discover how significant the various viscous effects were in the design of transonic wings[16]. An input pressure distribution was obtained by analyzing Lockheed wing-A using full viscous effects ; these included boundary layer displacement thickness, wake thickness and wake curvature. This was considered to be the type of real pressure distribution which would be available to the designer. This pressure distribution was then used in three cases. In the first case, the wing was designed inviscidly. In the second case, the wing was designed without the wake options but included the boundary displacement thickness effects. And in the third case, all viscous effect were used in the design of the wing. The design region for all three cases extended from 30-70% semispan and began 10% aft of the leading edge of the airfoil, but the inverse boundary condition was only enforced at the 30, 50 and 70% semispan station and the displacements were linearly interpolated to the stations delimitted. The initial airfoil section at 50% semispan was formed by thinning the supercritical target section by 6% and removing the cove region. The initial sections at the edges of the design region were the same as the target sections, while the remaining sections delimitted were obtained through linear interpolation.

The results for these cases are presented in figures 17. Neglecting wake effects seems to have a small effect on the resulting design. The sections are little thicker

than the sections designed with full viscous effects. This is probably because wake curvature effects reduce the lift of the wing resulting in smaller boundary layer displacement thicknesses than those obtained without wake effects. Because of this, the section designed without wake effects was relofted less, leading to a thicker section. On the other hand, the wing sections designed inviscidly are profoundly different at 30 and 70% semispan, but only slightly different at 50% semispan. The large differences at the inboard and outboard stations are due to the influence of the inviscid pressures outside the design region which probably cause a large mismatch in the potentials at the design-analysis interface. And the remarkable agreement in the middle of the design region, except in the cove region where the boundary layer is thick, is due to the influence of the viscous boundary condition at the edges of the design region. (This was verified by designing the entire wing inviscidly using viscous pressure distributions. This case led to airfoil sections which varied smoothly in the spanwise direction. These results will be shown in the final paper) After the wings were designed, all three were then analyzed with full viscous effects to assess the significance of the changes made to the wing on the pressure distributions and to see how well these pressures matched the target pressures. Knowing that the wing designed with full viscous effects is correct, it is quite obvious from figure 18 and Table 1 that the wing designed inviscidly is quite unsatisfactory. The shock is not far enough aft and the lift produced is sometimes 20% smaller than that desired.

Initial profile effects

One of the disadvantages of the inverse method is that a-priori knowledge about the correct shape of the leading edge must be known to achieve the correct airfoil shape. It was thought that because FLO30's grid package packs grid lines close

to the leading edge of the airfoil, that the design could be started quite close to the leading edge thus relieving the designer of the burden of choosing the correct nose shape. Two test cases were conducted to investigate the dependence of the final design on the initial airfoil section. Both used Lockheed wing-A at the same conditions mentioned earlier for the viscous study. For the first case, the initial airfoils were the same as those in the viscous study. These airfoils all had leading edges which were in the same family as the target section. The design was started 10% aft of the leading edge. In the second case, NACA 0012 sections were used at all design stations; the leading edge of these sections were not in the same family as the target airfoil sections. For this case, the pressure boundary condition began 5% aft of the leading edge. Referring to figures 19 and 20, it can be said that although slightly better results were obtained for the first case, the airfoils designed were quite insensitive to the initial section.

Aspect Ratio and Sweep Effects

Three cases will be shown in order to roughly delimit the range of aspect ratios and leading edge sweep angles. These include Lockheed Wing A and B and will hopefully include Wing C in the final paper. These wings have aspect ratios of 8, 3.8, and 2.6, leading edge sweep angles of 27,35, and 45 degrees and taper ratios of .4,.4, and .3 respectively. The target pressure distributions were obtained by a direct analysis of the target wings in a fully viscous environment. The initial section for Wing-A was a NACA 0012, while a NACA 0006 was used for Wing-B. The design region for Wing-B extended from 10-100% semispan and began 5% aft of the leading edge. Both wings were designed using all available viscous options. Fine grid results for Wing-B are shown in figure 21, while medium grid results for

Wing-A are shown in figure 22. As can be seen the designed and target sections for both Wings are in excellent agreement in the interior of the design region and closely match at the edges of the design region.

Conclusions

Progress in the direct-inverse wing design method in curvilinear coordinates has been made. This included the remedying of a spanwise oscillation problem and the assessment of grid skewness, viscous interaction, and the initial airfoil section on the final design. It was found that : in response to the spanwise oscillation problem that designing at every other spanwise station produced the best results for the cases presented, a smoothly varying grid is especially needed for the accurate design at the wing tip, boundary layer displacement thicknesses must be included in a successful wing design, the design of high and medium aspect ratio wings is possible with this code, and that the final airfoil section designed is fairly independent of the initial section.

I. ACKNOWLEDGEMENTS

The work presented in this paper was primarily supported by the National Aeronautics and Space Administration under Grant NAG-1-619 with Richard L. Campbell of the Langley Research Center as technical monitor. The authors express their appreciation to Richard L. Campbell and Edgar Waggoner of NASA Langley and to Thomas Gally for their assistance and helpful suggestions. Much thanks also goes to the Computer Service Center at Texas A&M University for their very generous computer support.

References

[1] Davis, W., "TRO-2D: A Code for Rational Transonic Aero Optimization," AIAA Paper 85-0425, January 1985.

[2] Hicks. R., "Wing Design by Numerical Optimization," AIAA Paper 77-1247, August 1985.

[3] Campbell, R.C., and Smith, L.A., " ," *AIAA 5th Applied Aerodynamics Conference*, Monterey, California, August 17-19, pp. 527-538.

[4] Carlson, L. A., "Transonic Airfoil Design Using Cartesian Coordinates," NASA CR-2578, April 1976.

[5] Carlson, L. A., "TRANDES: A Fortran Program for Transonic Airfoil Analysis or Design," NASA CR-2821, June 1977.

[6] Anderson, W. K., and Carlson, L. A., "Inverse Transonic Wing Design on a Vector Processor," Texas A&M Research Foundation Report TAMRF-4535-8212, December 1982.

[7] Weed, R. A., Anderson, W. K., and Carlson, L. A., "A Direct-Inverse Three-Dimensional Transonic Wing Design Method for Vector Computers," AIAA Paper 84-2156, August 1984.

[8] Shankar, V. and Malmuth, N.D.,, "Computational Transonic Inverse Procedure for Wing Design," AIAA Paper 80-1390R, 1980.

[9] Gally, T. A. and Carlson, L. A., "Inverse Transonic Wing Design Using Inverse Methods in Curvilinear Coordinates," *5th Applied Aerodynamics Conference*, Monterey, California, August 17-19, pp. 516-526.

[10] Melson, N. D. and Streett, C. L., "TAWFIVE: A User's Guide," NASA TM84619, September 1983.

[11] Jameson, Anthony, "Transonic Potential Flow Calcu lations Using Conservative Form," *Proceedings of AIAA 2nd Computational Fluid Dynamics Conference*, Hartfort, Conn., June 1975, pp. 148-161.

[12] Jameson, Anthony and Caughey, D. A., "A Finite Volume Method for Transonic Potential Flow Calculations," *Proceedings of AIAA 3rd Computational Fluid Dynamics Conference*, Albuquerque, N. M., June 1977, pp. 35-54.

[13] Jameson, Anthony, "Iterative Solution of Transonic Flows over Airfoils and Wings, Including Flows at Mach 1," *Comm. Pure Appl. Math.*, vol. 27, 1974, pp. 283-309.

[14] Caughey, D. A. and Jameson, Anthony, "Progress in Finite-Volume Calculation for Wing-Fuselage Combinations," AIAA Paper 79-1513R, 1979.

[15] Gally, T. A., "Inverse Transonic Wing Design Using Finite-Volume Methods in Curvilinear Coordinates," Master's Thesis, Texas A&M University, May 1987.

[16] Carlson, L.A., Ratcliff, R.R., Gally, T. A. , "Inverse Wing Design In Transonic Flow Including Viscous Interaction," *Transonic Symposium*, Hampton, Virginia , April 19-21, 1988, pp. .

STAGGERED BOX FINITE VOLUME SCHEME

Compensation Terms defined

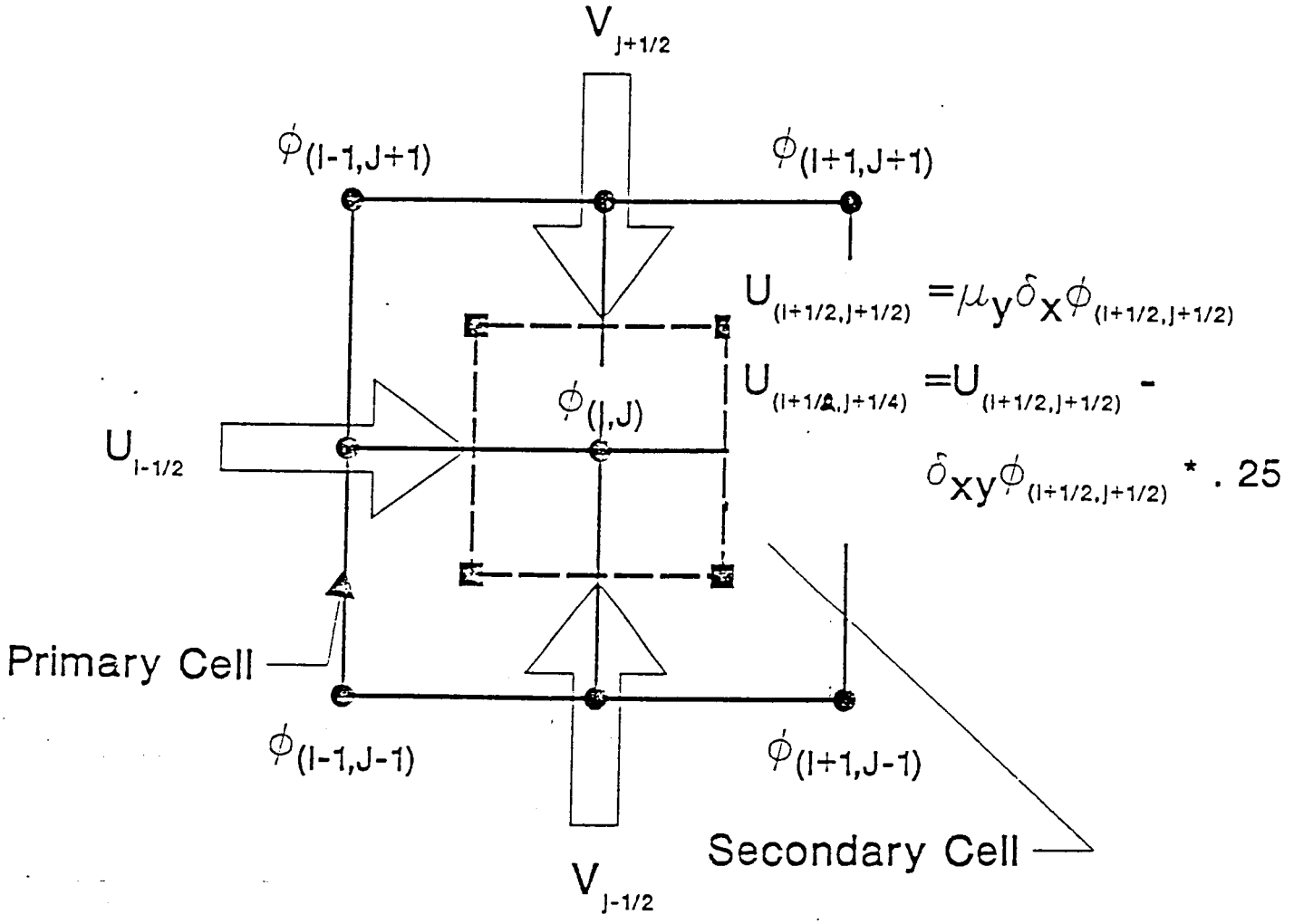

Figure 1. Staggered Box Finite-Volume Cell

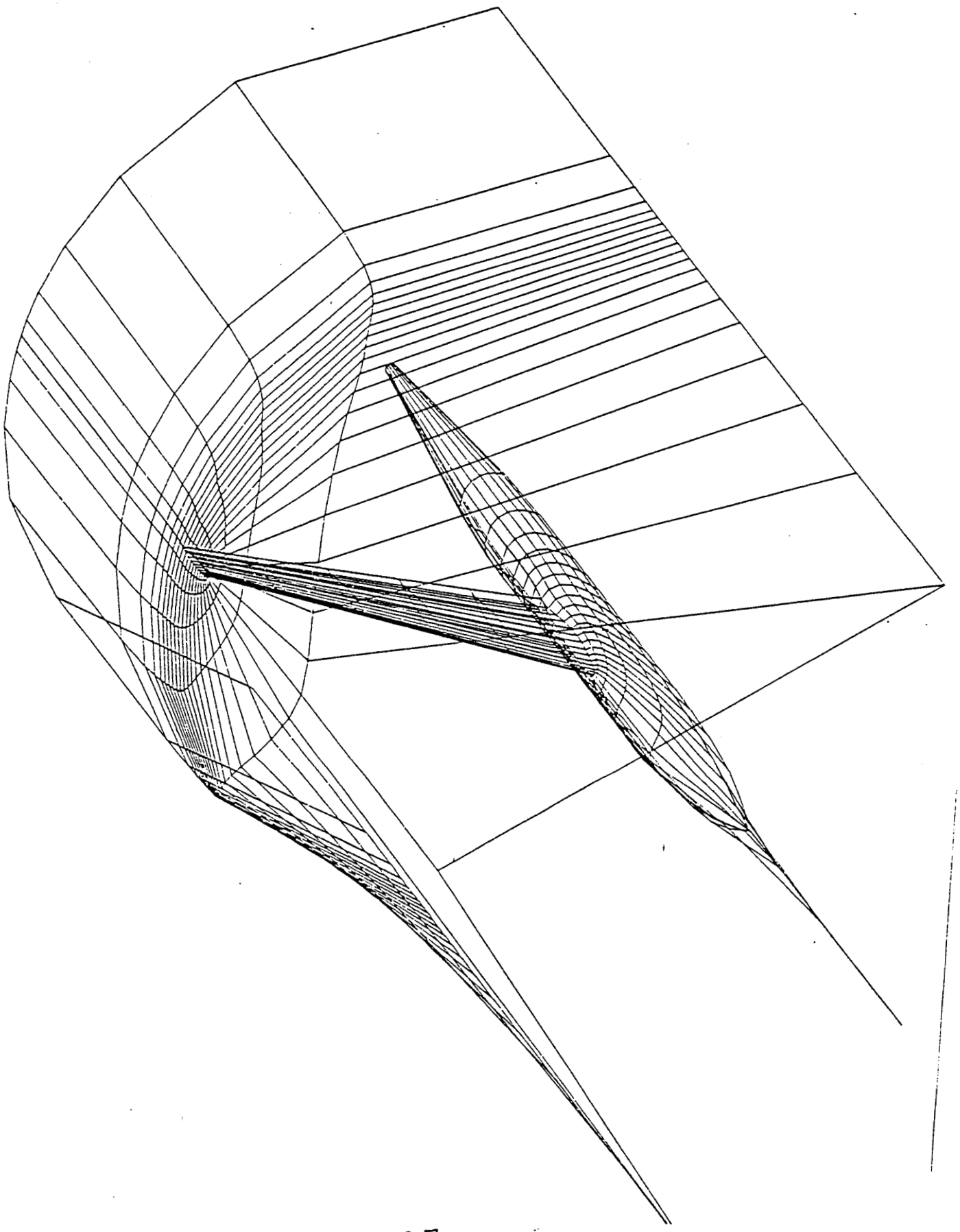

Figure 2. Conformal Grid Topography

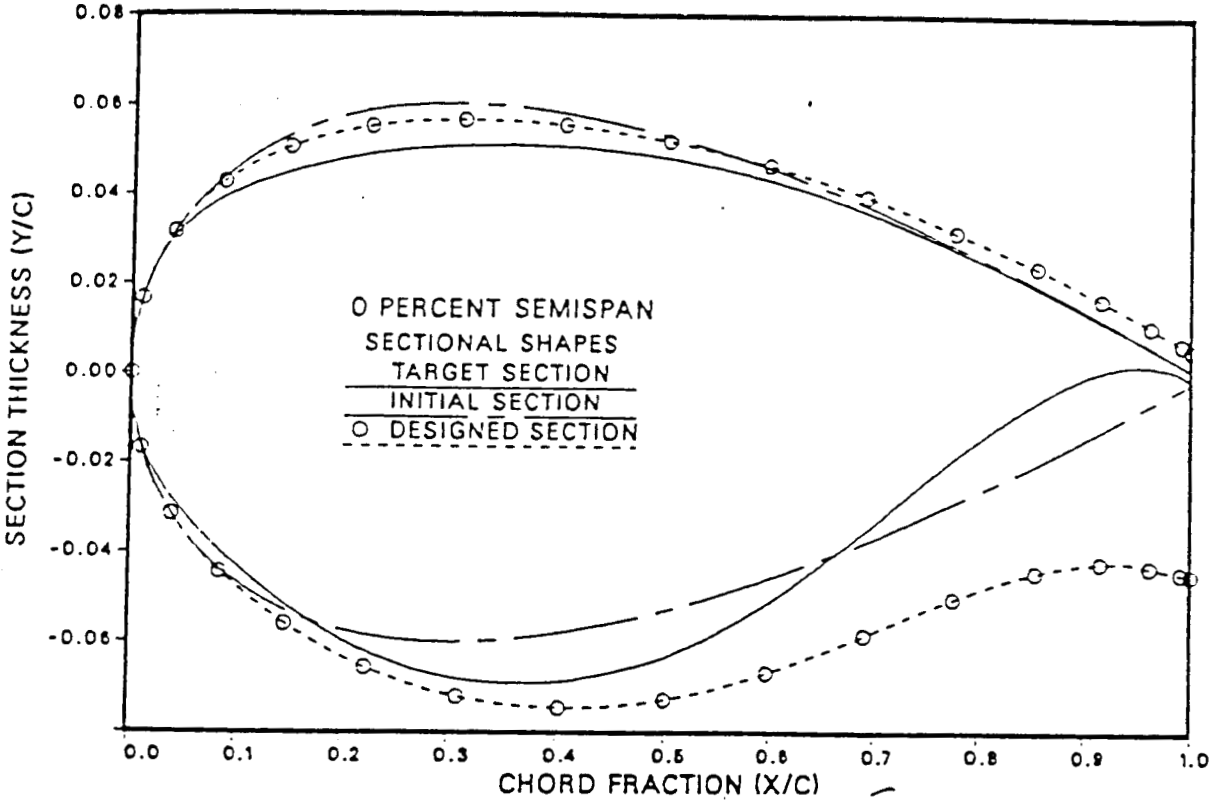

Figure 3a

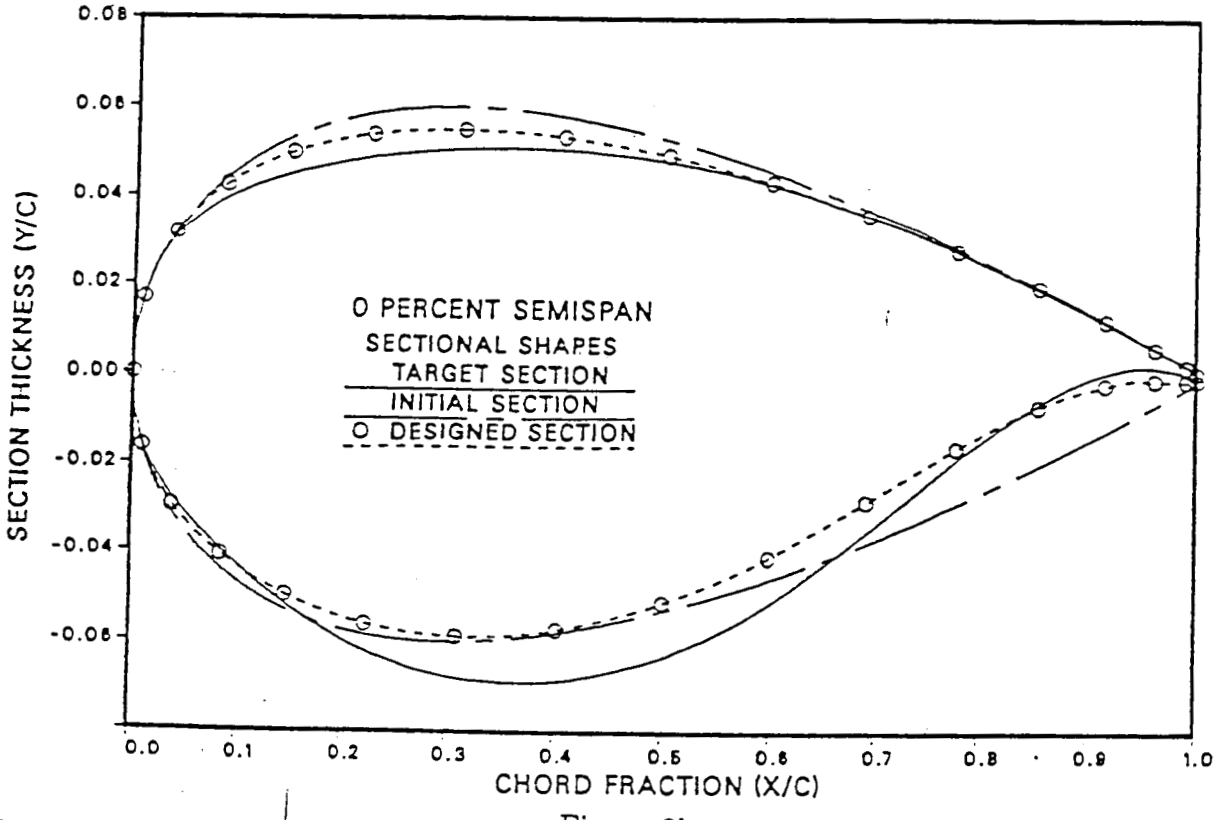

Figure 3b

Figure 3a-3d. Typical History of an Airfoil Section Designed at the Root of the Wing Shown at Every Seven Surface Updates

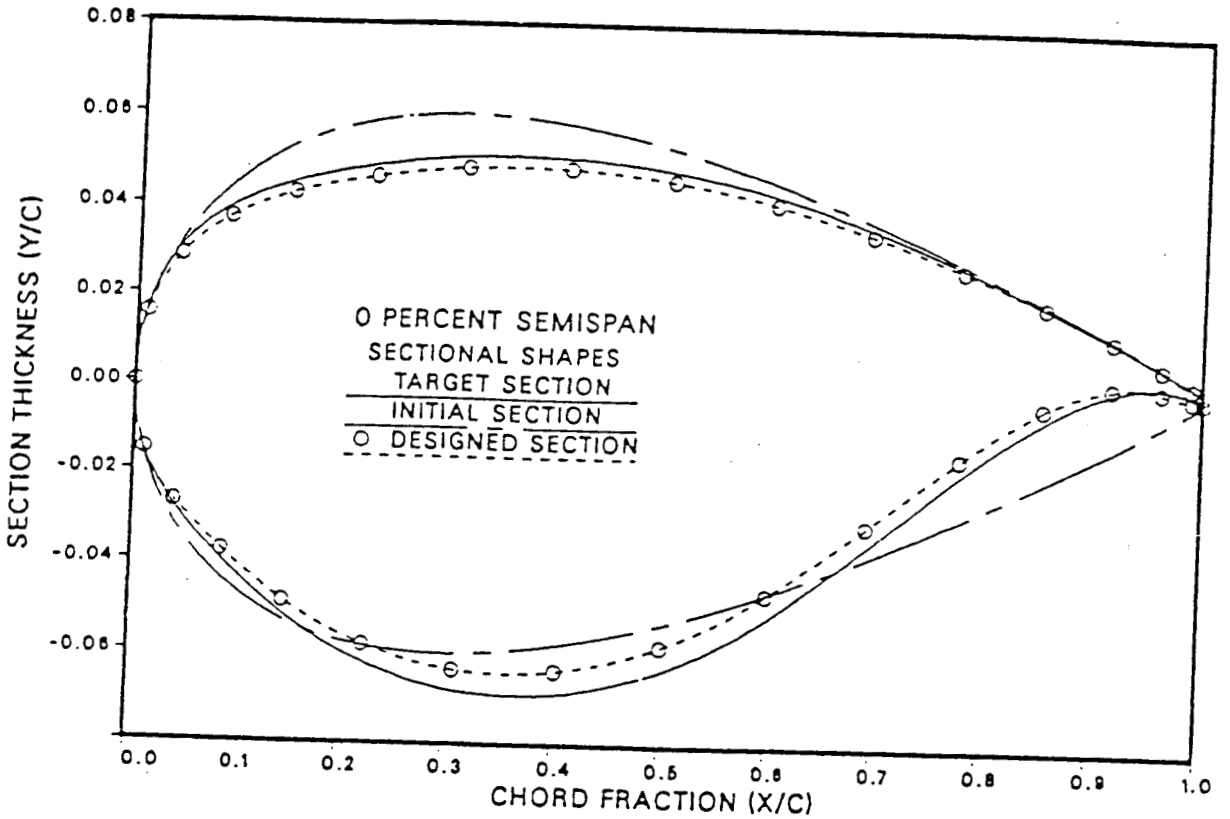

Figure 3c

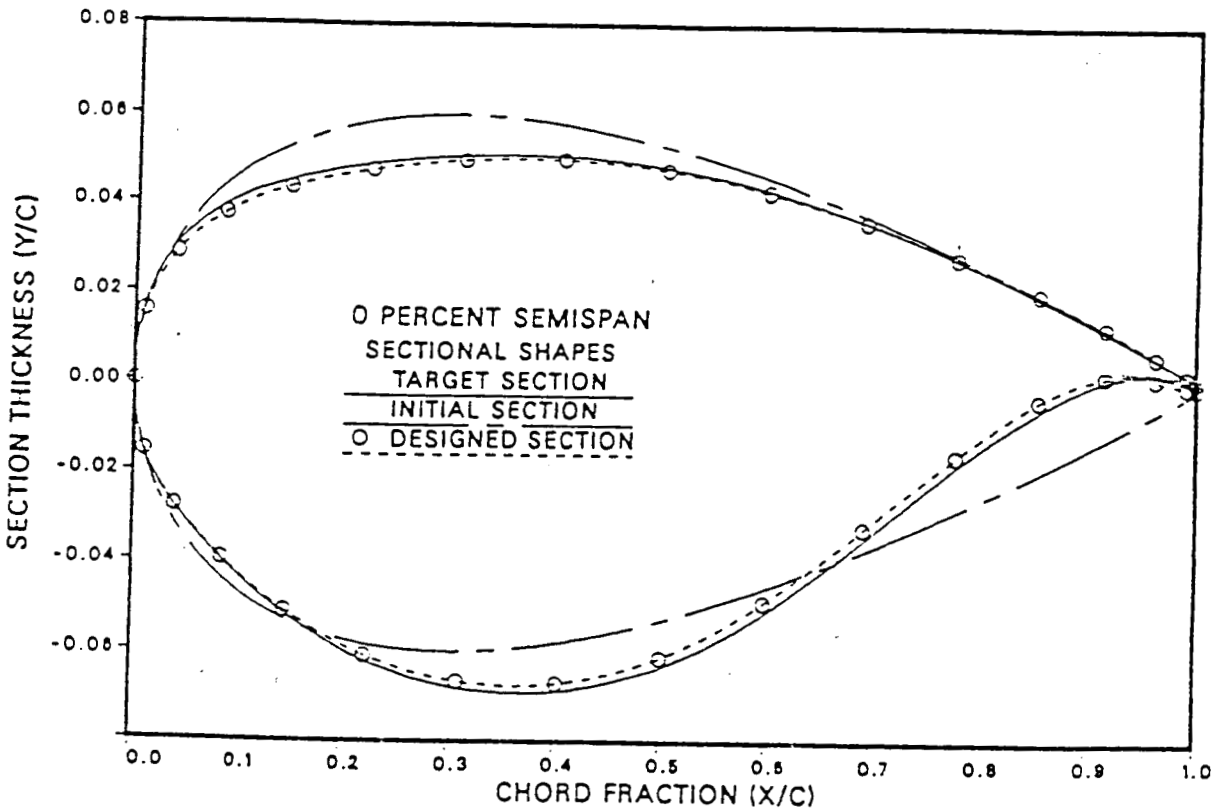

Figure 3d

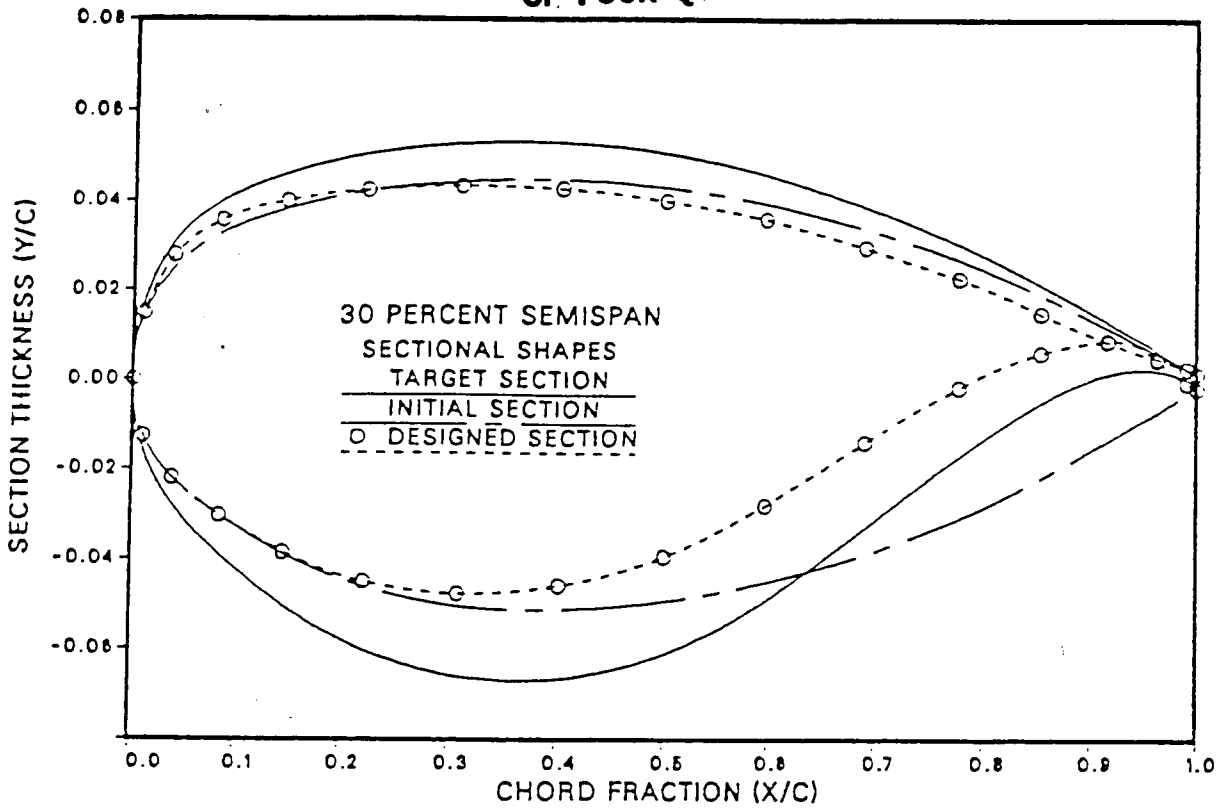

Figure 4a

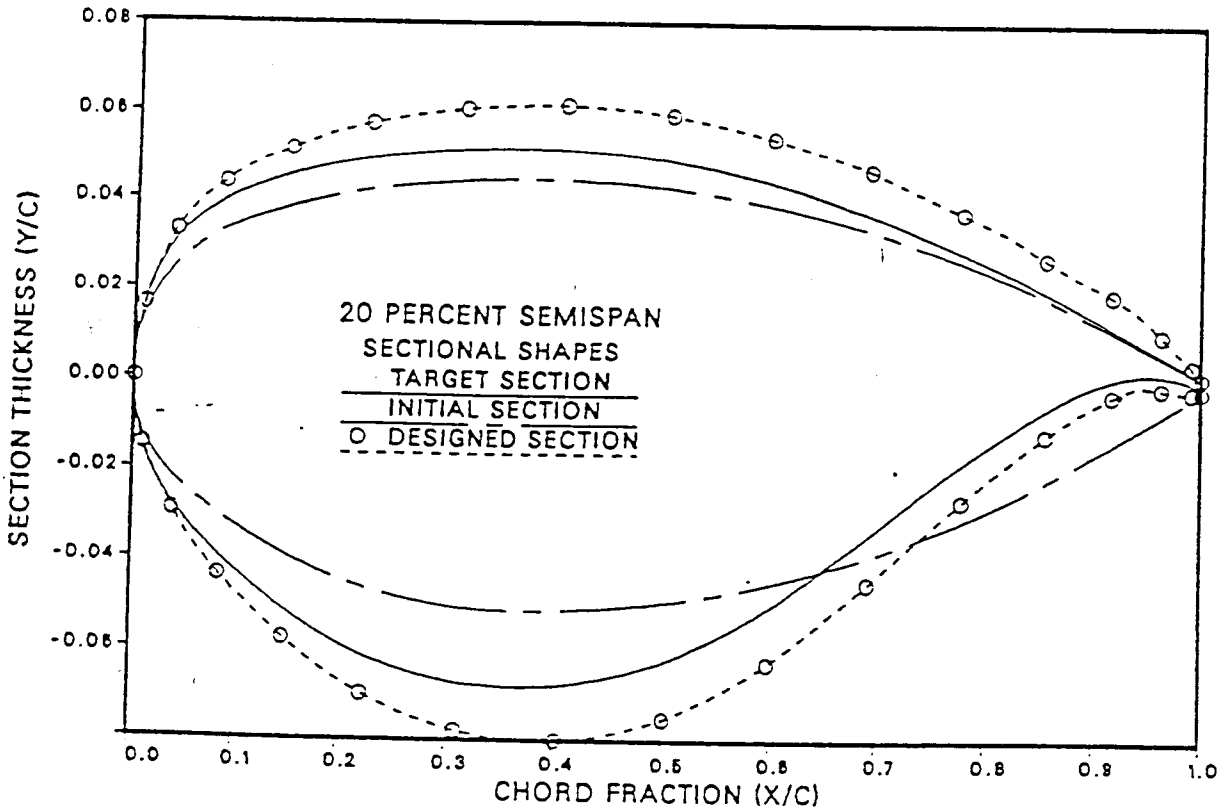

Figure 4a-4b. Alternating Thick-Thin Sections
Caused by the Oscillation of the Parabola

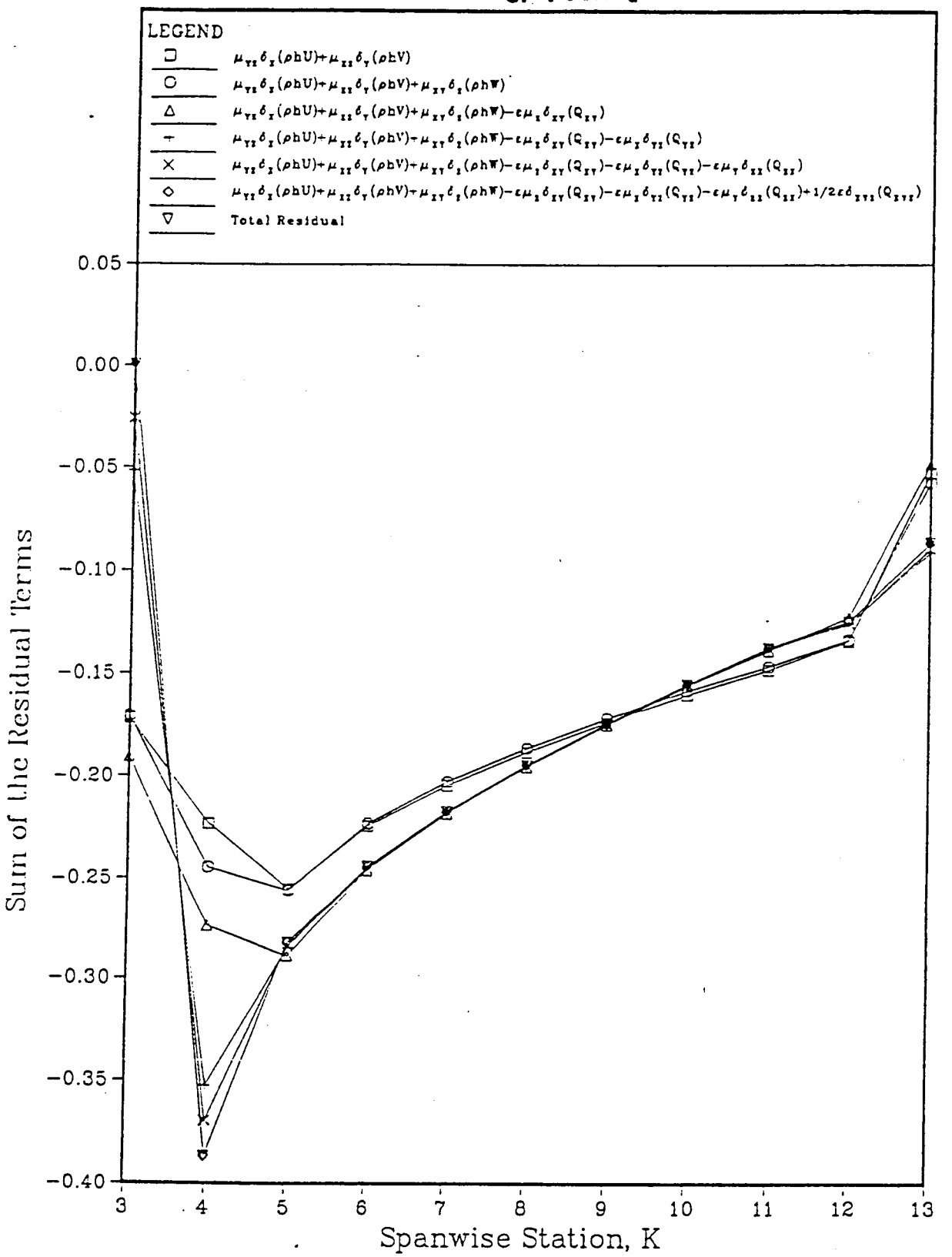

Residual Sum For x = 1.000 (lower surface)
GLOBAL ITERATION 1

Figure 5a

Figure 5a-5c. Typical Time History of the Residual and the Terms Composing It at the Lower Trailing Edge

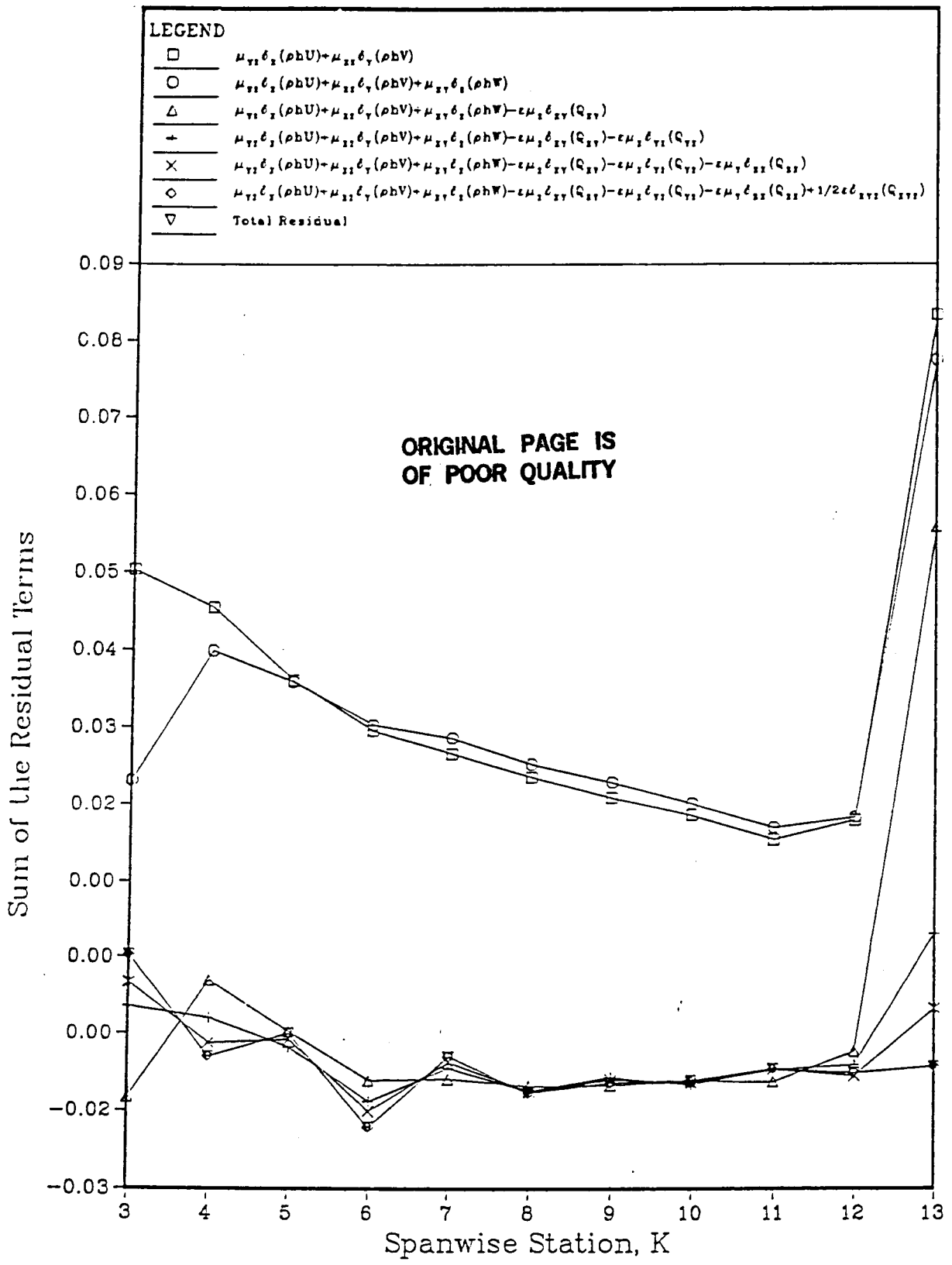

Residual Sum For x = 1.000 (lower surface)
GLOBAL ITERATION 14

Figure 5b

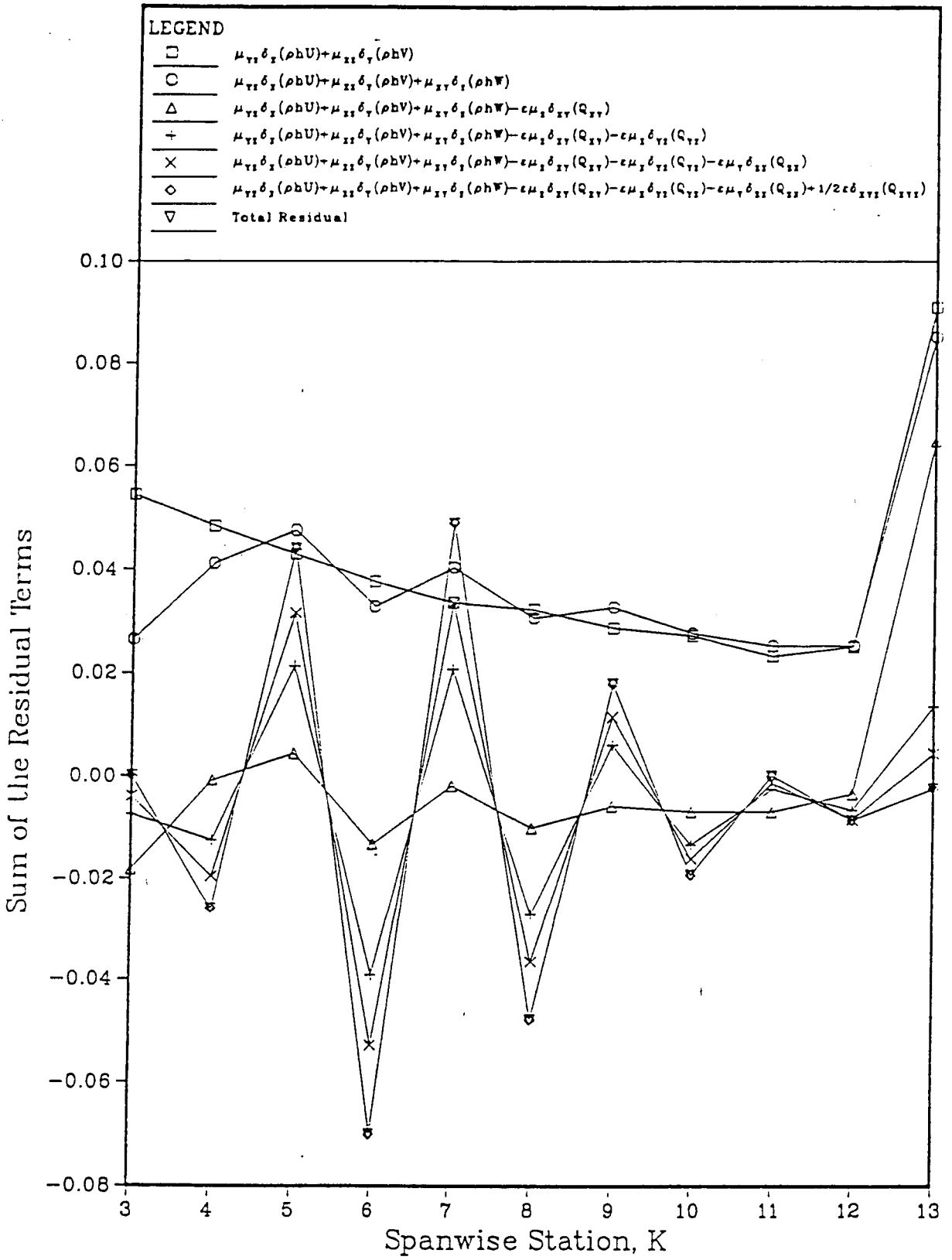

Residual Sum For x = 1.000 (lower surface)
GLOBAL ITERATION 26

Figure 5c

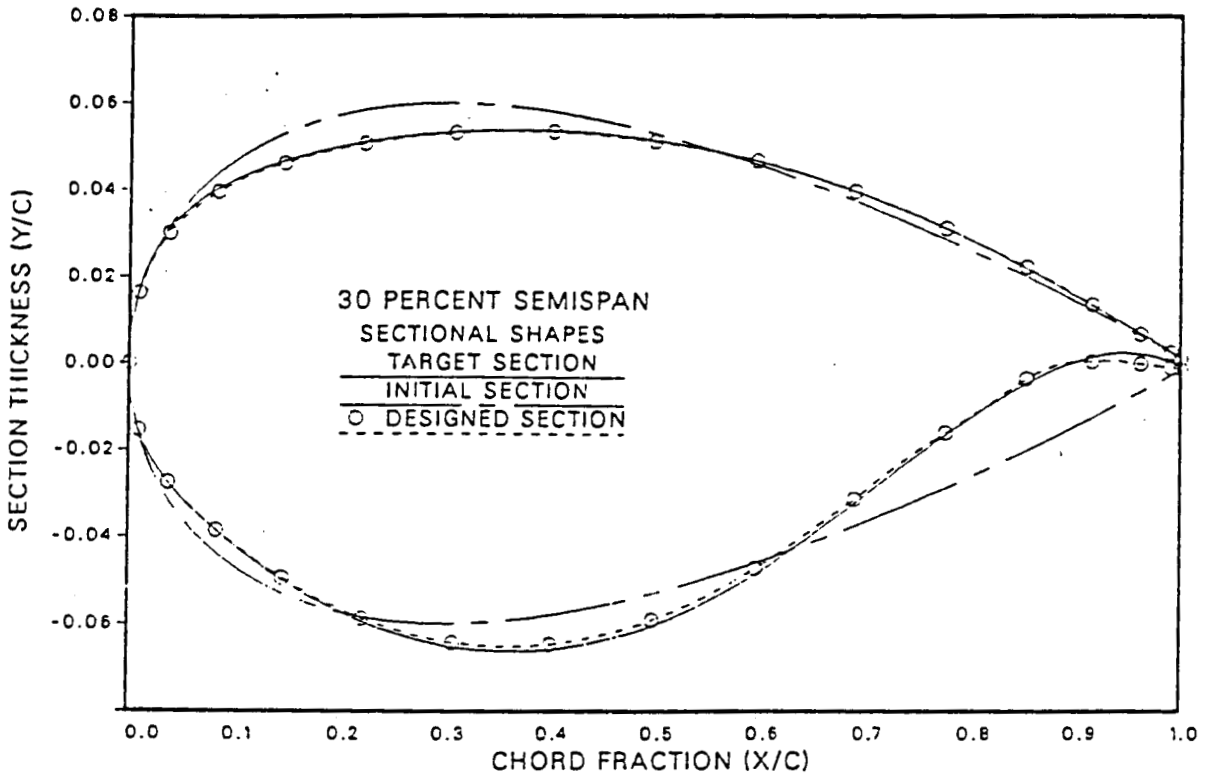

Figure 6a

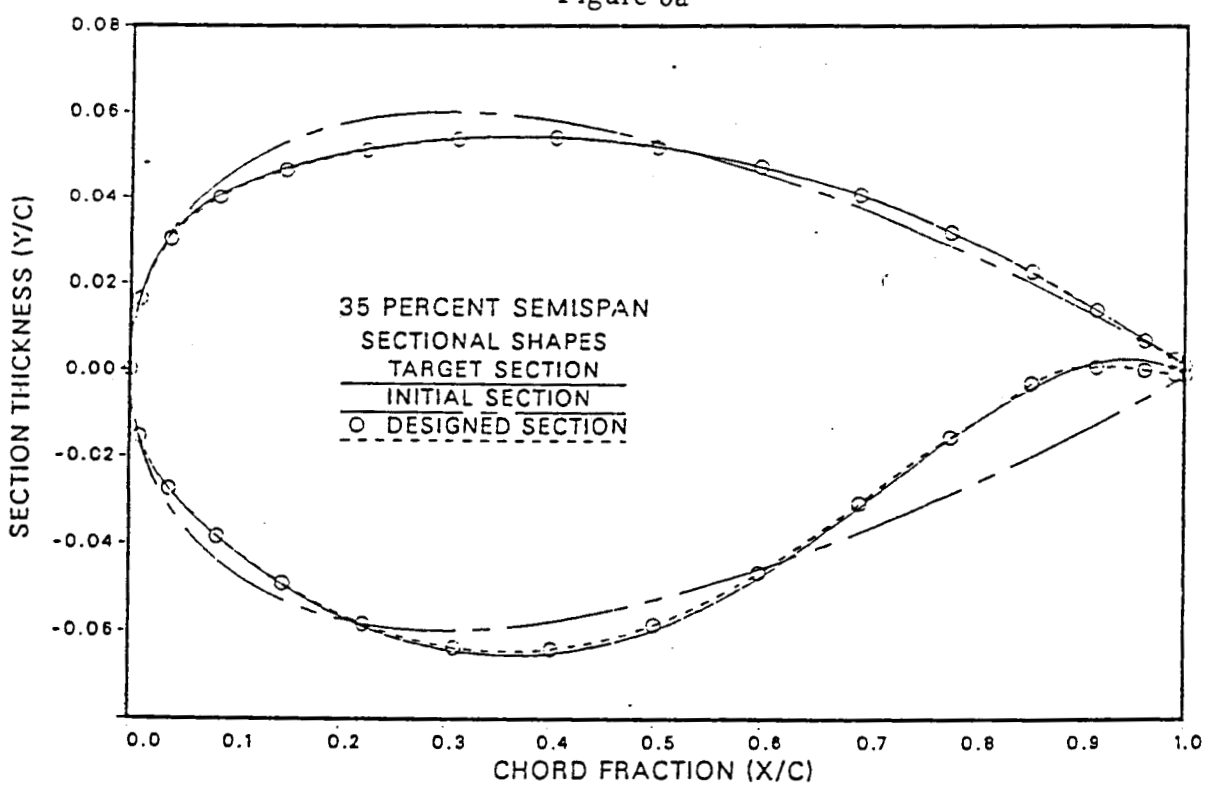

Figure 6a-6d. Airfoil Sections Designed Using Method A

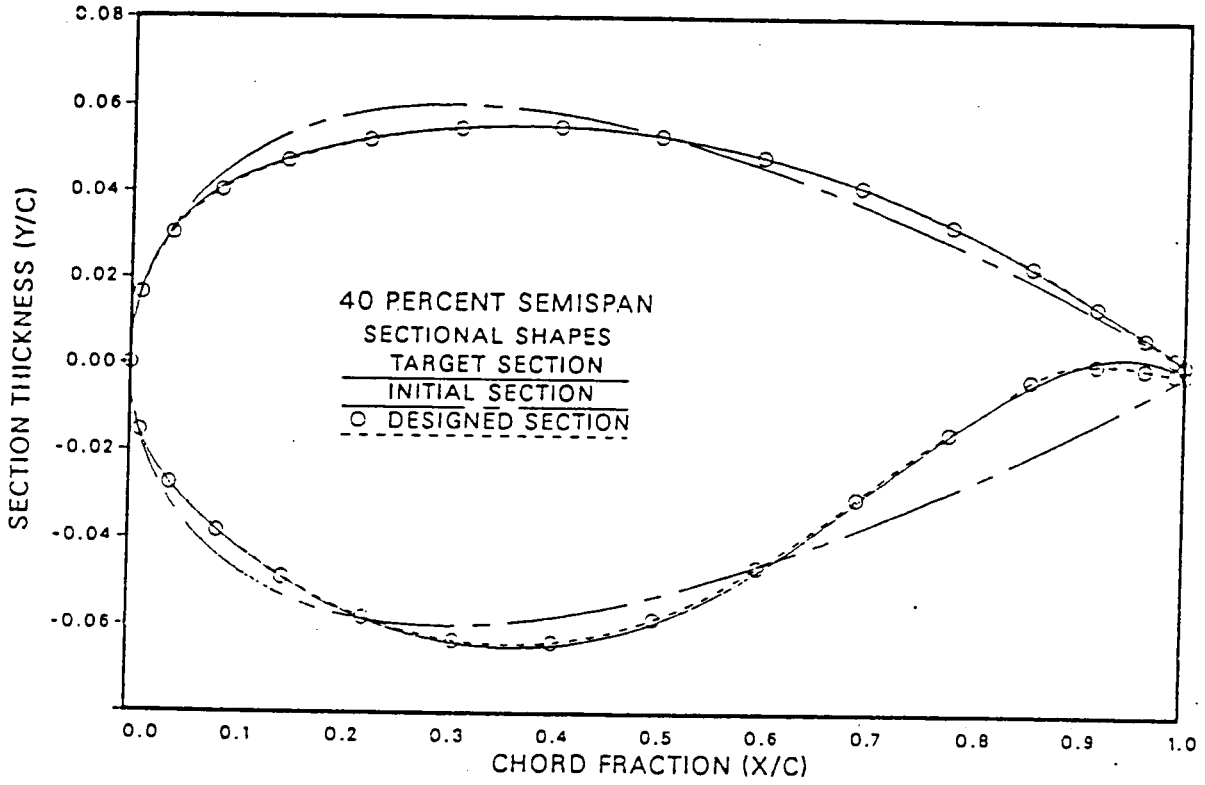

Figure 6b

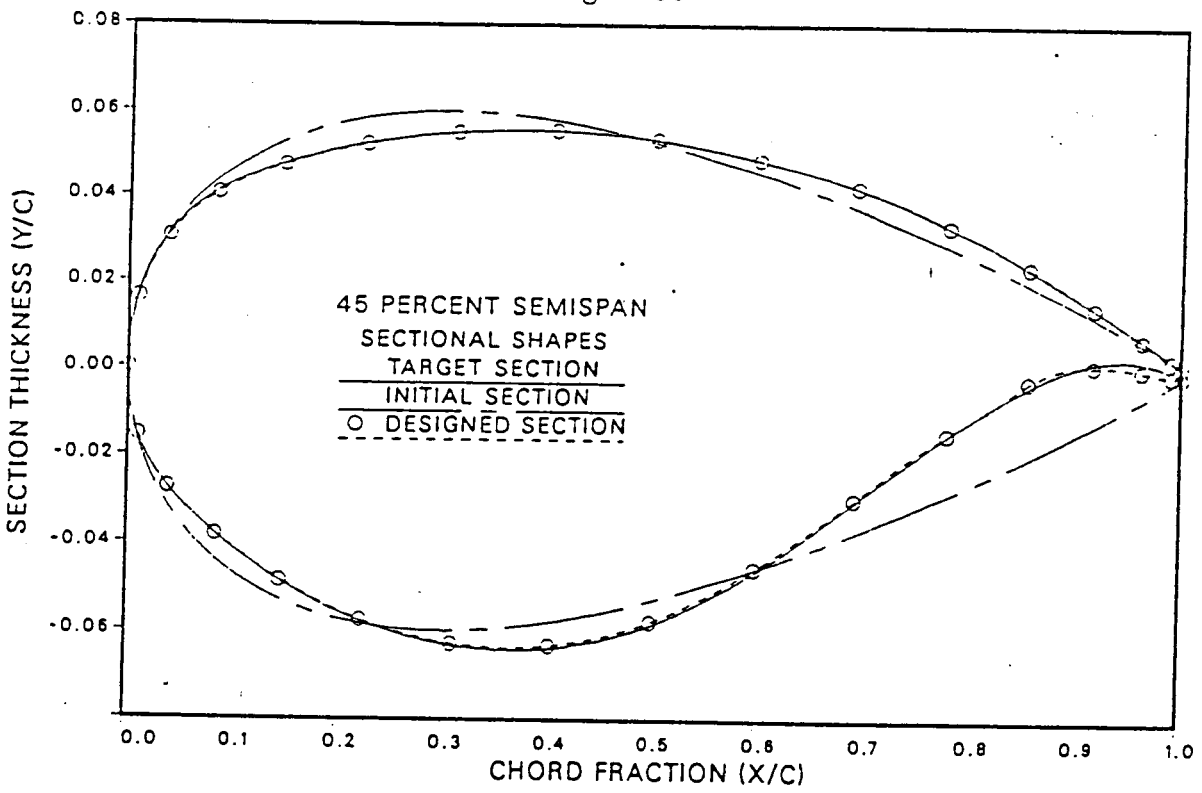

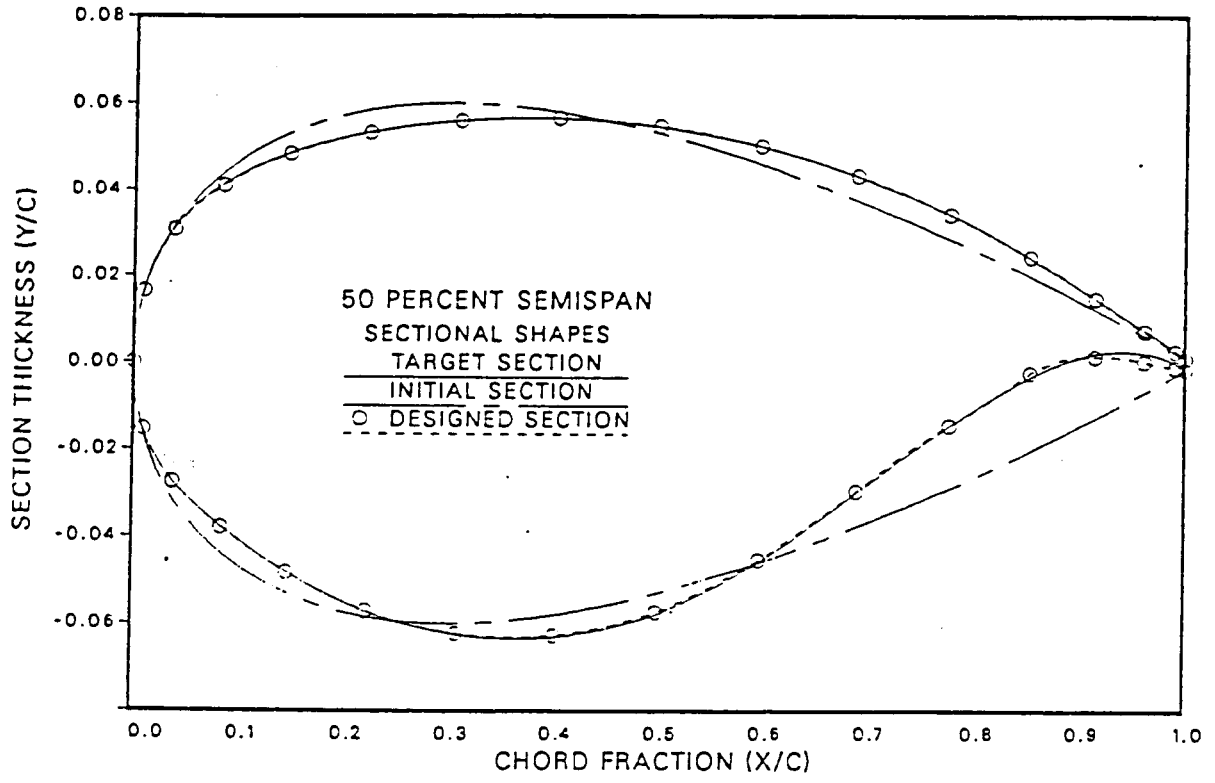
0.08
0.06
0.04
0.02
0.00
-0.02
-0.04
-0.06
SECTION THICKNESS (Y/C)
50 PERCENT SEMISPAN
SECTIONAL SHAPES
TARGET SECTION
INITIAL SECTION
DESIGNED SECTION
0.0
0.1
0.2
0.3
0.4
0.5
0.6
0.7
0.8
0.9
1.0
CHORD FRACTION (X/C)

Figure 6c

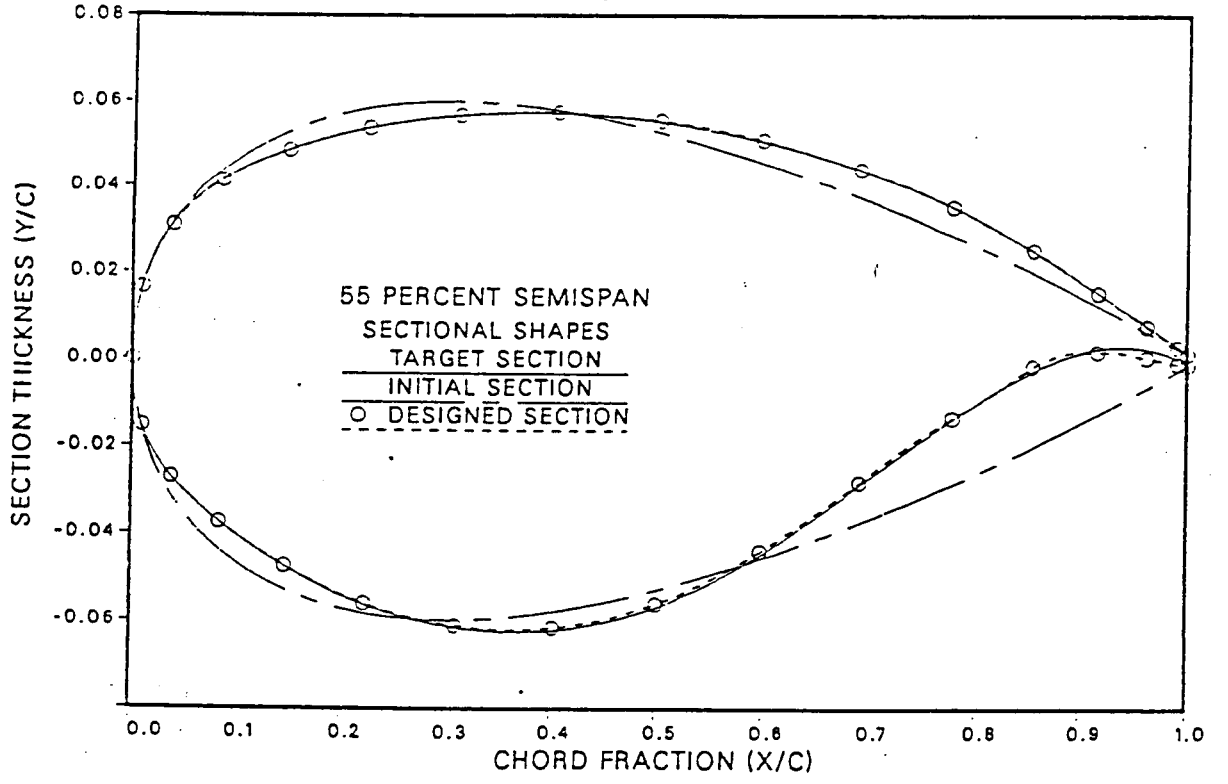
0.08
0.06
0.04
0.02
0.00
-0.02
-0.04
-0.06
SECTION THICKNESS (Y/C)
55 PERCENT SEMISPAN
SECTIONAL SHAPES
TARGET SECTION
INITIAL SECTION
DESIGNED SECTION
0.0
0.1
0.2
0.3
0.4
0.5
0.6
0.7
0.8
0.9
1.0
CHORD FRACTION (X/C)

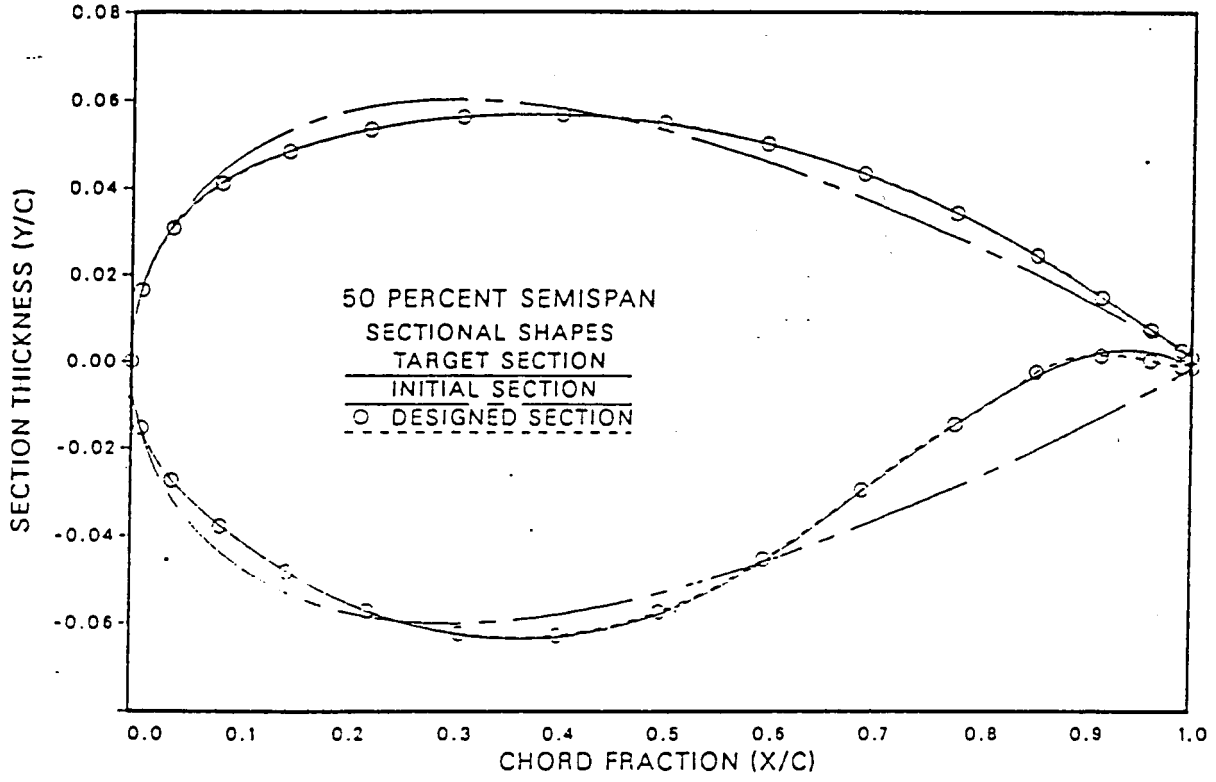
0.08
0.06
0.04
0.02
0.00
-0.02
-0.04
-0.06
SECTION THICKNESS (Y/C)
50 PERCENT SEMISPAN
SECTIONAL SHAPES
TARGET SECTION
INITIAL SECTION
DESIGNED SECTION
0.0
0.1
0.2
0.3
0.4
0.5
0.6
0.7
0.8
0.9
1.0
CHORD FRACTION (X/C)

Figure 6c

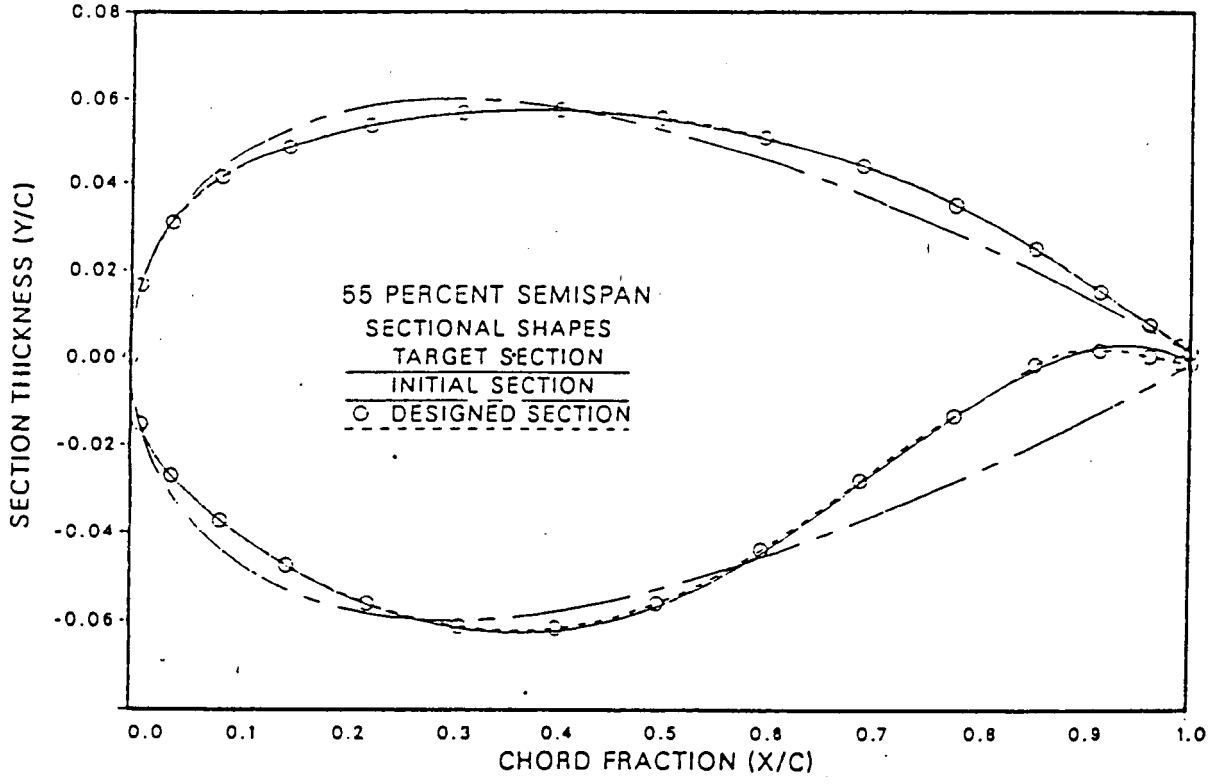
0.08
0.06
0.04
0.02
0.00
-0.02
-0.04
-0.06
SECTION THICKNESS (Y/C)
55 PERCENT SEMISPAN
SECTIONAL SHAPES
TARGET SECTION
INITIAL SECTION
DESIGNED SECTION
0.0
0.1
0.2
0.3
0.4
0.5
0.6
0.7
0.8
0.9
1.0
CHORD FRACTION (X/C)

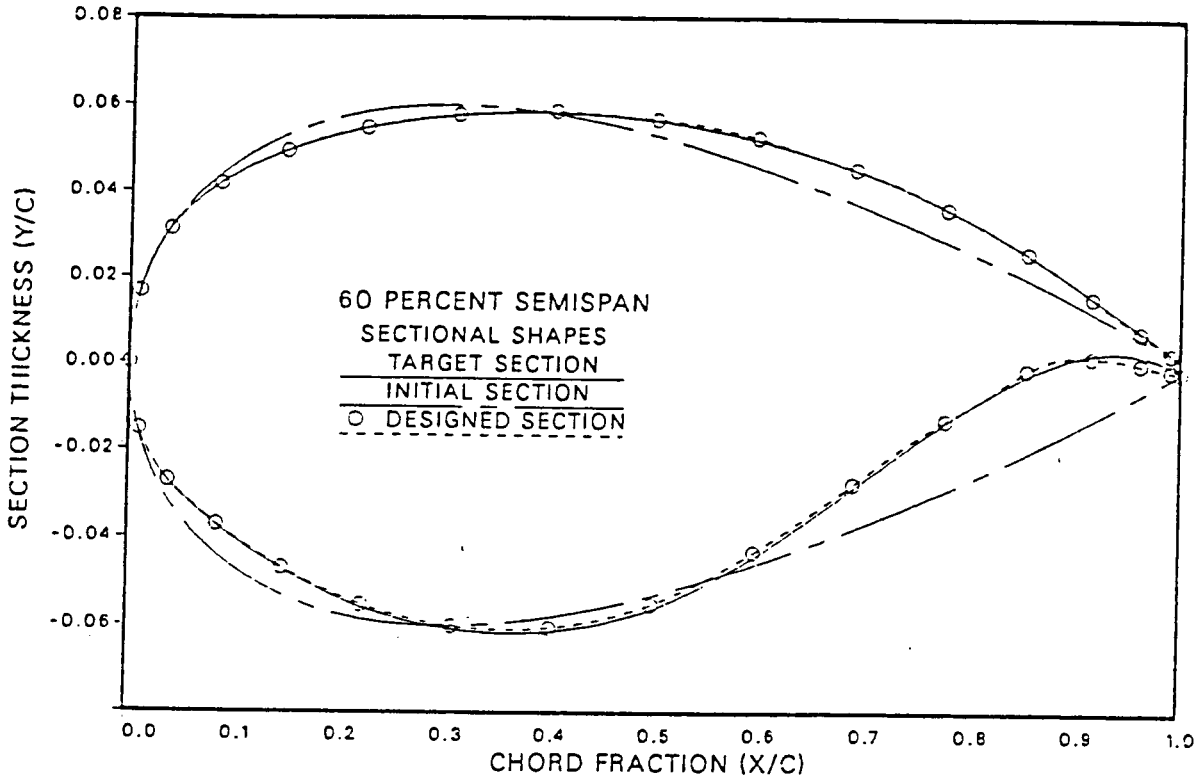
0.08
0.06
0.04
0.02
0.00
-0.02
-0.04
-0.06
SECTION THICKNESS (Y/C)
60 PERCENT SEMISPAN
SECTIONAL SHAPES
TARGET SECTION
INITIAL SECTION
DESIGNED SECTION
0.0
0.1
0.2
0.3
0.4
0.5
0.6
0.7
0.8
0.9
1.0
CHORD FRACTION (X/C)

Figure 6d

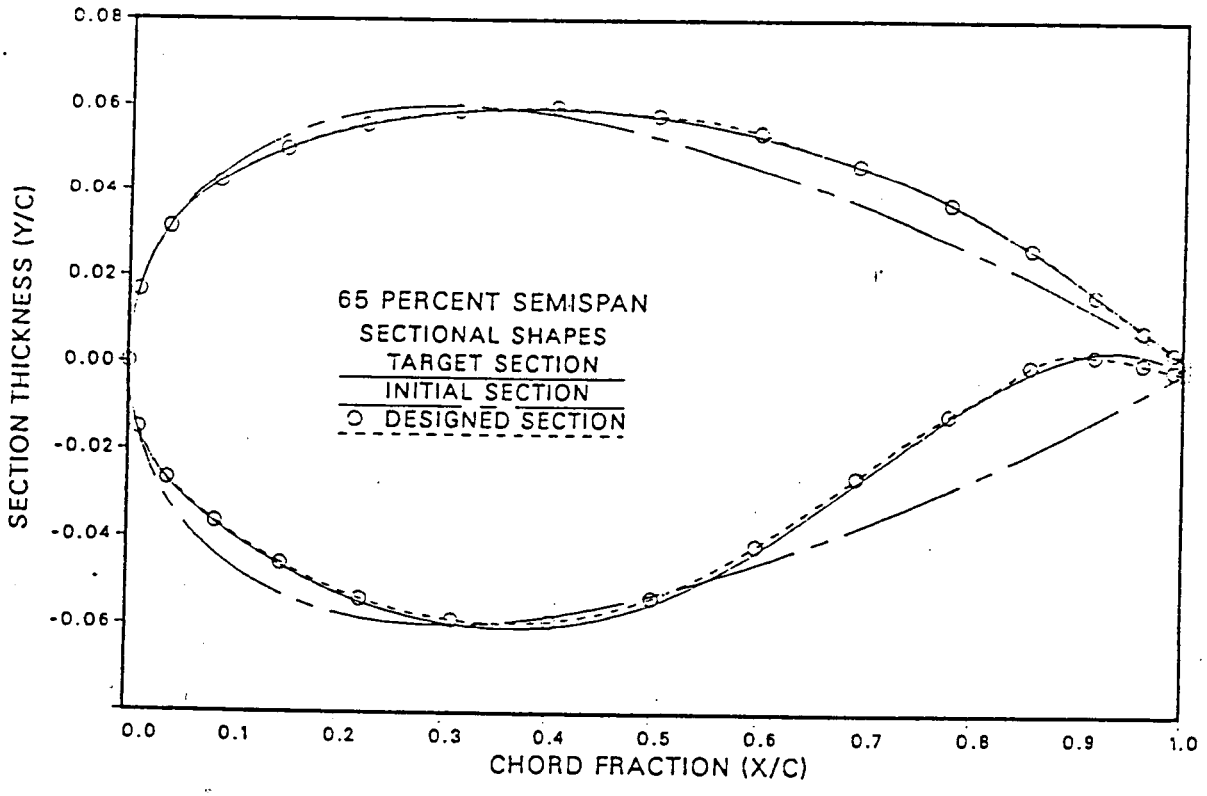
0.08
0.06
0.04
0.02
0.00
-0.02
-0.04
-0.06
SECTION THICKNESS (Y/C)
65 PERCENT SEMISPAN
SECTIONAL SHAPES
TARGET SECTION
INITIAL SECTION
DESIGNED SECTION
0.0
0.1
0.2
0.3
0.4
0.5
0.6
0.7
0.8
0.9
1.0
CHORD FRACTION (X/C)

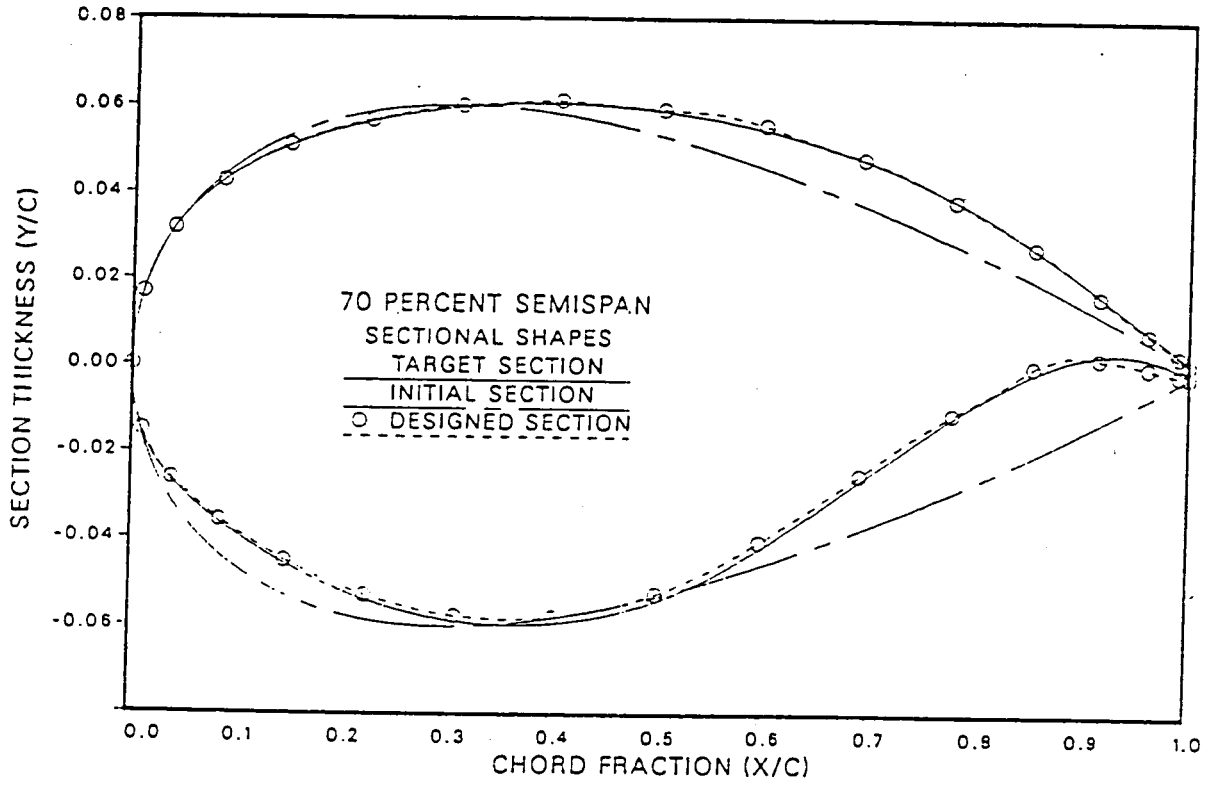
0.08
0.06
0.04
0.02
0.00
-0.02
-0.04
-0.06
SECTION THICKNESS (Y/C)
70 PERCENT SEMISPAN
SECTIONAL SHAPES
TARGET SECTION
INITIAL SECTION
DESIGNED SECTION
0.0
0.1
0.2
0.3
0.4
0.5
0.6
0.7
0.8
0.9
1.0
CHORD FRACTION (X/C)

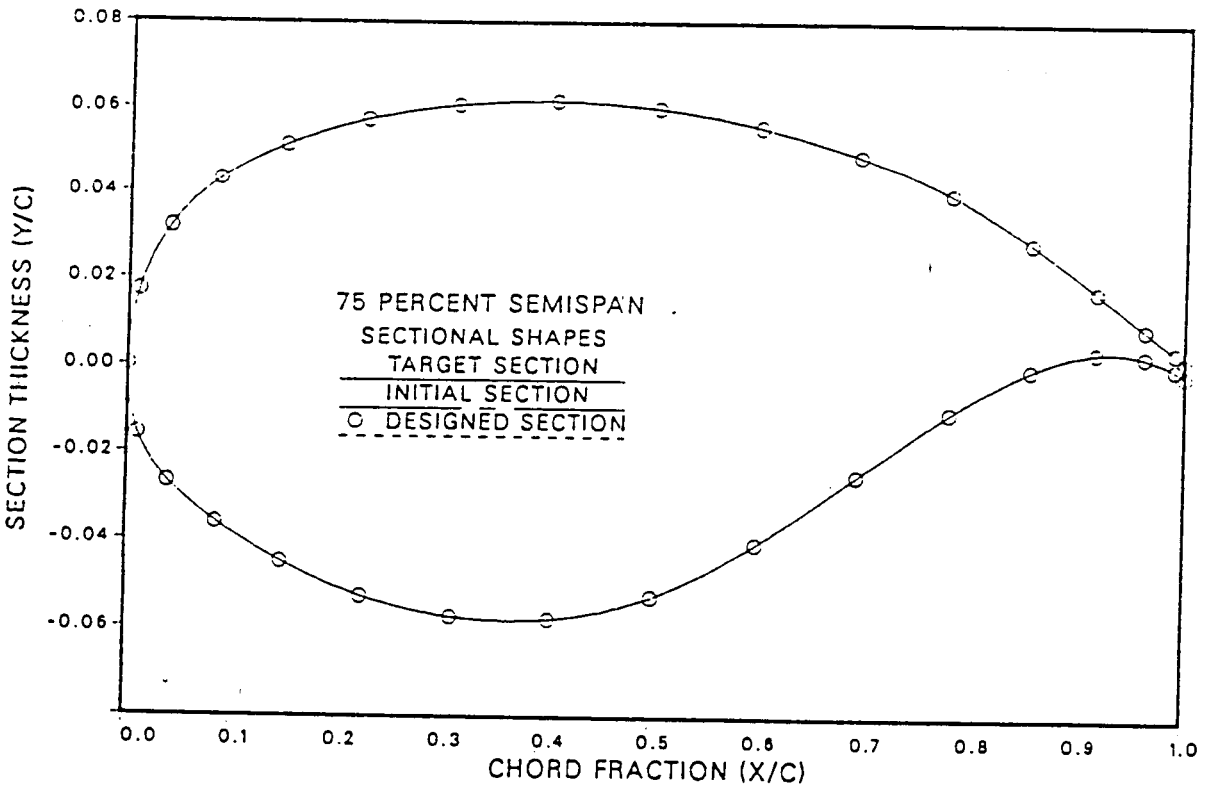
0.08
0.06
0.04
0.02
0.00
-0.02
-0.04
-0.06
SECTION THICKNESS (Y/C)
75 PERCENT SEMISPAN
SECTIONAL SHAPES
TARGET SECTION
INITIAL SECTION
DESIGNED SECTION
0.0
0.1
0.2
0.3
0.4
0.5
0.6
0.7
0.8
0.9
1.0
CHORD FRACTION (X/C)

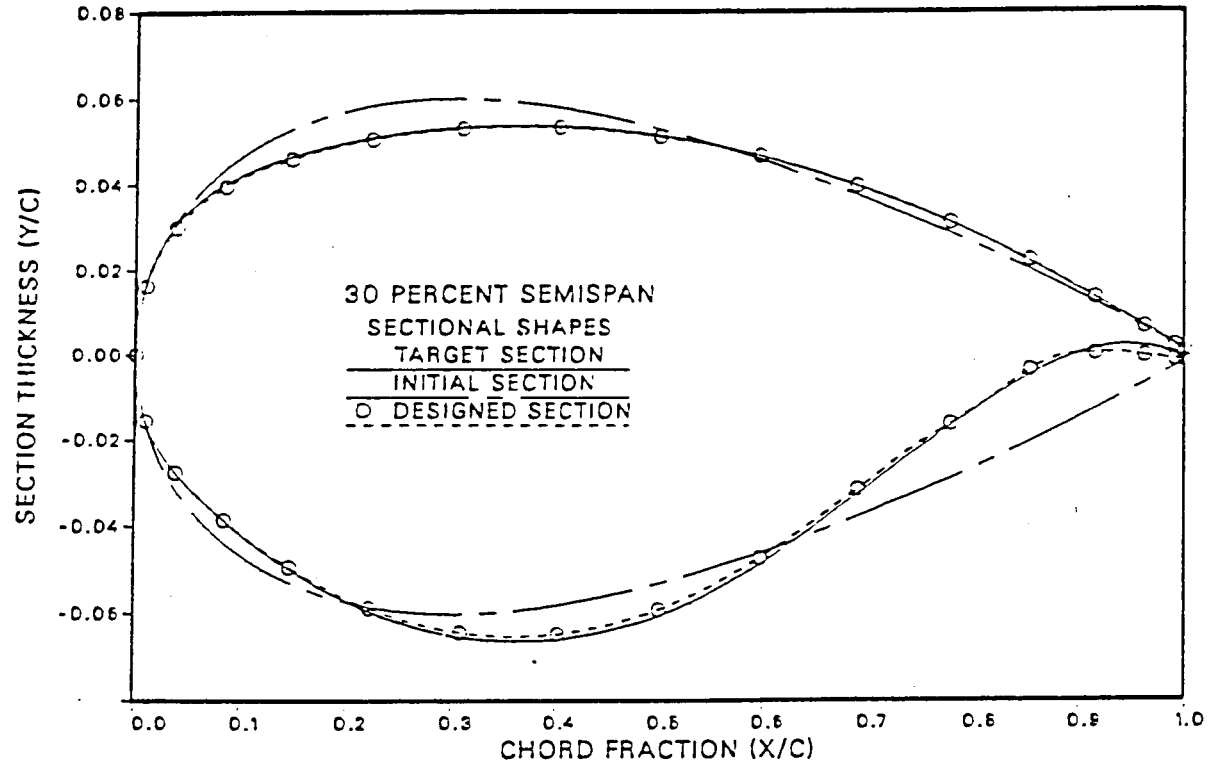

Figure 7a

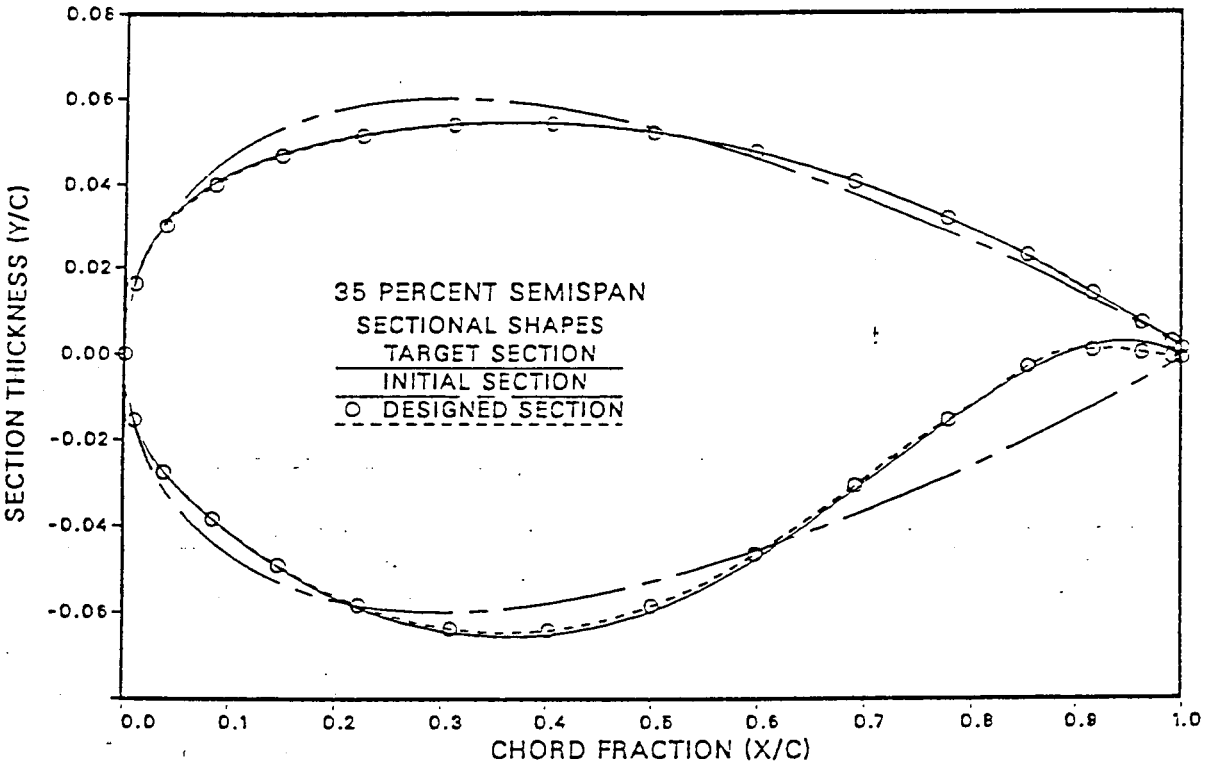

Figure 7a-7d. Airfoil Sections Designed Using Method B

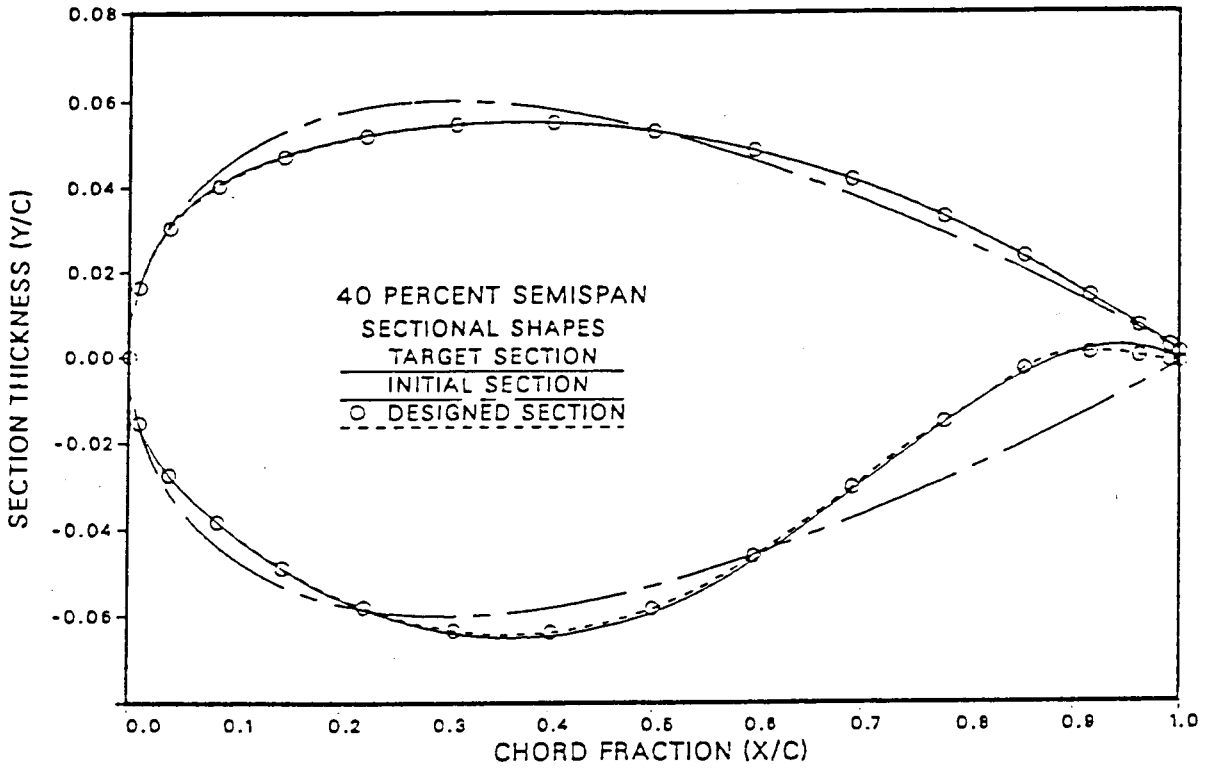
0.08
0.06
0.04
0.02
0.00
-0.02
-0.04
-0.06
SECTION THICKNESS (Y/C)
40 PERCENT SEMISPAN
SECTIONAL SHAPES
TARGET SECTION
INITIAL SECTION
O DESIGNED SECTION
0.0
0.1
0.2
0.3
0.4
0.5
0.6
0.7
0.8
0.9
1.0
CHORD FRACTION (X/C)

Figure 7b

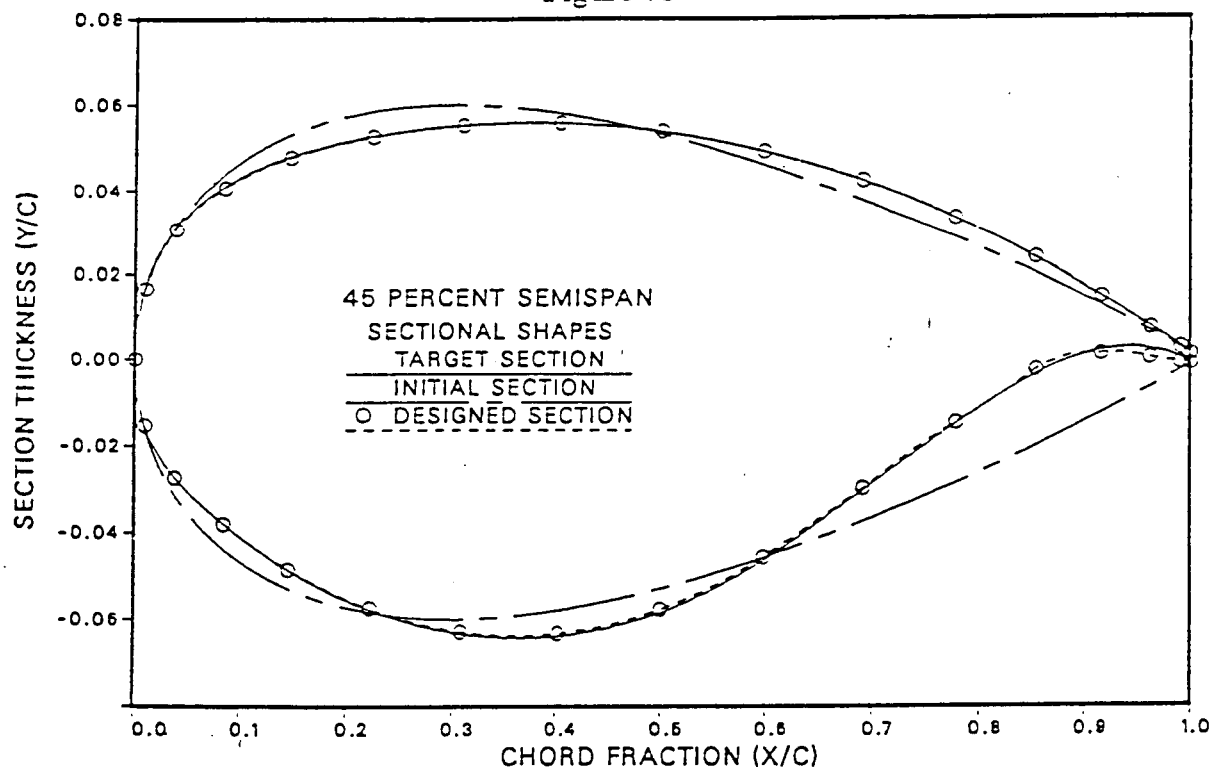
0.08
0.06
0.04
0.02
0.00
-0.02
-0.04
-0.06
SECTION THICKNESS (Y/C)
45 PERCENT SEMISPAN
SECTIONAL SHAPES
TARGET SECTION
INITIAL SECTION
O DESIGNED SECTION
0.0
0.1
0.2
0.3
0.4
0.5
0.6
0.7
0.8
0.9
1.0
CHORD FRACTION (X/C)

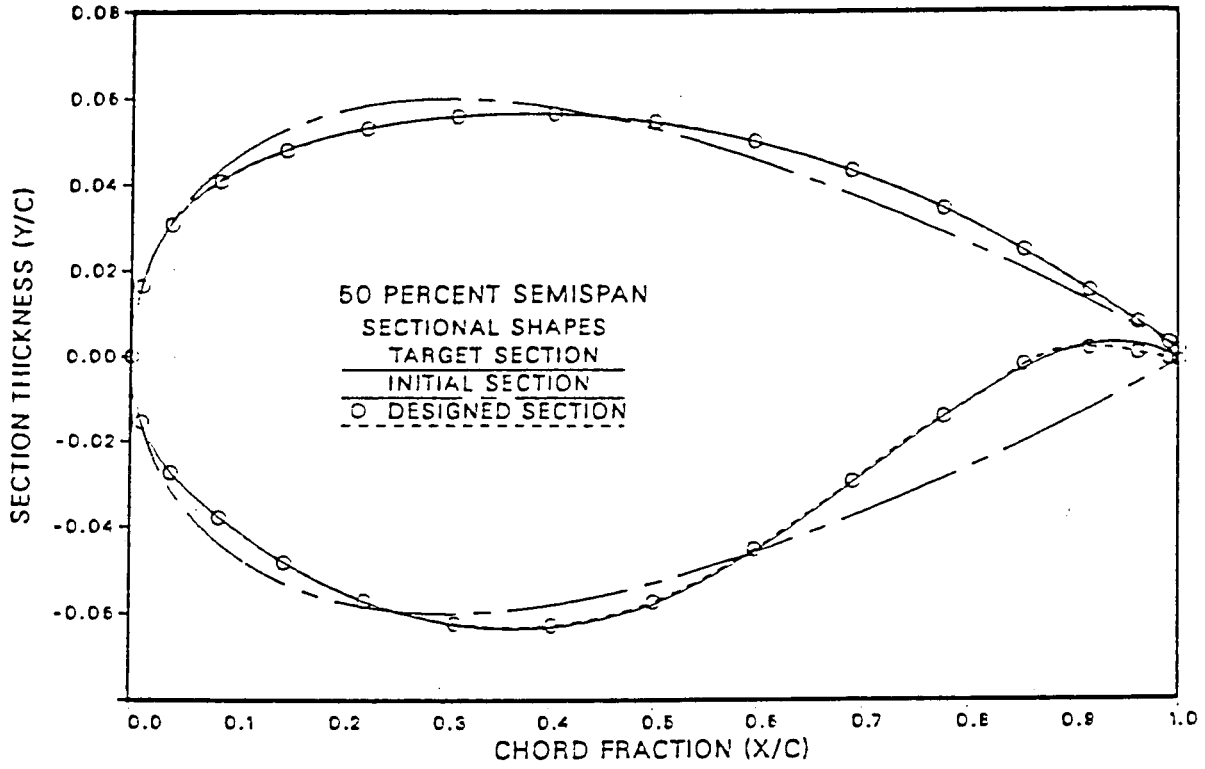
50 PERCENT SEMISPAN
SECTIONAL SHAPES
TARGET SECTION
INITIAL SECTION
DESIGNED SECTION
SECTION THICKNESS (Y/C)
CHORD FRACTION (X/C)
0.08
0.06
0.04
0.02
0.00
-0.02
-0.04
-0.06
0.0
0.1
0.2
0.3
0.4
0.5
0.6
0.7
0.8
0.9
1.0

Figure 7c

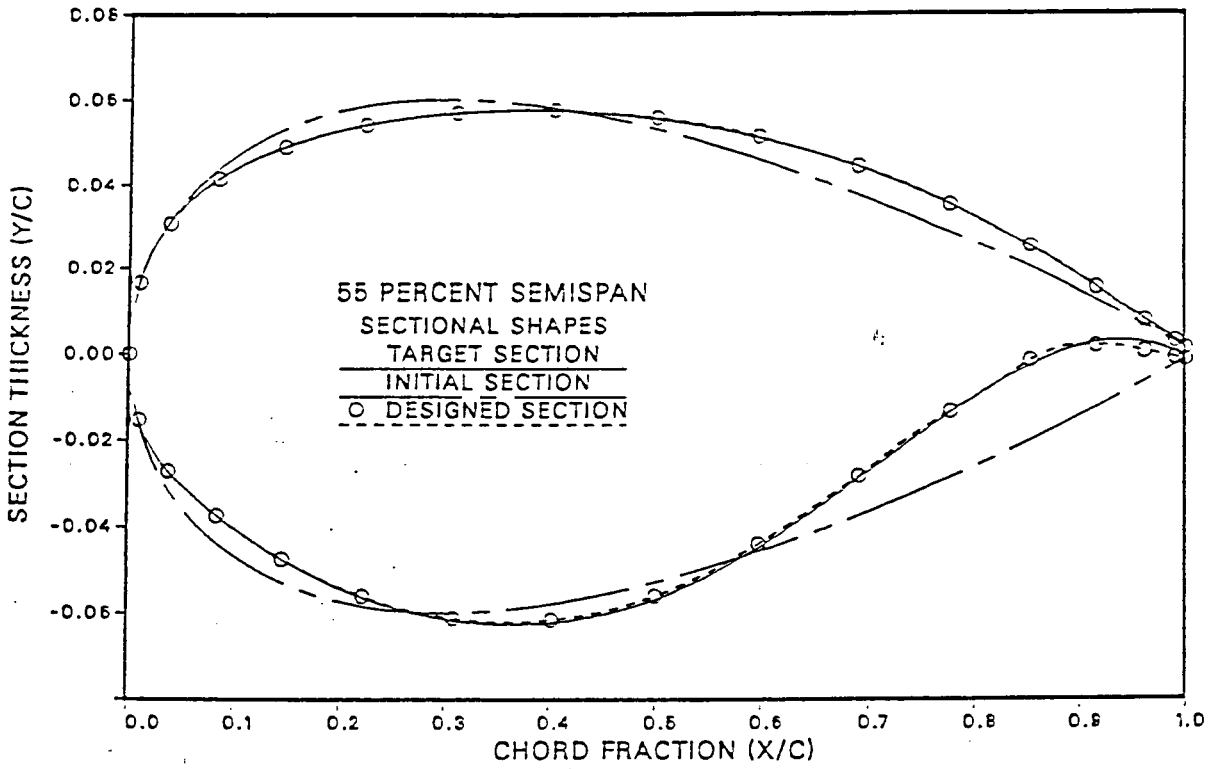
55 PERCENT SEMISPAN
SECTIONAL SHAPES
TARGET SECTION
INITIAL SECTION
DESIGNED SECTION
SECTION THICKNESS (Y/C)
CHORD FRACTION (X/C)
0.08
0.06
0.04
0.02
0.00
-0.02
-0.04
-0.06
0.0
0.1
0.2
0.3
0.4
0.5
0.6
0.7
0.8
0.9
1.0

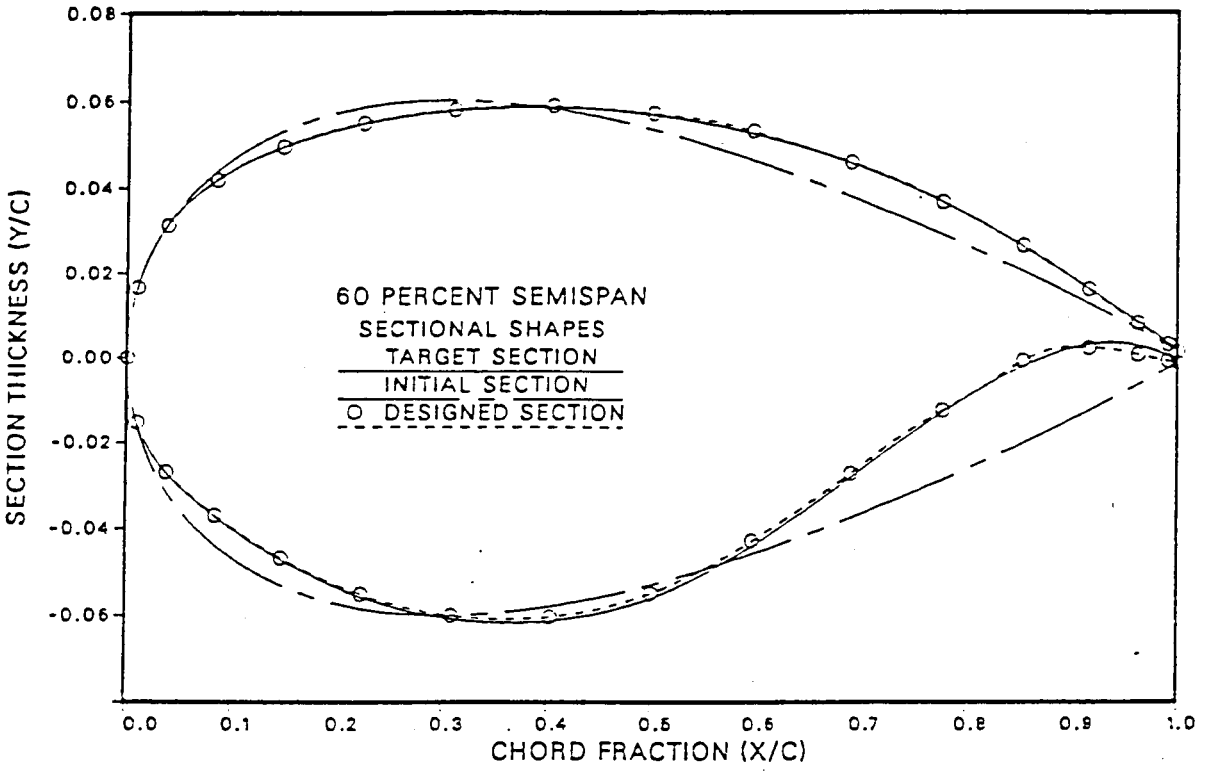
0.08
0.06
0.04
0.02
0.00
-0.02
-0.04
-0.06
SECTION THICKNESS (Y/C)
60 PERCENT SEMISPAN
SECTIONAL SHAPES
TARGET SECTION
INITIAL SECTION
O DESIGNED SECTION
0.0
0.1
0.2
0.3
0.4
0.5
0.6
0.7
0.8
0.9
1.0
CHORD FRACTION (X/C)

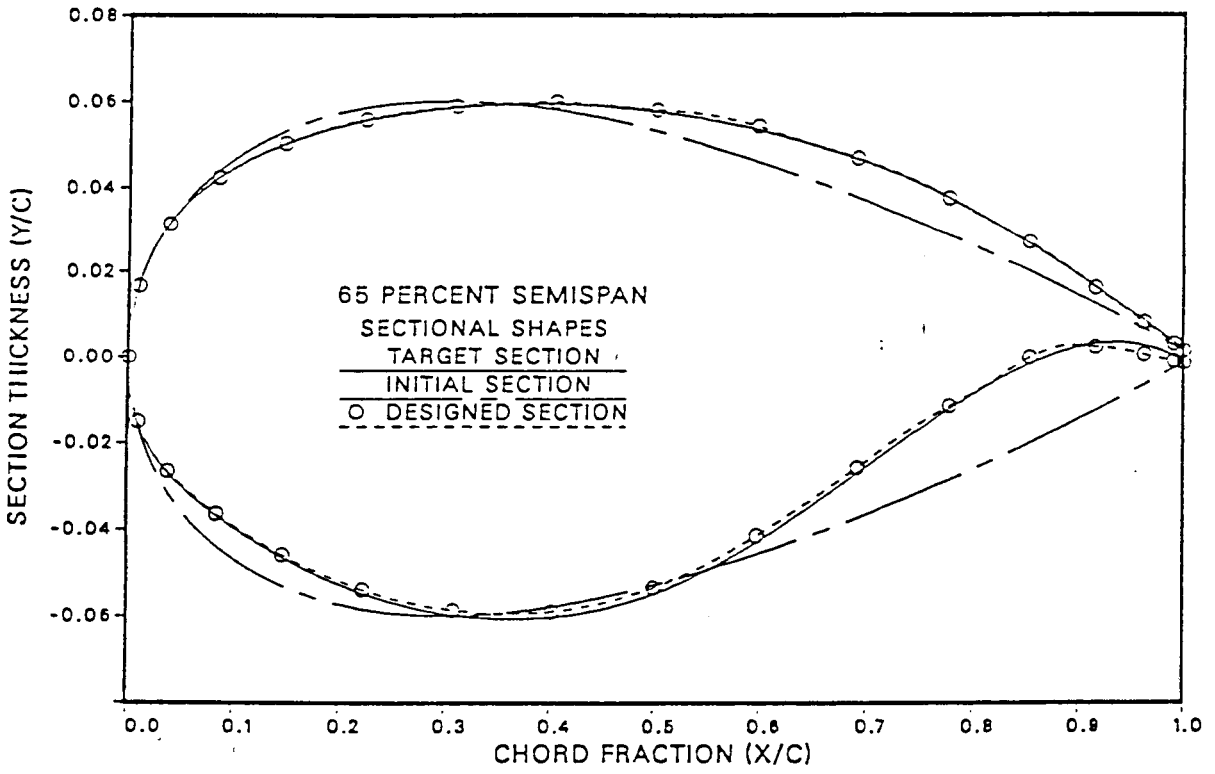
0.08
0.06
0.04
0.02
0.00
-0.02
-0.04
-0.06
SECTION THICKNESS (Y/C)
65 PERCENT SEMISPAN
SECTIONAL SHAPES
TARGET SECTION
INITIAL SECTION
O DESIGNED SECTION
0.0
0.1
0.2
0.3
0.4
0.5
0.6
0.7
0.8
0.9
1.0
CHORD FRACTION (X/C)

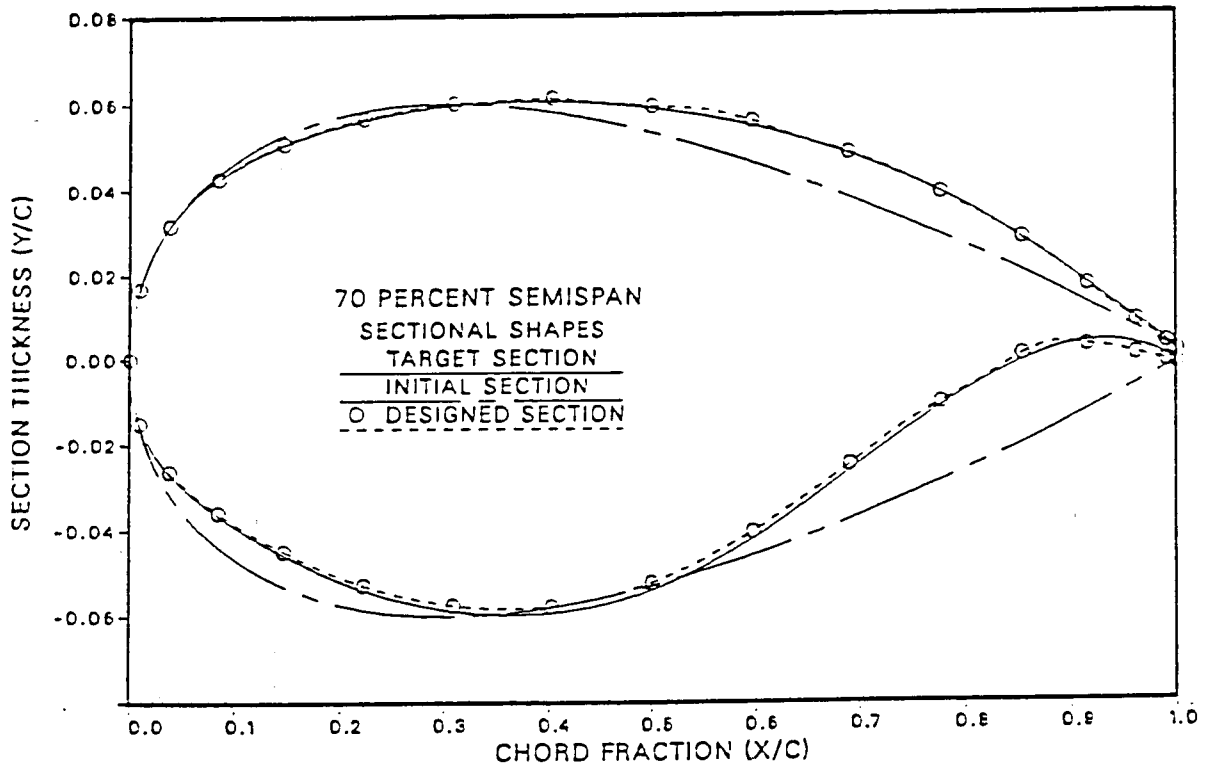
0.08
0.06
0.04
0.02
0.00
-0.02
-0.04
-0.06
SECTION THICKNESS (Y/C)
70 PERCENT SEMISPAN
SECTIONAL SHAPES
TARGET SECTION
INITIAL SECTION
O DESIGNED SECTION
0.0
0.1
0.2
0.3
0.4
0.5
0.6
0.7
0.8
0.9
1.0
CHORD FRACTION (X/C)

Figure 7d

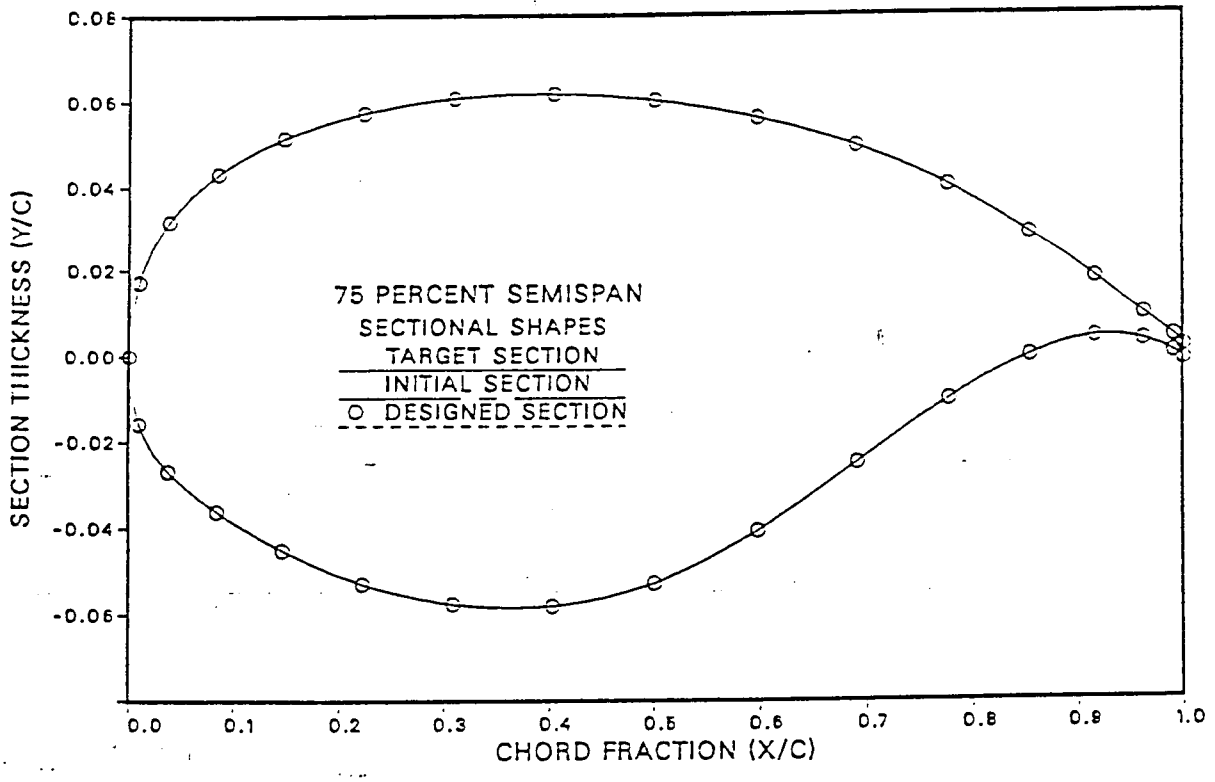
0.08
0.06
0.04
0.02
0.00
-0.02
-0.04
-0.06
SECTION THICKNESS (Y/C)
75 PERCENT SEMISPAN
SECTIONAL SHAPES
TARGET SECTION
INITIAL SECTION
O DESIGNED SECTION
0.0
0.1
0.2
0.3
0.4
0.5
0.6
0.7
0.8
0.9
1.0
CHORD FRACTION (X/C)

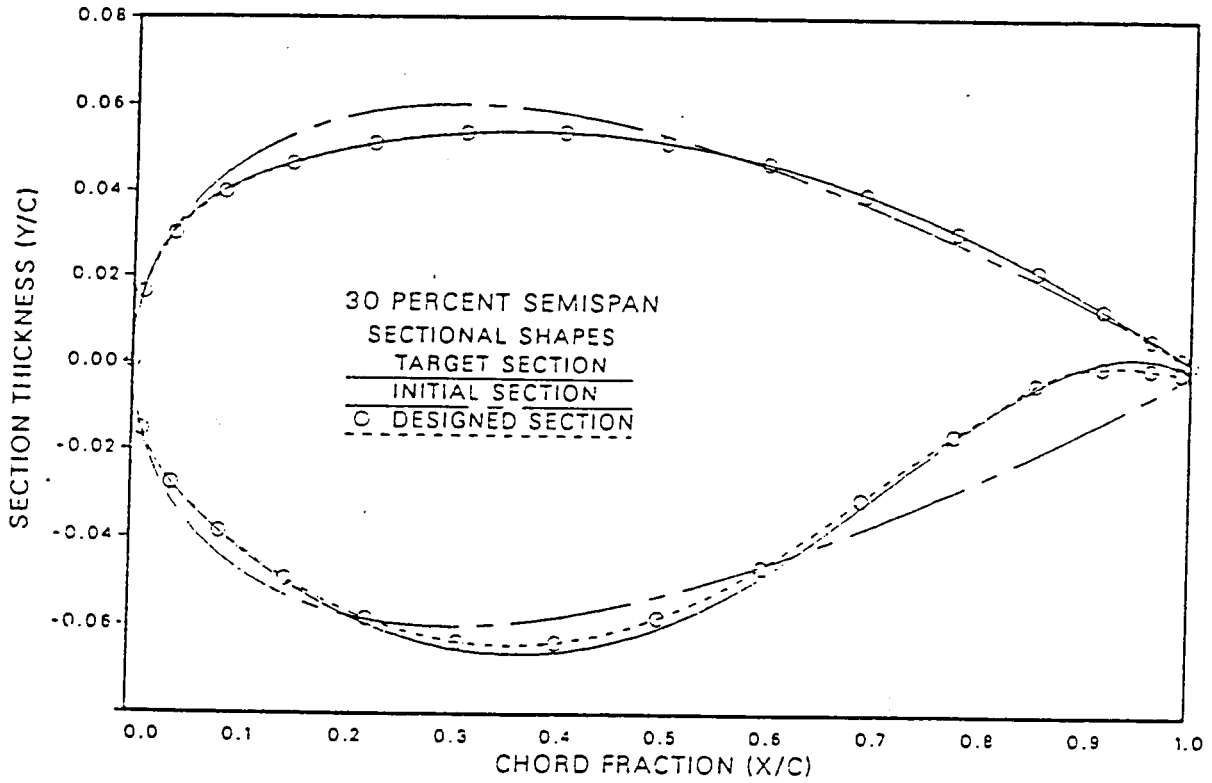
0.08
0.06
0.04
0.02
0.00
-0.02
-0.04
-0.06
SECTION THICKNESS (Y/C)
30 PERCENT SEMISPAN
SECTIONAL SHAPES
TARGET SECTION
INITIAL SECTION
DESIGNED SECTION
0.0
0.1
0.2
0.3
0.4
0.5
0.6
0.7
0.8
0.9
1.0
CHORD FRACTION (X/C)

Figure 8a

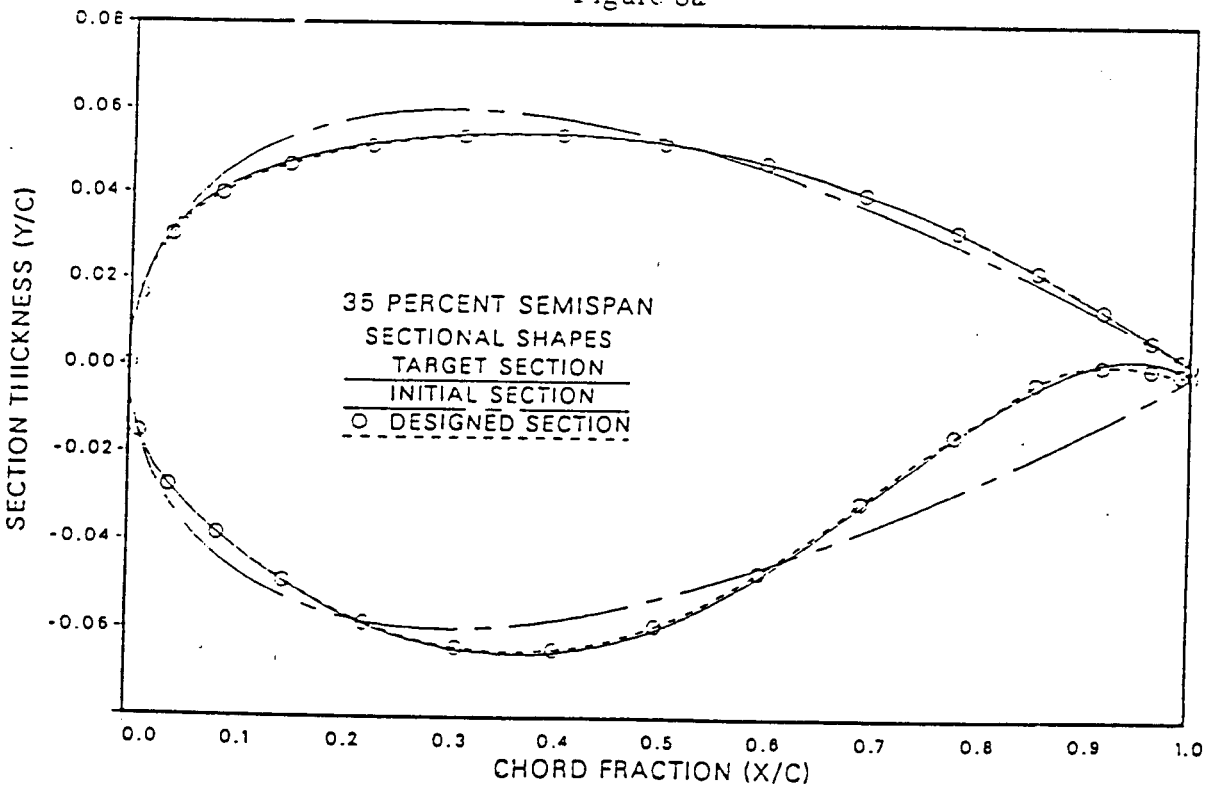
0.08
0.06
0.04
0.02
0.00
-0.02
-0.04
-0.06
SECTION THICKNESS (Y/C)
35 PERCENT SEMISPAN
SECTIONAL SHAPES
TARGET SECTION
INITIAL SECTION
DESIGNED SECTION
0.0
0.1
0.2
0.3
0.4
0.5
0.6
0.7
0.8
0.9
1.0
CHORD FRACTION (X/C)

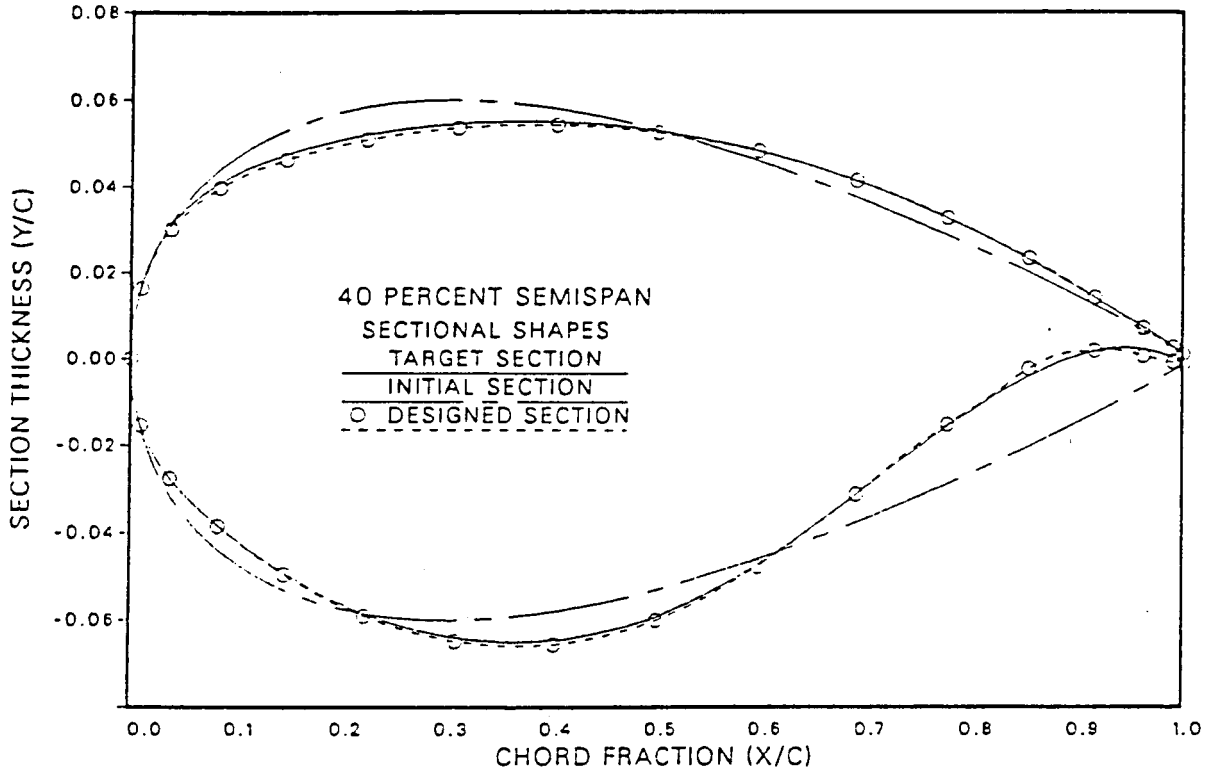
0.08
0.06
0.04
0.02
0.00
-0.02
-0.04
-0.06
SECTION THICKNESS (Y/C)
40 PERCENT SEMISPAN
SECTIONAL SHAPES
TARGET SECTION
INITIAL SECTION
DESIGNED SECTION
0.0
0.1
0.2
0.3
0.4
0.5
0.6
0.7
0.8
0.9
1.0
CHORD FRACTION (X/C)

Figure 8b

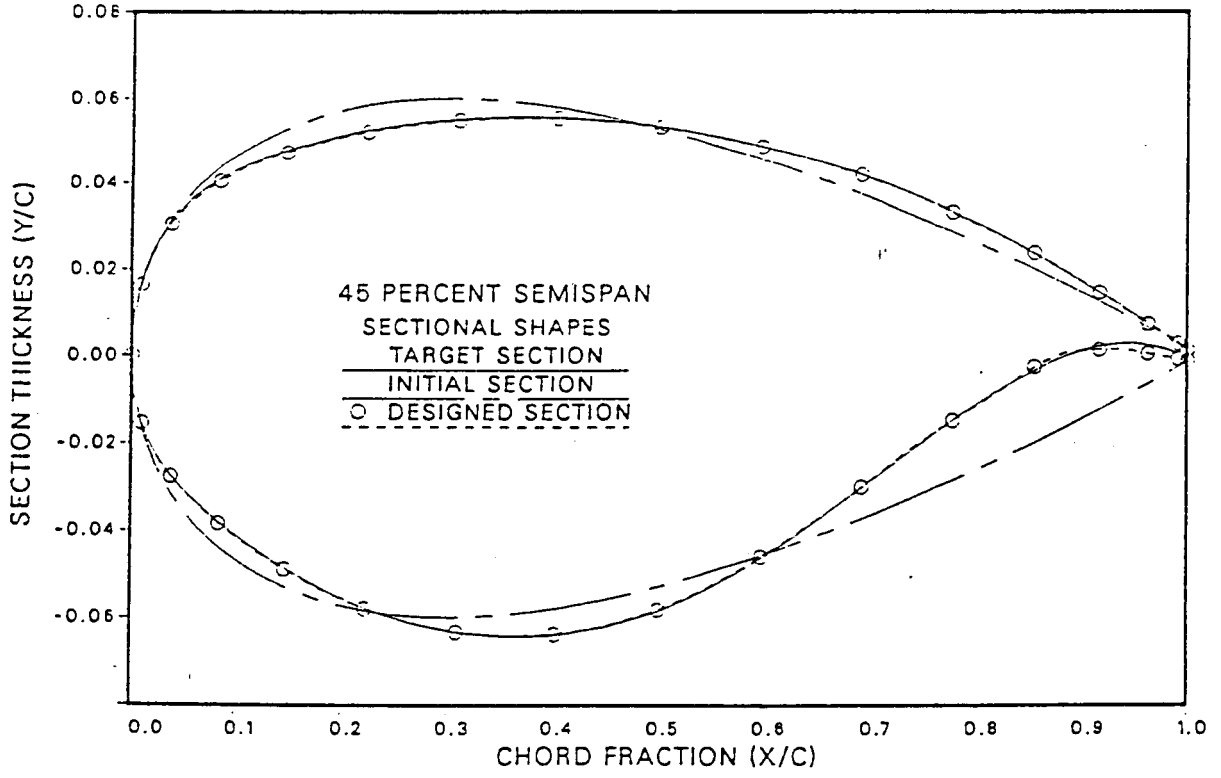
0.08
0.06
0.04
0.02
0.00
-0.02
-0.04
-0.06
SECTION THICKNESS (Y/C)
45 PERCENT SEMISPAN
SECTIONAL SHAPES
TARGET SECTION
INITIAL SECTION
DESIGNED SECTION
0.0
0.1
0.2
0.3
0.4
0.5
0.6
0.7
0.8
0.9
1.0
CHORD FRACTION (X/C)

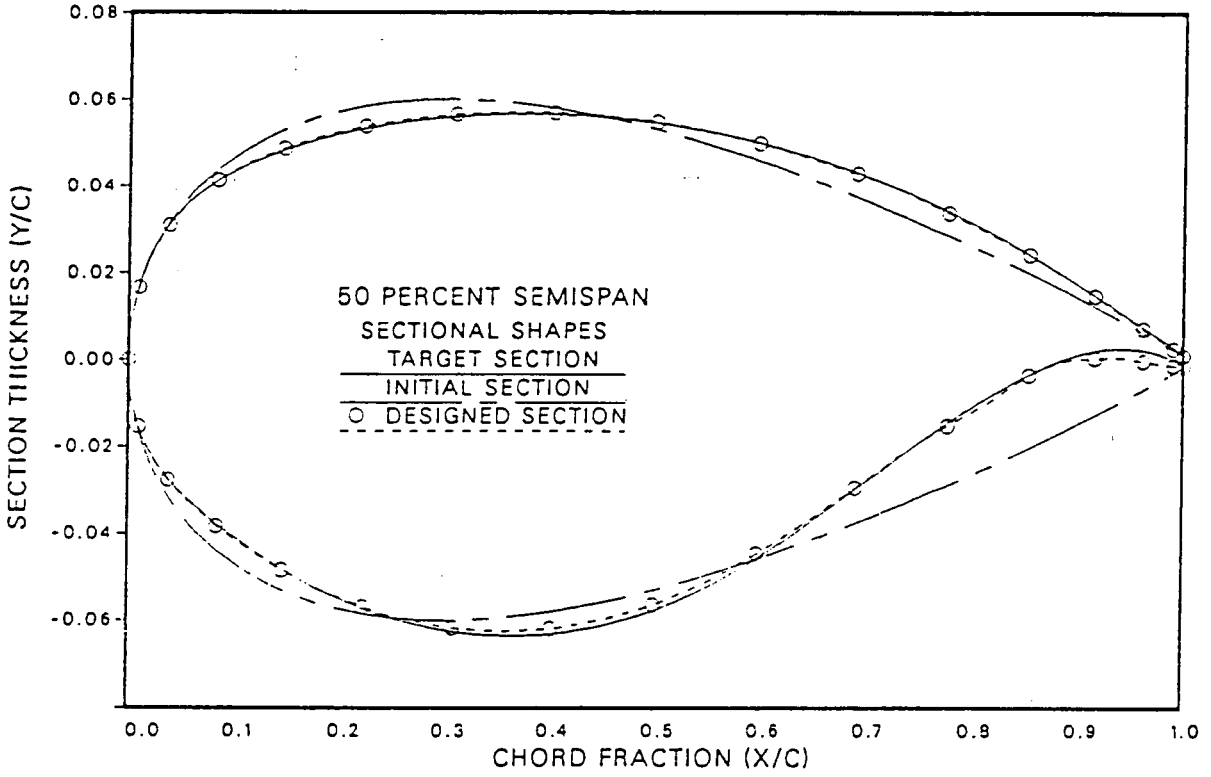
0.08
0.06
0.04
0.02
0.00
-0.02
-0.04
-0.06
SECTION THICKNESS (Y/C)
50 PERCENT SEMISPAN
SECTIONAL SHAPES
TARGET SECTION
INITIAL SECTION
DESIGNED SECTION
0.0
0.1
0.2
0.3
0.4
0.5
0.6
0.7
0.8
0.9
1.0
CHORD FRACTION (X/C)

Figure 8c

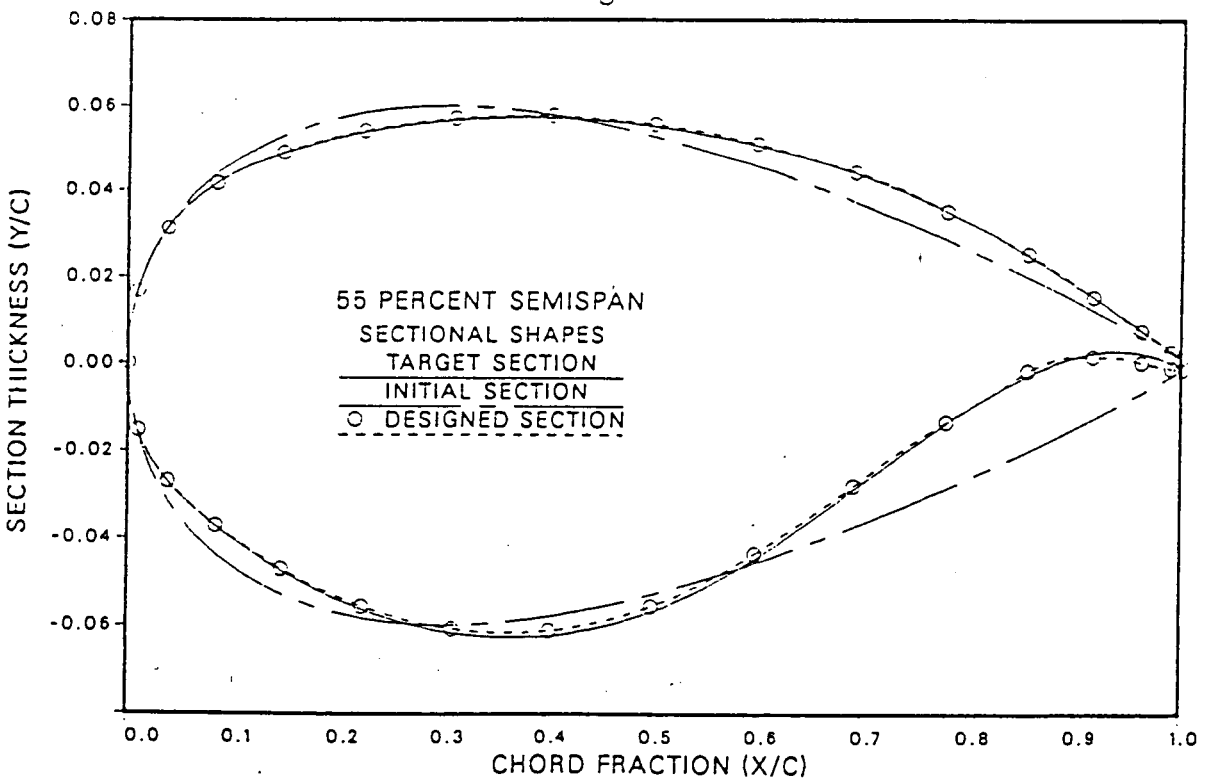
0.08
0.06
0.04
0.02
0.00
-0.02
-0.04
-0.06
SECTION THICKNESS (Y/C)
55 PERCENT SEMISPAN
SECTIONAL SHAPES
TARGET SECTION
INITIAL SECTION
DESIGNED SECTION
0.0
0.1
0.2
0.3
0.4
0.5
0.6
0.7
0.8
0.9
1.0
CHORD FRACTION (X/C)

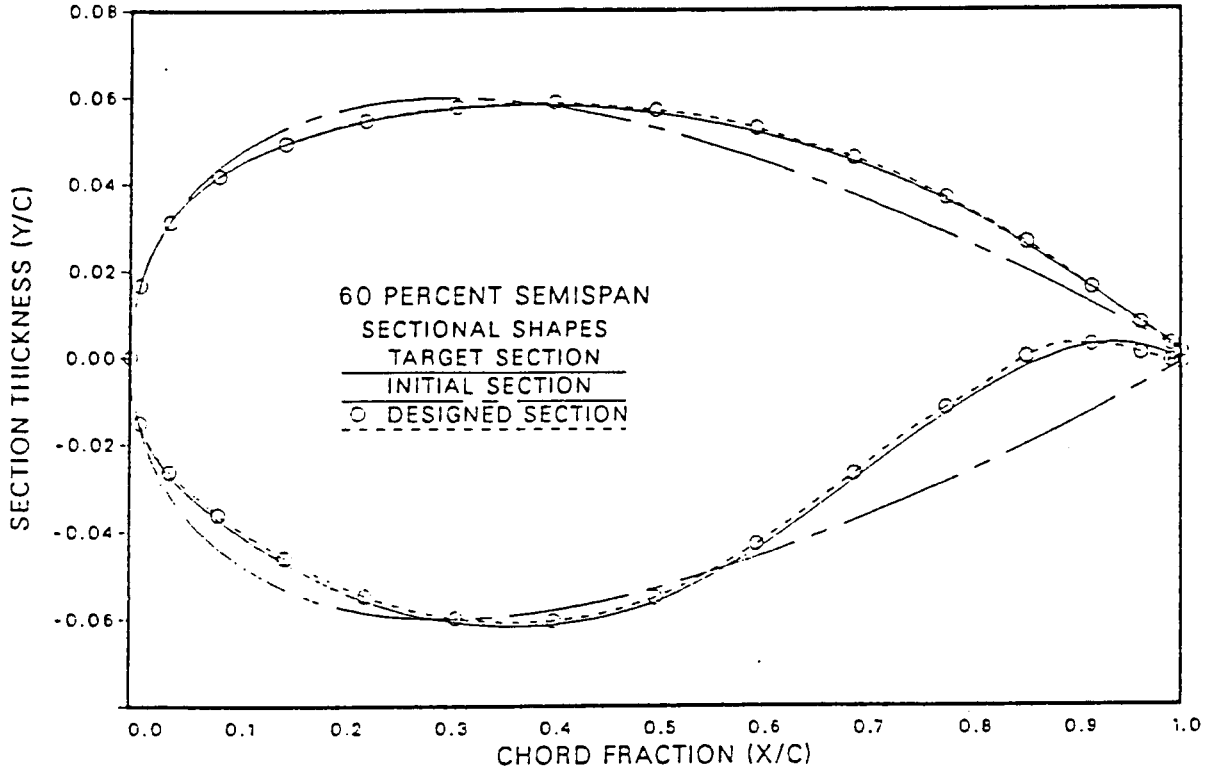
0.08
0.06
0.04
0.02
0.00
-0.02
-0.04
-0.06
SECTION THICKNESS (Y/C)
60 PERCENT SEMISPAN
SECTIONAL SHAPES
TARGET SECTION
INITIAL SECTION
DESIGNED SECTION
0.0
0.1
0.2
0.3
0.4
0.5
0.6
0.7
0.8
0.9
1.0
CHORD FRACTION (X/C)

Figure 8d

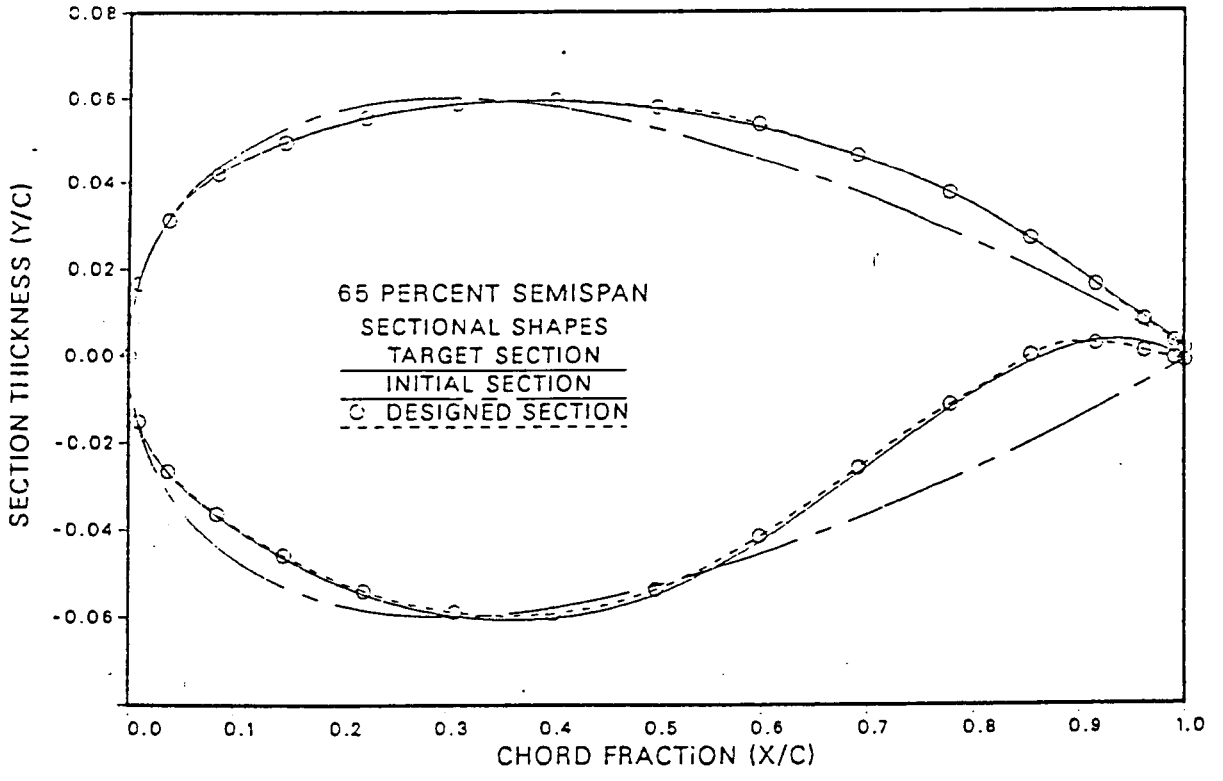
0.08
0.06
0.04
0.02
0.00
-0.02
-0.04
-0.06
SECTION THICKNESS (Y/C)
65 PERCENT SEMISPAN
SECTIONAL SHAPES
TARGET SECTION
INITIAL SECTION
DESIGNED SECTION
0.0
0.1
0.2
0.3
0.4
0.5
0.6
0.7
0.8
0.9
1.0
CHORD FRACTION (X/C)

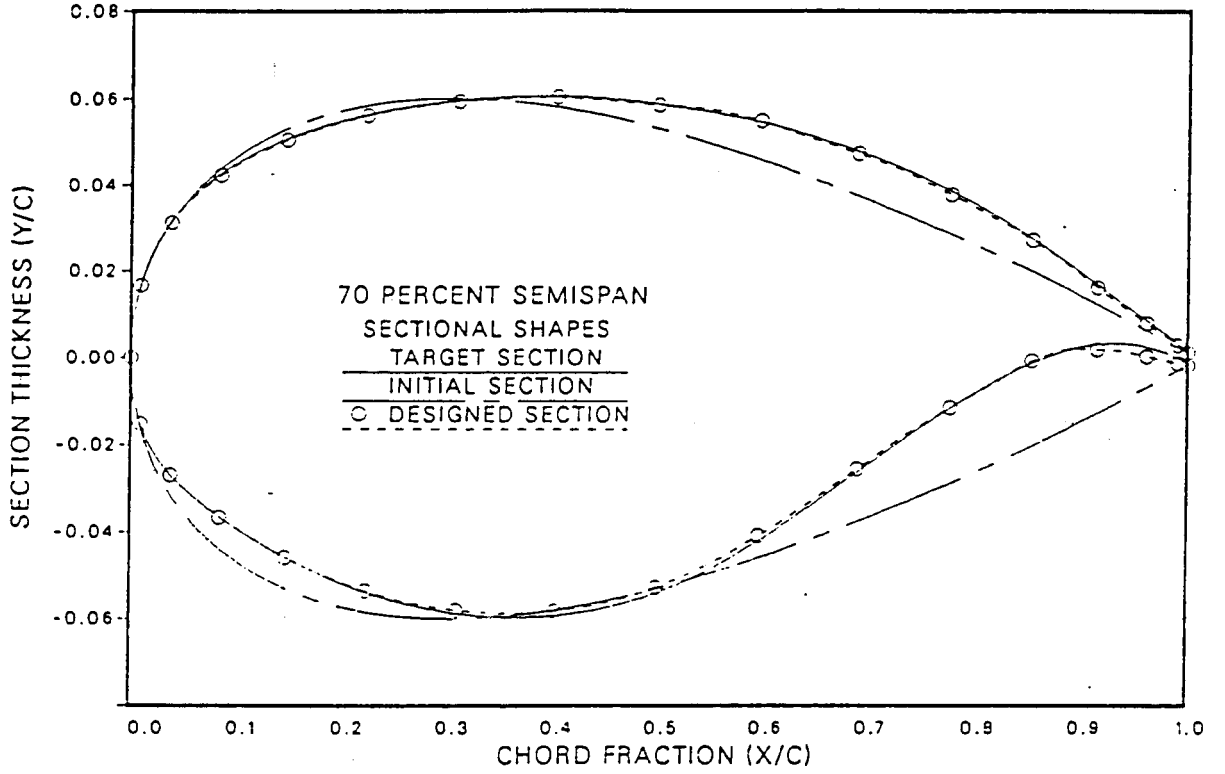
0.08
0.06
0.04
0.02
0.00
-0.02
-0.04
-0.06
SECTION THICKNESS (Y/C)
70 PERCENT SEMISPAN
SECTIONAL SHAPES
TARGET SECTION
INITIAL SECTION
DESIGNED SECTION
0.0
0.1
0.2
0.3
0.4
0.5
0.6
0.7
0.8
0.9
1.0
CHORD FRACTION (X/C)

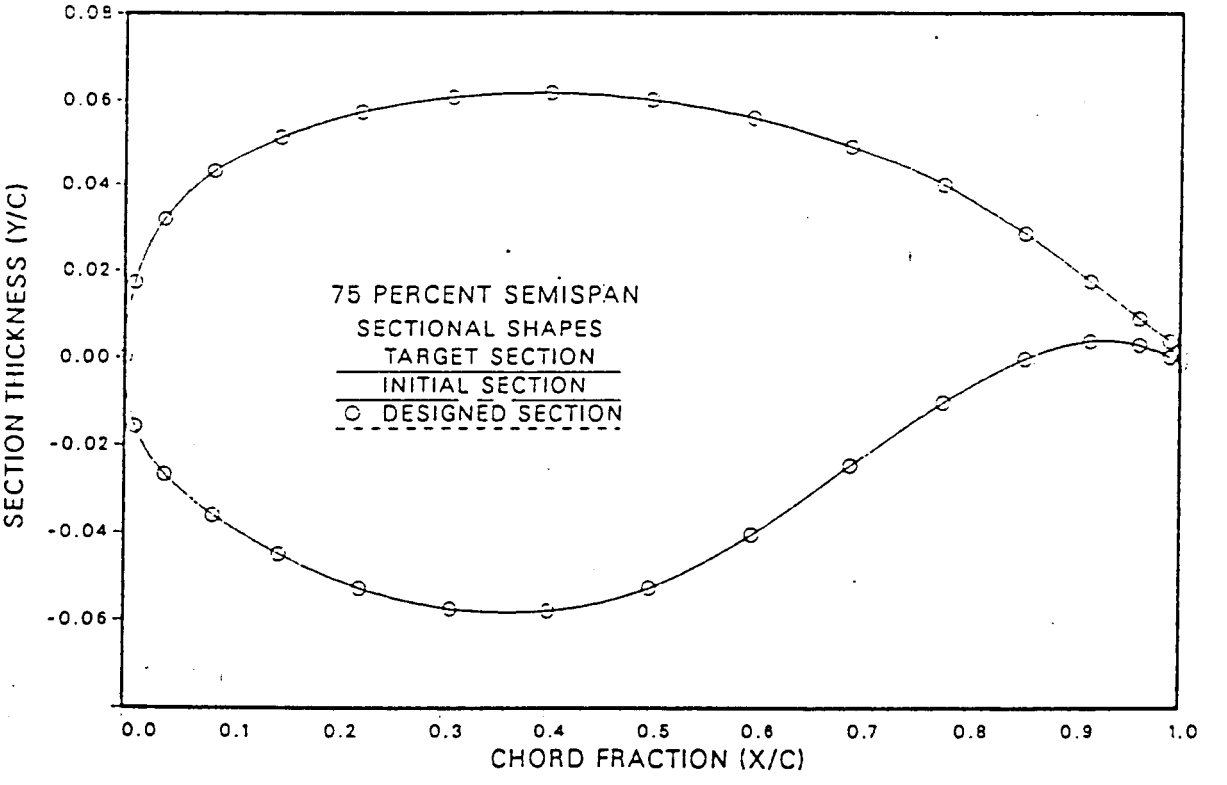
0.08
0.06
0.04
0.02
0.00
-0.02
-0.04
-0.06
SECTION THICKNESS (Y/C)
75 PERCENT SEMISPAN
SECTIONAL SHAPES
TARGET SECTION
INITIAL SECTION
DESIGNED SECTION
0.0
0.1
0.2
0.3
0.4
0.5
0.6
0.7
0.8
0.9
1.0
CHORD FRACTION (X/C)

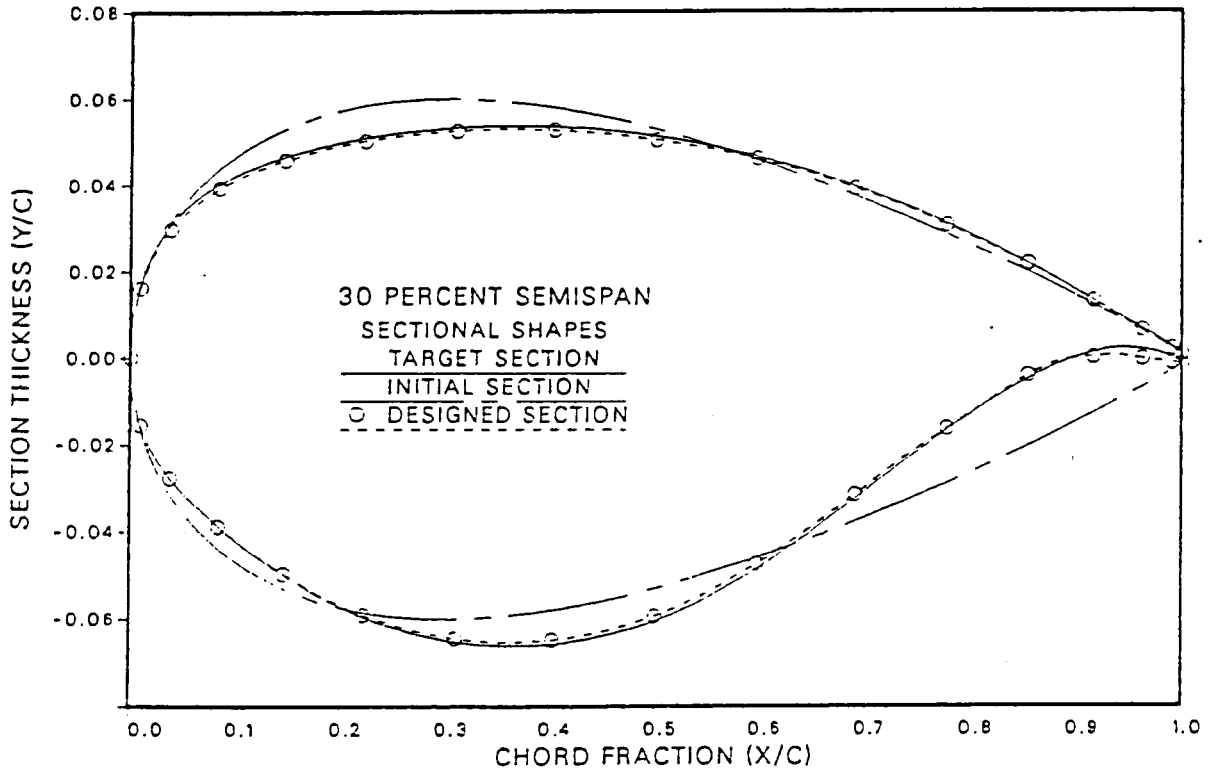

Figure 9a

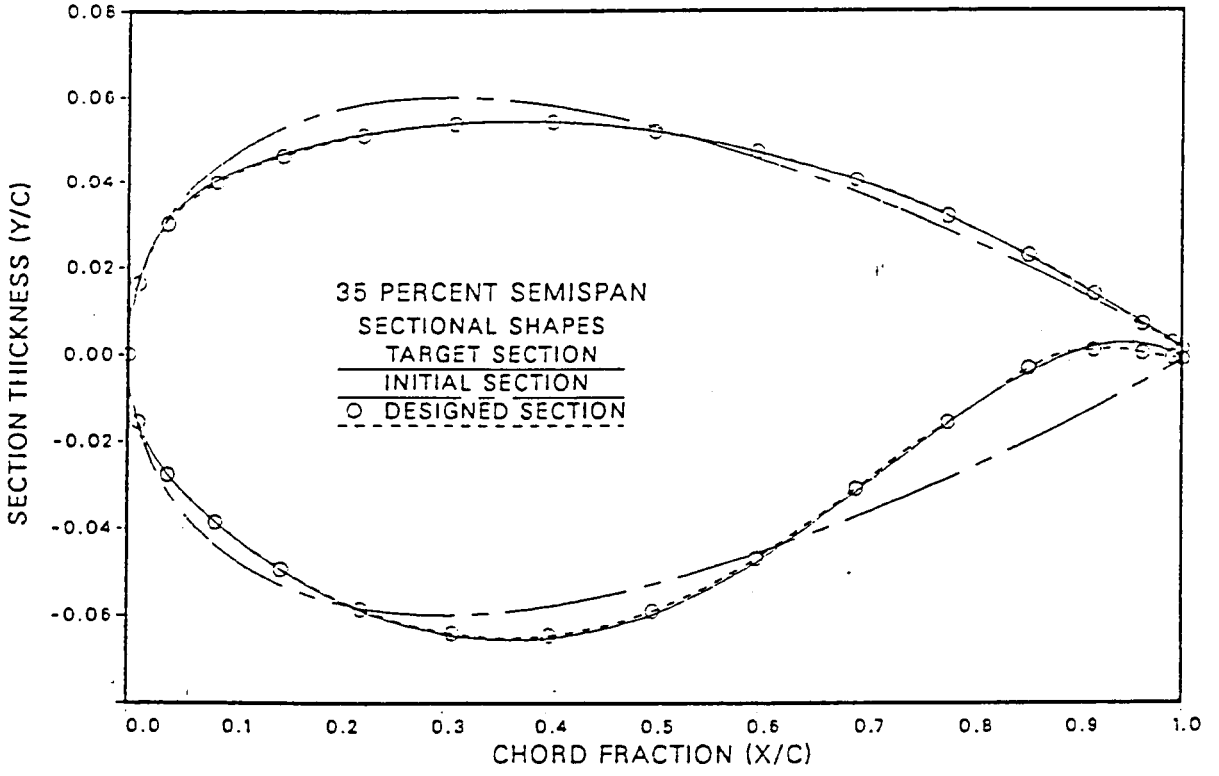

Figure 9a-9d. Airfoil Sections Designed Using Method D

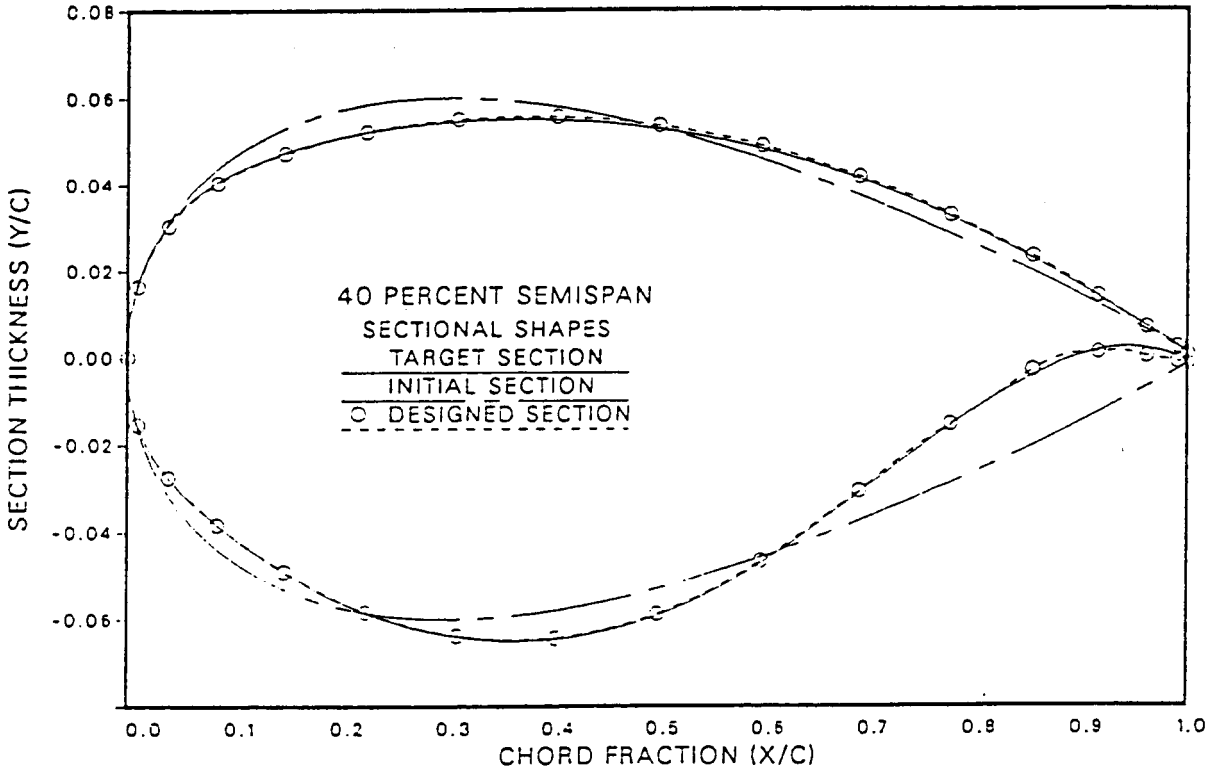
40 PERCENT SEMISPAN
SECTIONAL SHAPES
TARGET SECTION
INITIAL SECTION
DESIGNED SECTION
SECTION THICKNESS (Y/C)
CHORD FRACTION (X/C)
0.08
0.06
0.04
0.02
0.00
-0.02
-0.04
-0.06
0.0
0.1
0.2
0.3
0.4
0.5
0.6
0.7
0.8
0.9
1.0

Figure 9b

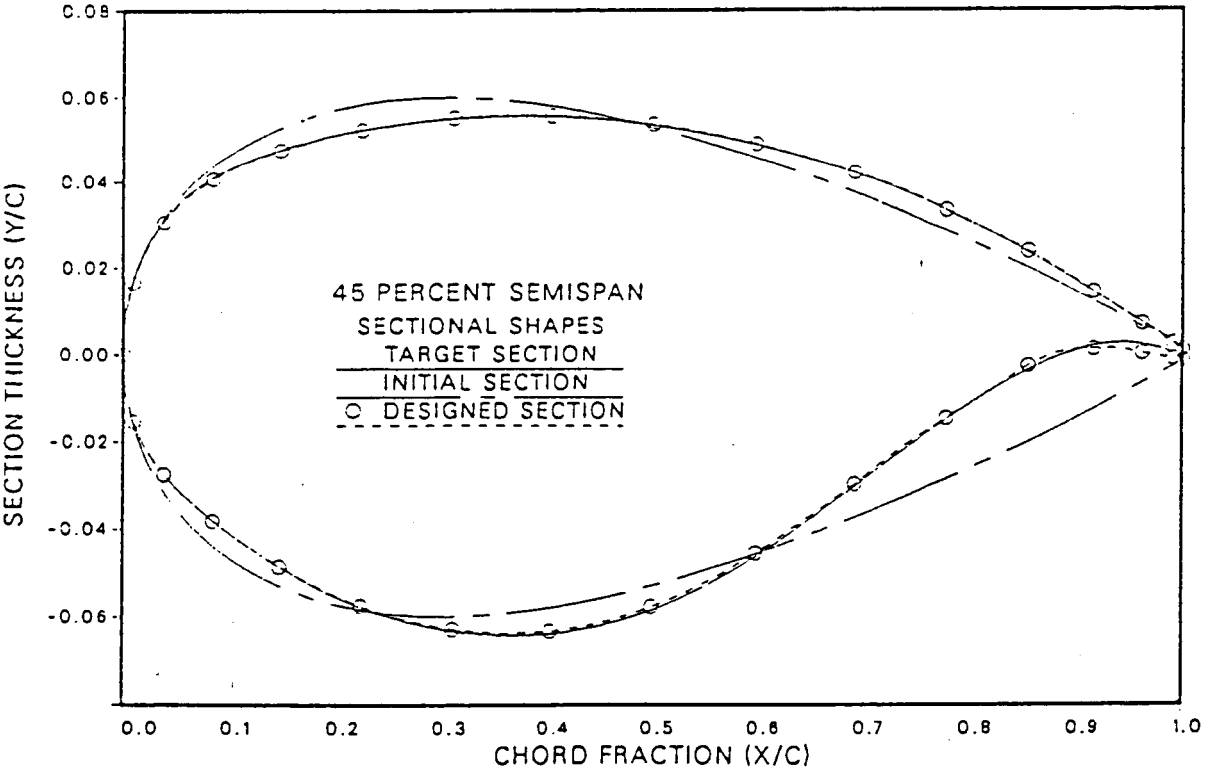
45 PERCENT SEMISPAN
SECTIONAL SHAPES
TARGET SECTION
INITIAL SECTION
DESIGNED SECTION
SECTION THICKNESS (Y/C)
CHORD FRACTION (X/C)
0.08
0.06
0.04
0.02
0.00
-0.02
-0.04
-0.06
0.0
0.1
0.2
0.3
0.4
0.5
0.6
0.7
0.8
0.9
1.0

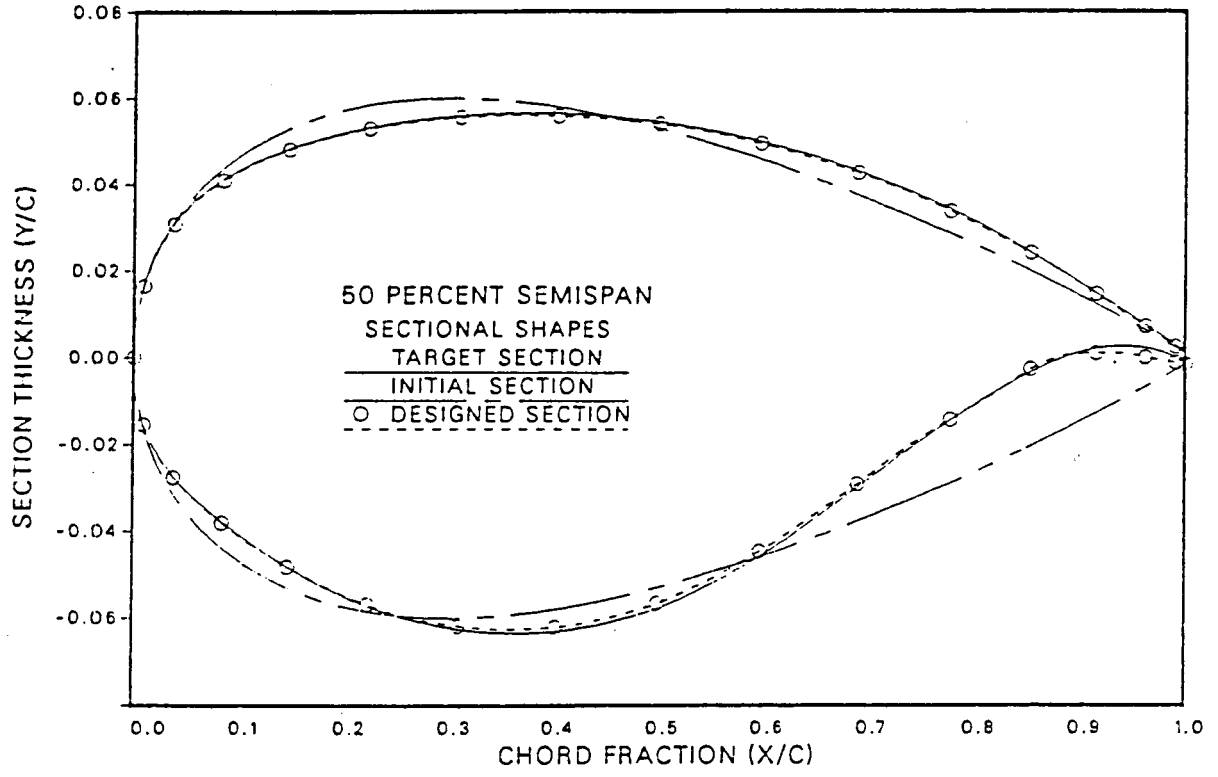
0.08
0.06
0.04
0.02
0.00
-0.02
-0.04
-0.06
SECTION THICKNESS (Y/C)
50 PERCENT SEMISPAN
SECTIONAL SHAPES
TARGET SECTION
INITIAL SECTION
O DESIGNED SECTION
0.0
0.1
0.2
0.3
0.4
0.5
0.6
0.7
0.8
0.9
1.0
CHORD FRACTION (X/C)

Figure 9c

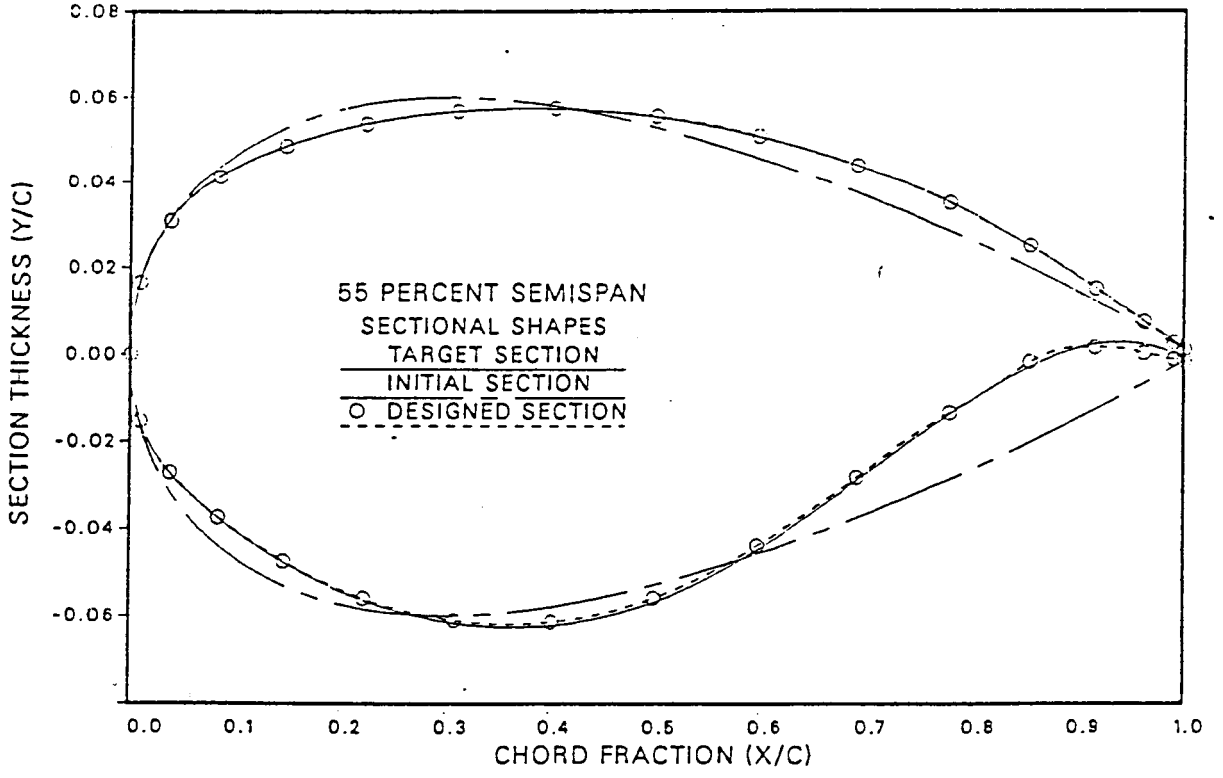
0.08
0.06
0.04
0.02
0.00
-0.02
-0.04
-0.06
SECTION THICKNESS (Y/C)
55 PERCENT SEMISPAN
SECTIONAL SHAPES
TARGET SECTION
INITIAL SECTION
O DESIGNED SECTION
0.0
0.1
0.2
0.3
0.4
0.5
0.6
0.7
0.8
0.9
1.0
CHORD FRACTION (X/C)

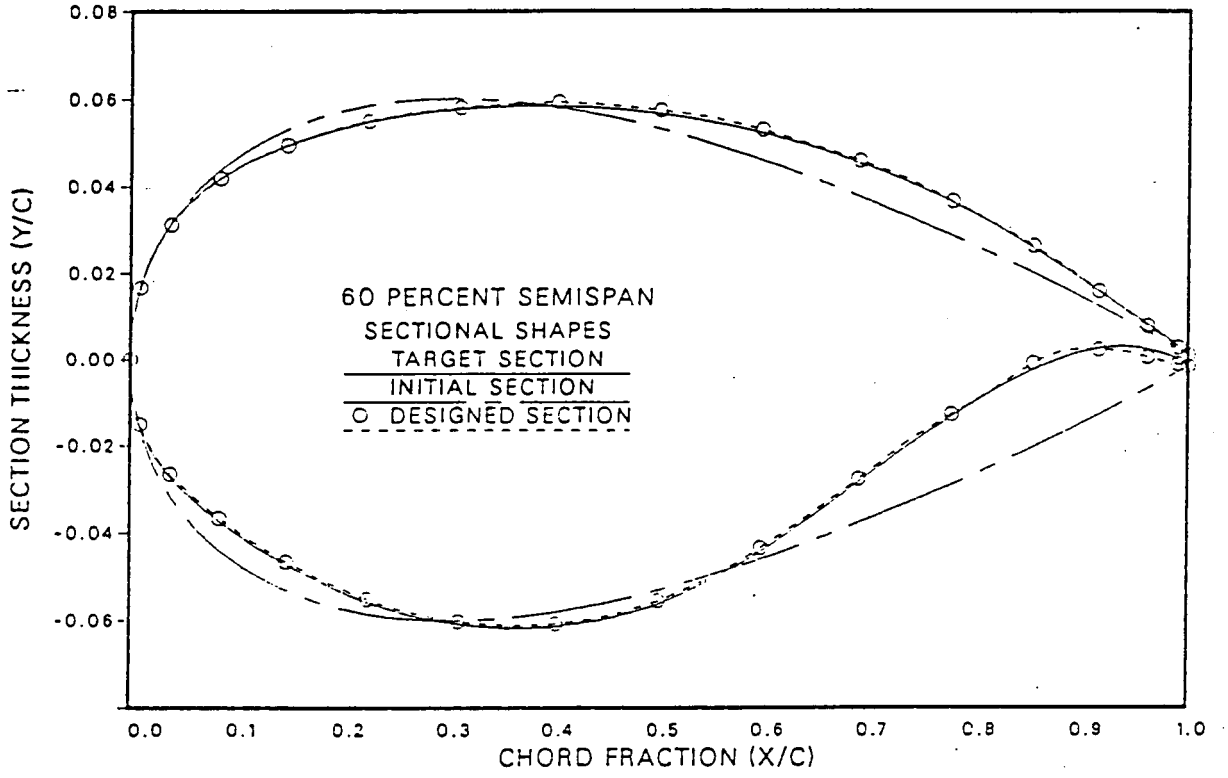
0.08
0.06
0.04
0.02
0.00
-0.02
-0.04
-0.06
SECTION THICKNESS (Y/C)
60 PERCENT SEMISPAN
SECTIONAL SHAPES
TARGET SECTION
INITIAL SECTION
DESIGNED SECTION
0.0
0.1
0.2
0.3
0.4
0.5
0.6
0.7
0.8
0.9
1.0
CHORD FRACTION (X/C)

Figure 9d

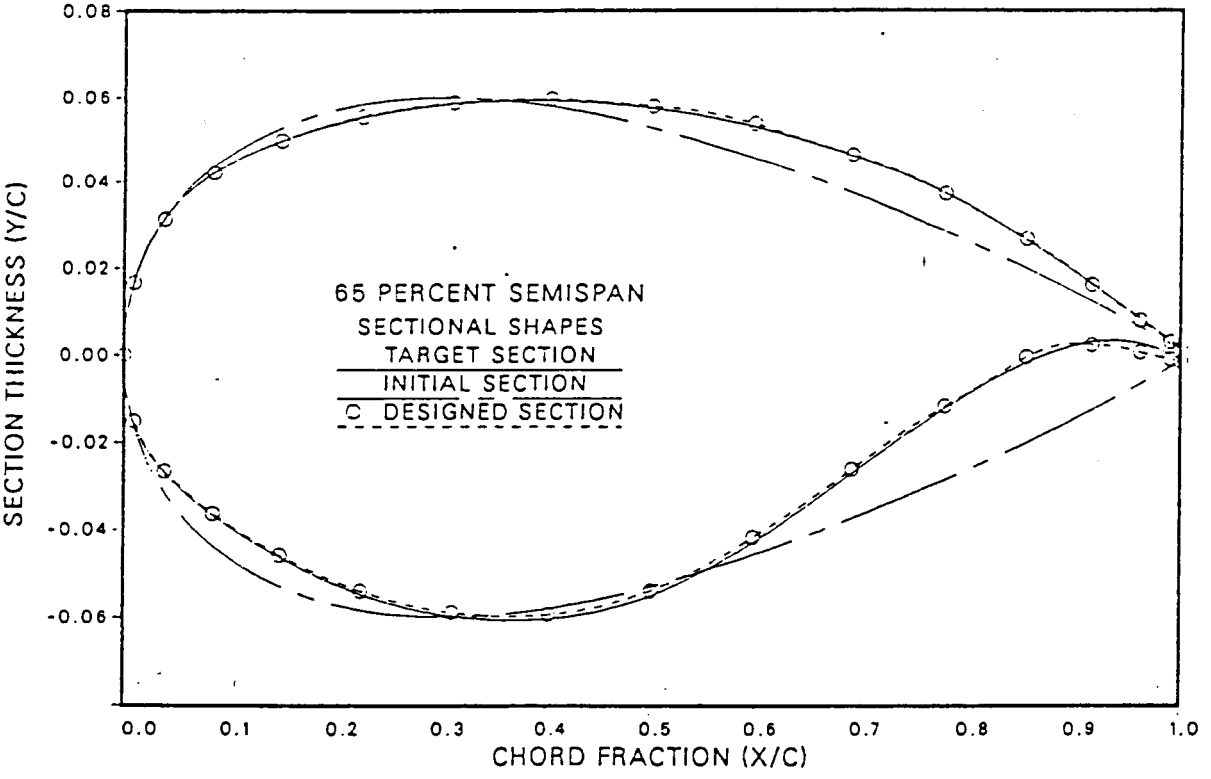
0.08
0.06
0.04
0.02
0.00
-0.02
-0.04
-0.06
SECTION THICKNESS (Y/C)
65 PERCENT SEMISPAN
SECTIONAL SHAPES
TARGET SECTION
INITIAL SECTION
DESIGNED SECTION
0.0
0.1
0.2
0.3
0.4
0.5
0.6
0.7
0.8
0.9
1.0
CHORD FRACTION (X/C)

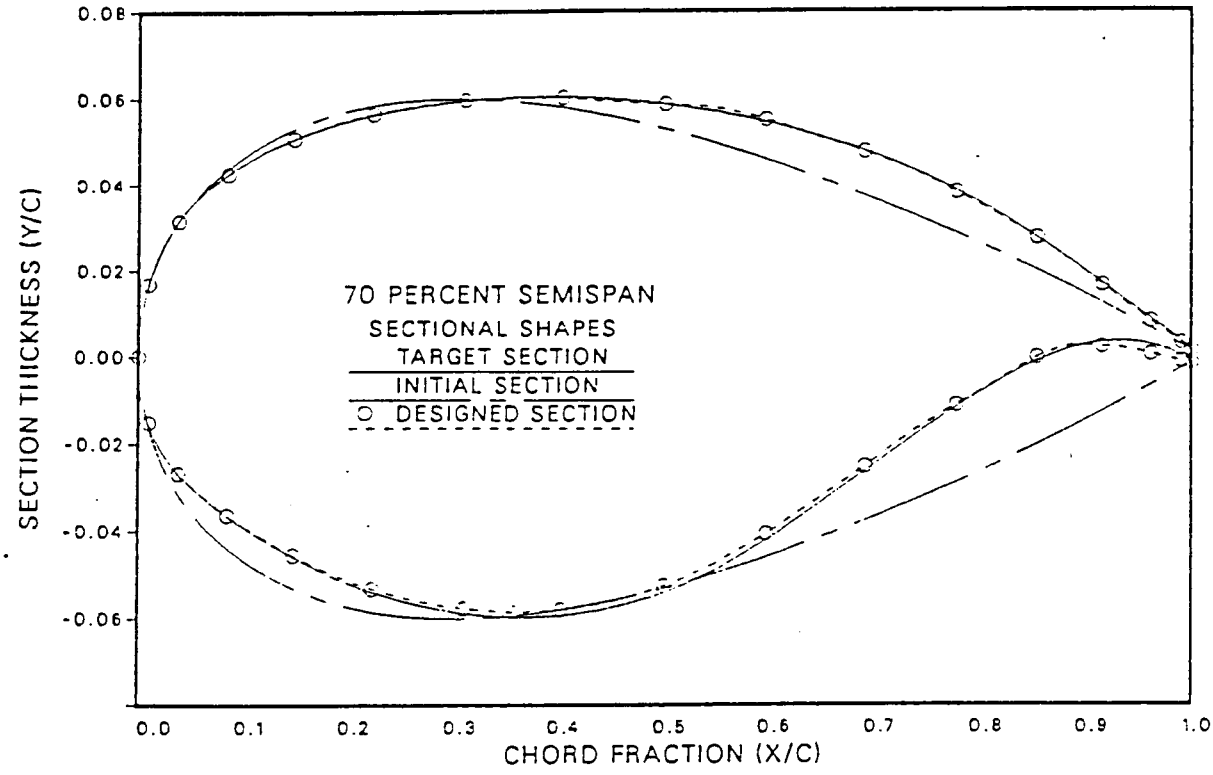
0.08
0.06
0.04
0.02
0.00
-0.02
-0.04
-0.06
SECTION THICKNESS (Y/C)
70 PERCENT SEMISPAN
SECTIONAL SHAPES
TARGET SECTION
INITIAL SECTION
DESIGNED SECTION
0.0
0.1
0.2
0.3
0.4
0.5
0.6
0.7
0.8
0.9
1.0
CHORD FRACTION (X/C)

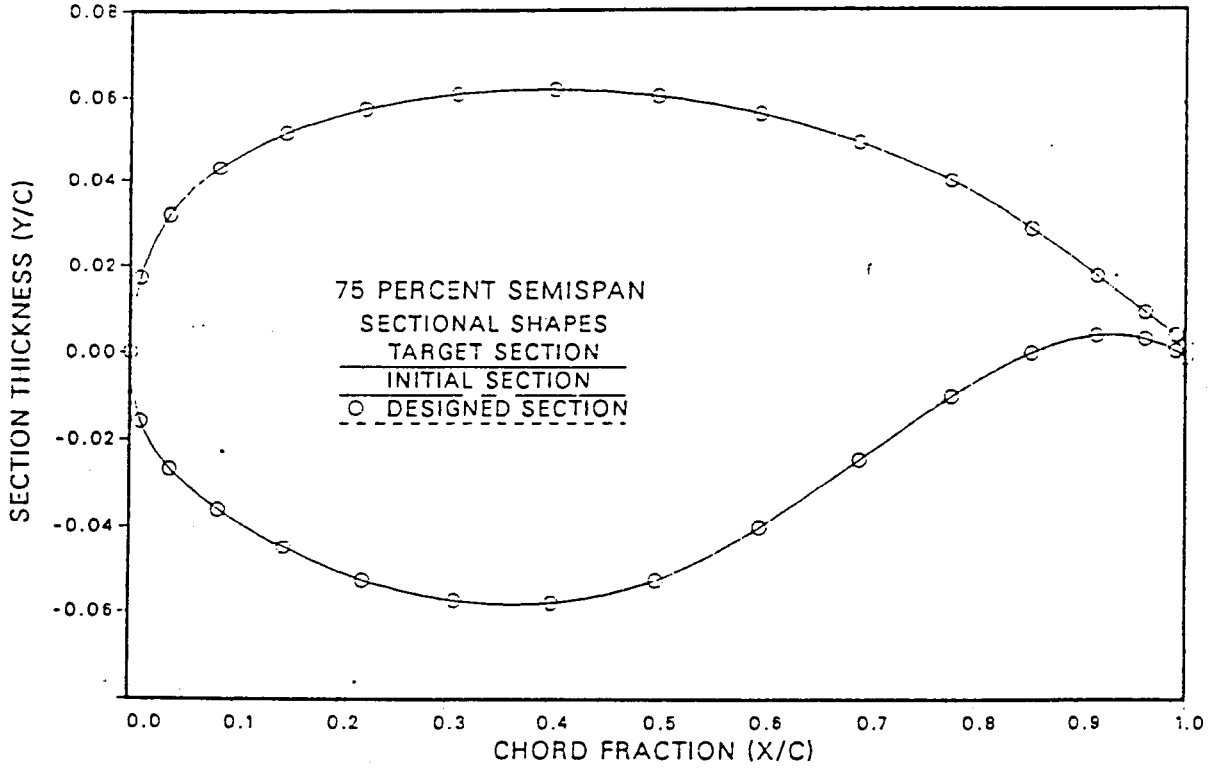
0.08
0.06
0.04
0.02
0.00
-0.02
-0.04
-0.06
SECTION THICKNESS (Y/C)
75 PERCENT SEMISPAN
SECTIONAL SHAPES
TARGET SECTION
INITIAL SECTION
DESIGNED SECTION
0.0
0.1
0.2
0.3
0.4
0.5
0.6
0.7
0.8
0.9
1.0
CHORD FRACTION (X/C)

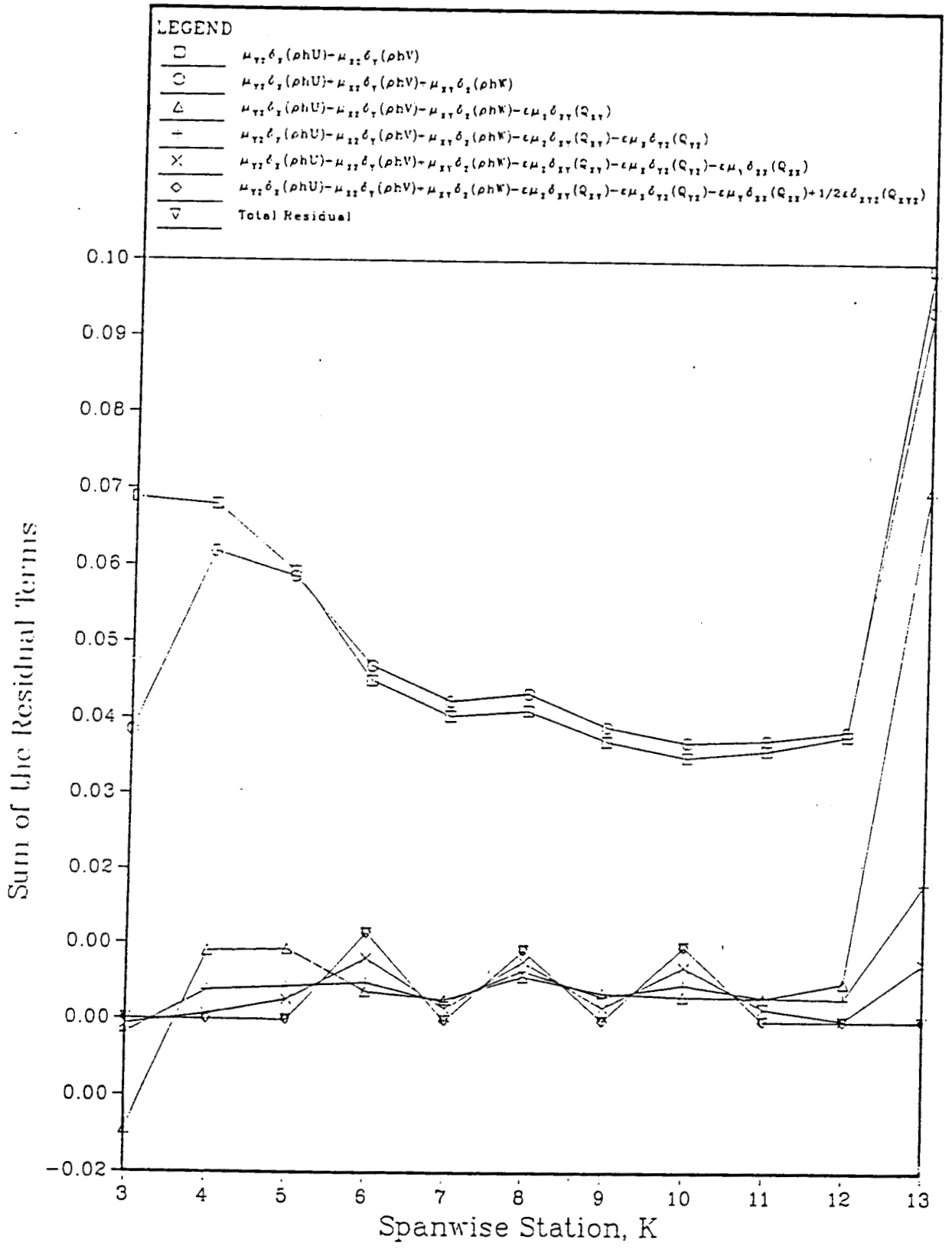

Residual Sum For x = 1.000 (lower surface)
GLOBAL ITERATION 26

Figure 10. Breakdown of the Residual at Convergence Using Method A

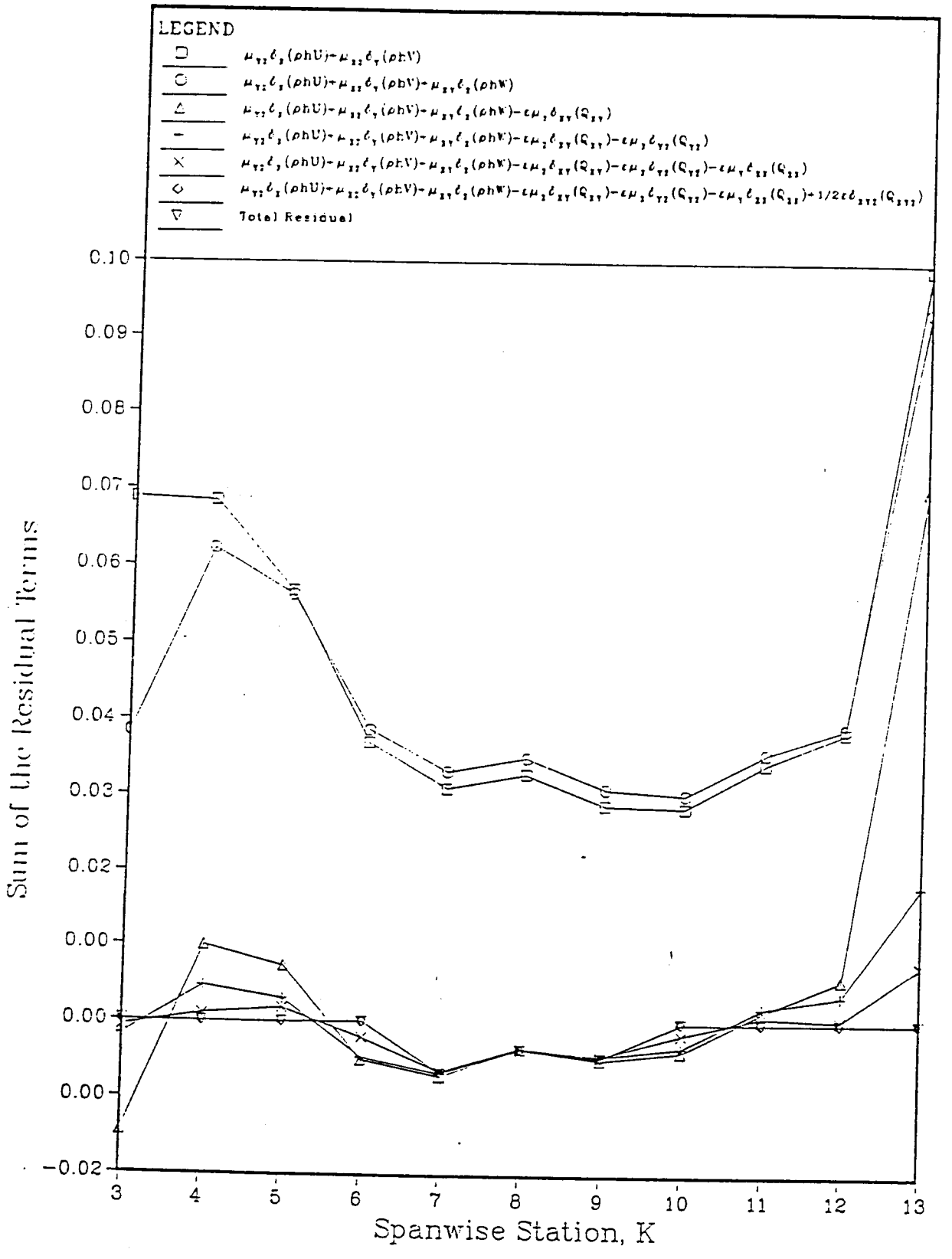

Figure 11. Breakdown of the Residual at Convergence Using Method B

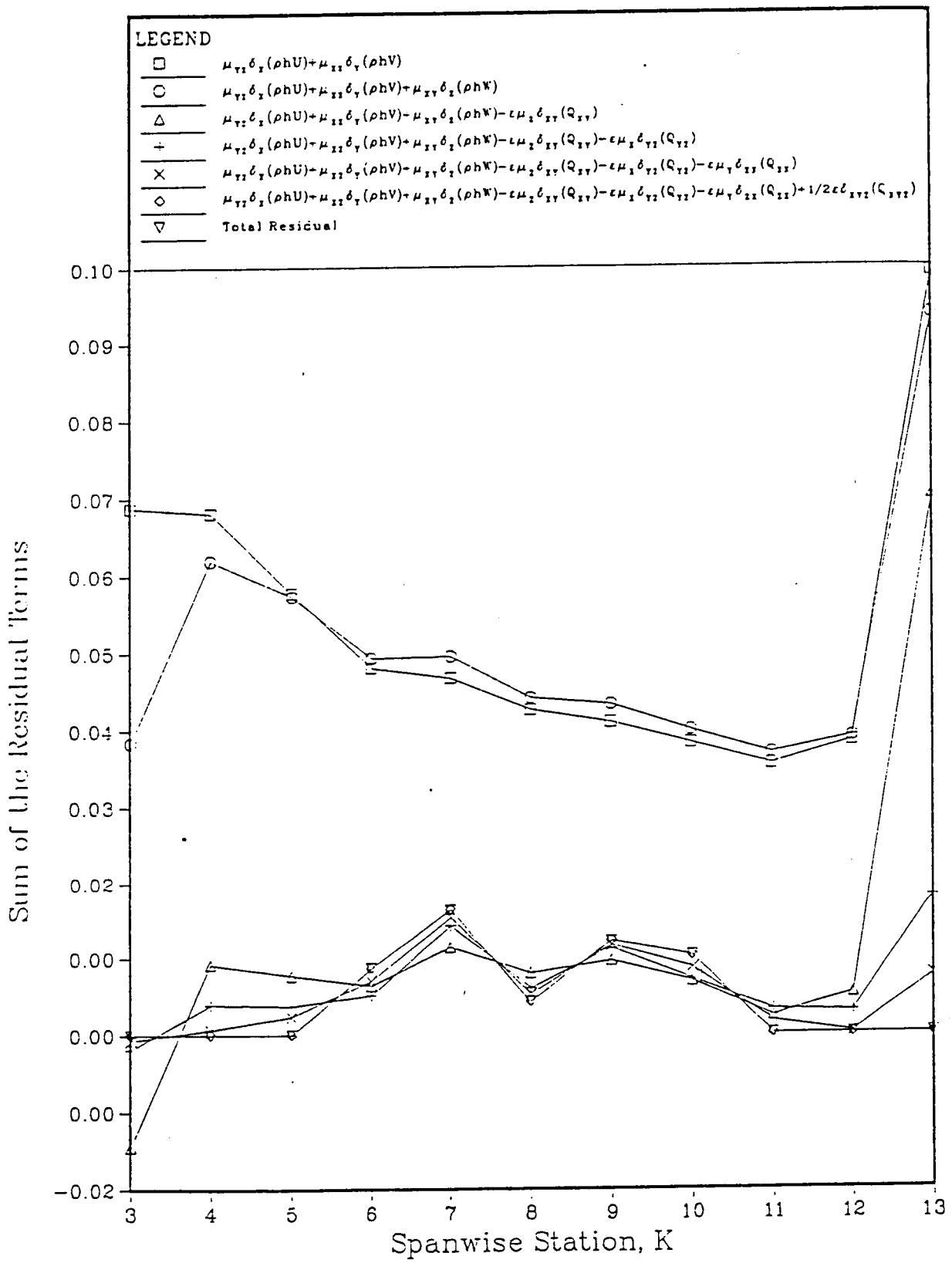

Residual Sum For x = 1.000 (lower surface)
GLOBAL ITERATION 26

Figure 12. Breakdown of the Residual at Convergence Using Method C

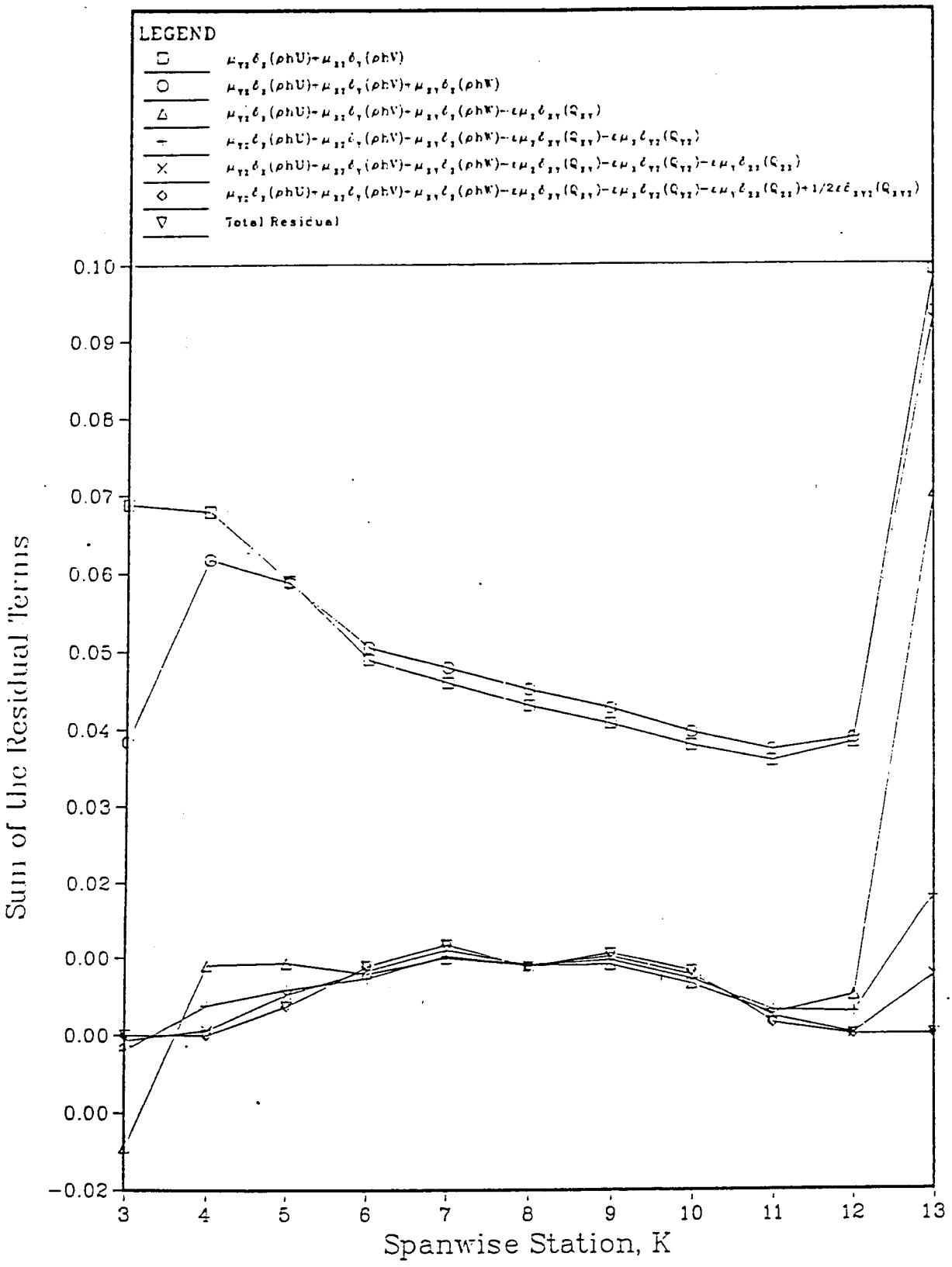

Residual Sum For x = 1.000 (lower surface)
GLOBAL ITERATION 26

Figure 13. Breakdown of the Residual at Convergence Using Method D

Figure 14a-14b. Comparison of a Fairly Unskewed and Skewed Grid at the Wing Surface

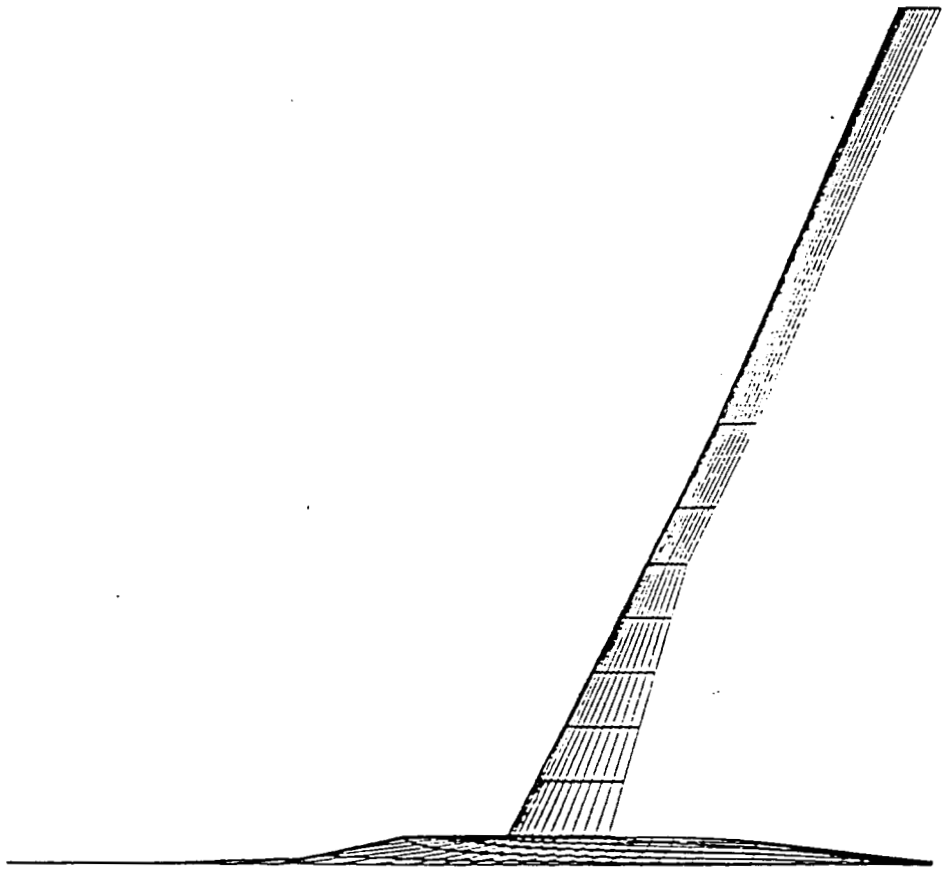

Figure 14a

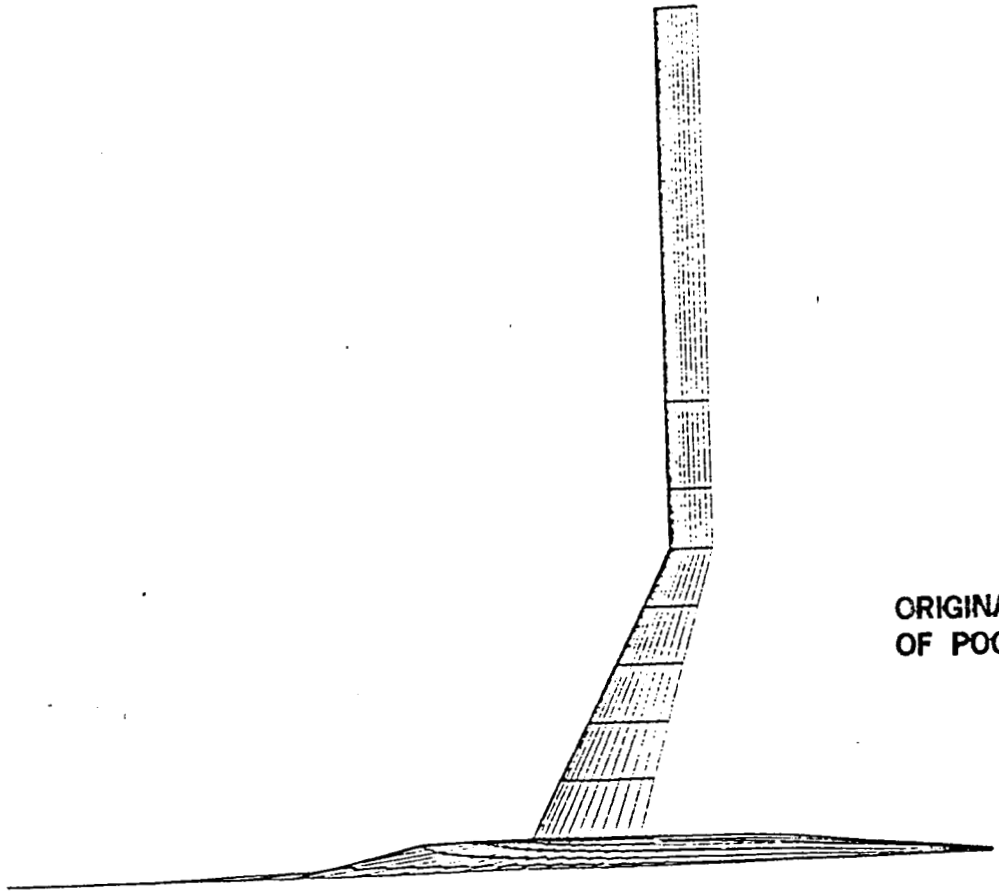

Figure 14b

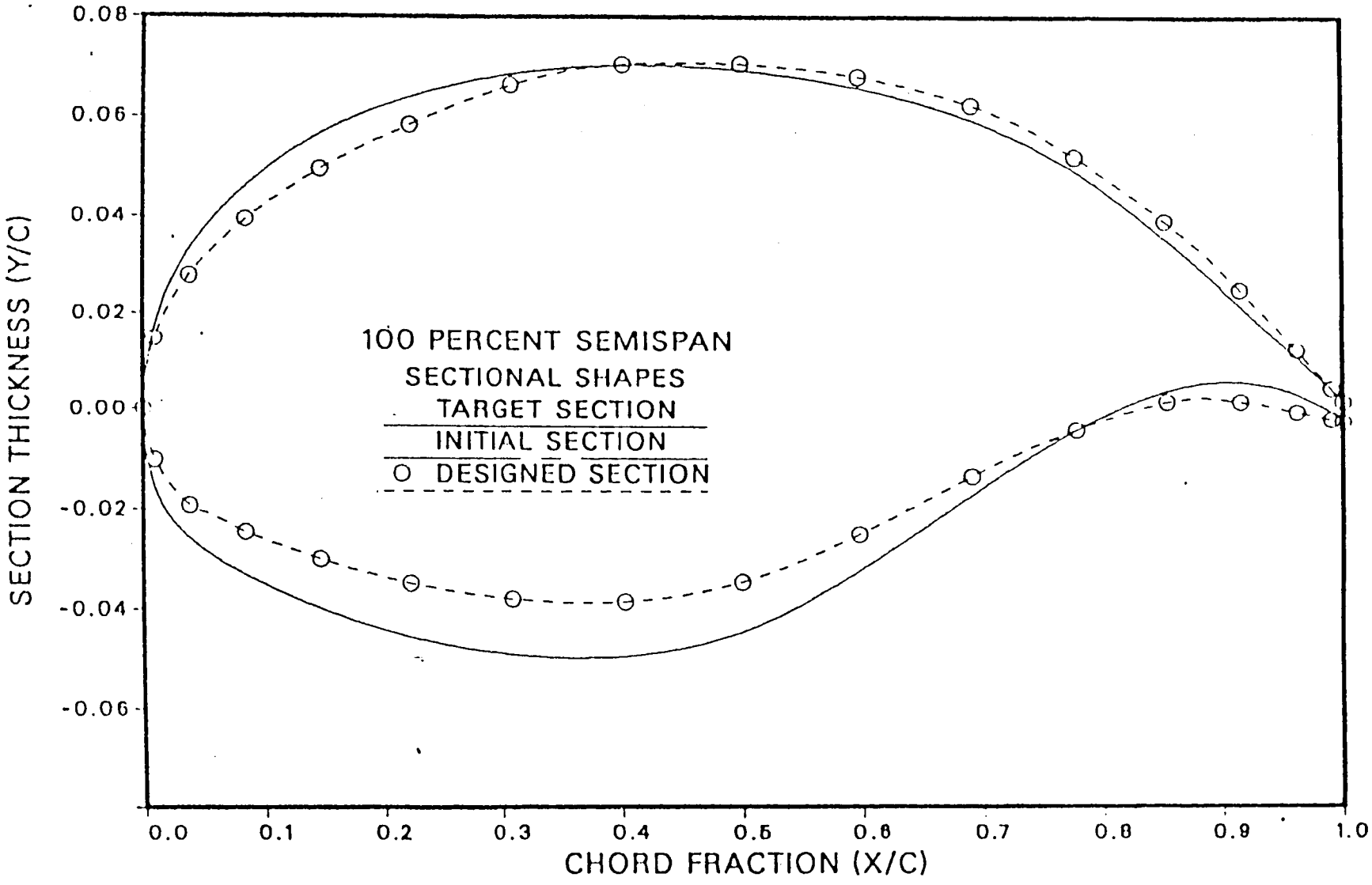

Figure 15. Section Designed Using the Skewed Grid

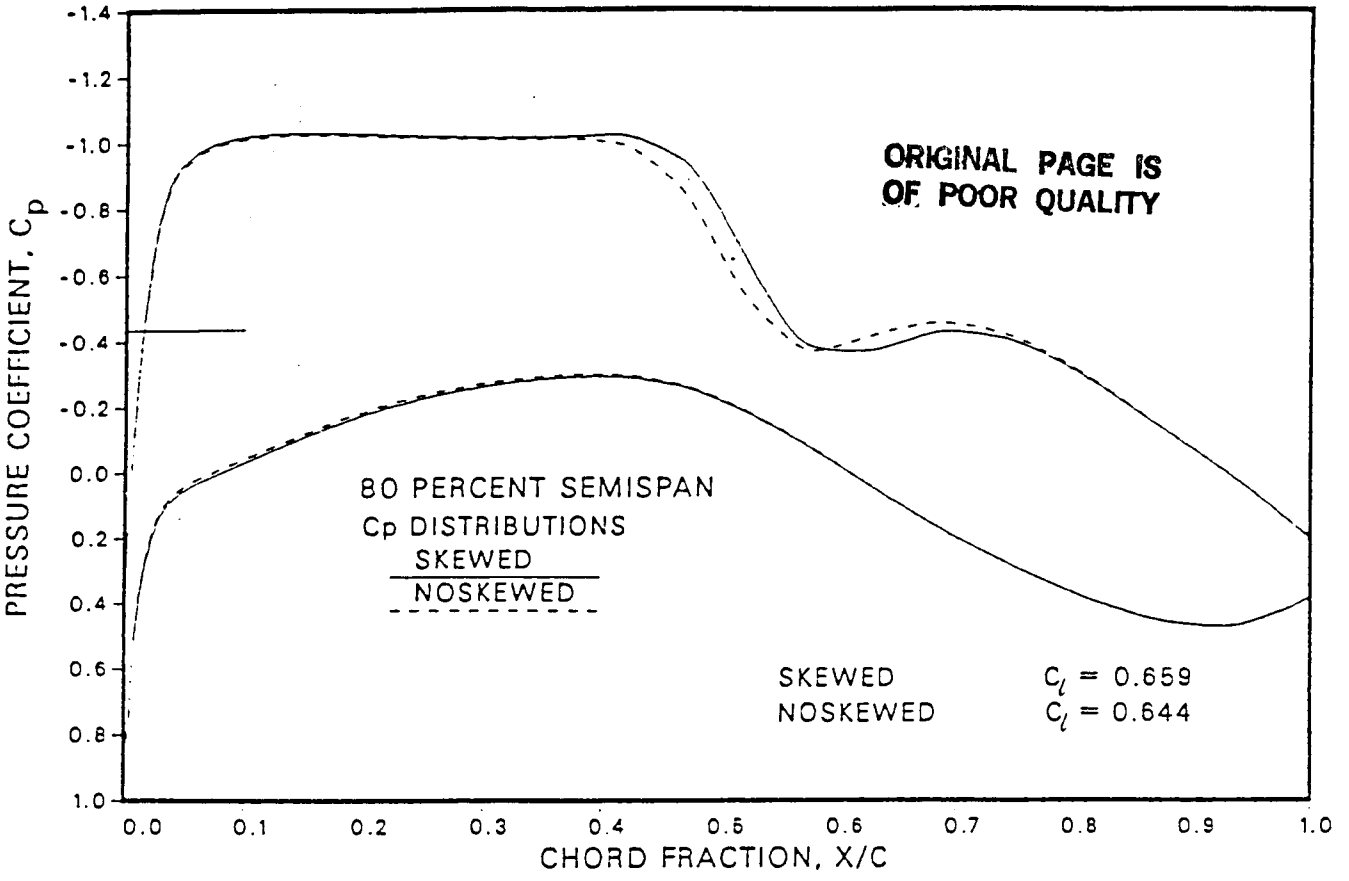

Figure 16a-16b. Comparison of Pressures Obtained From an Analysis of Wing-A Using the Grids in Figure 14

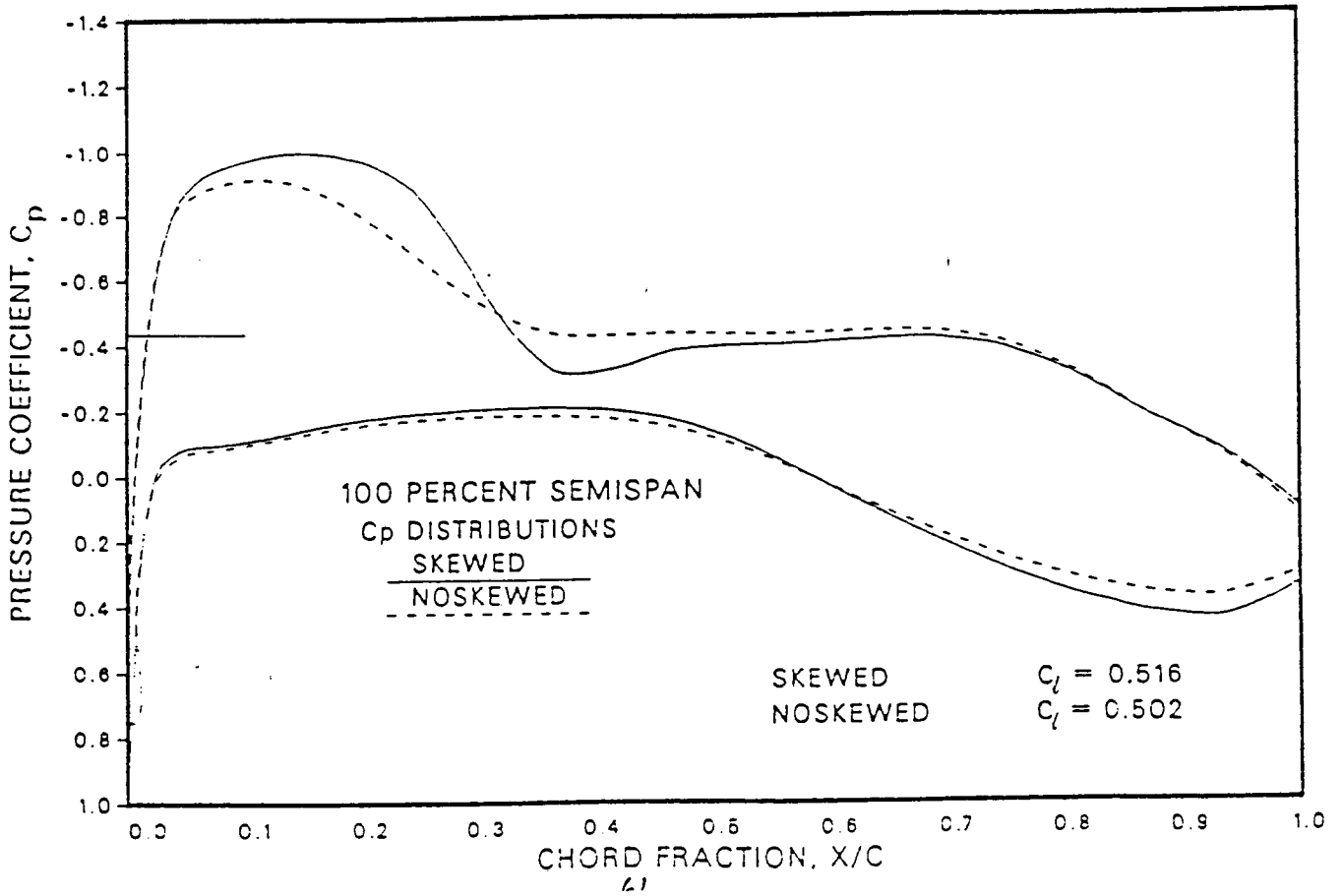

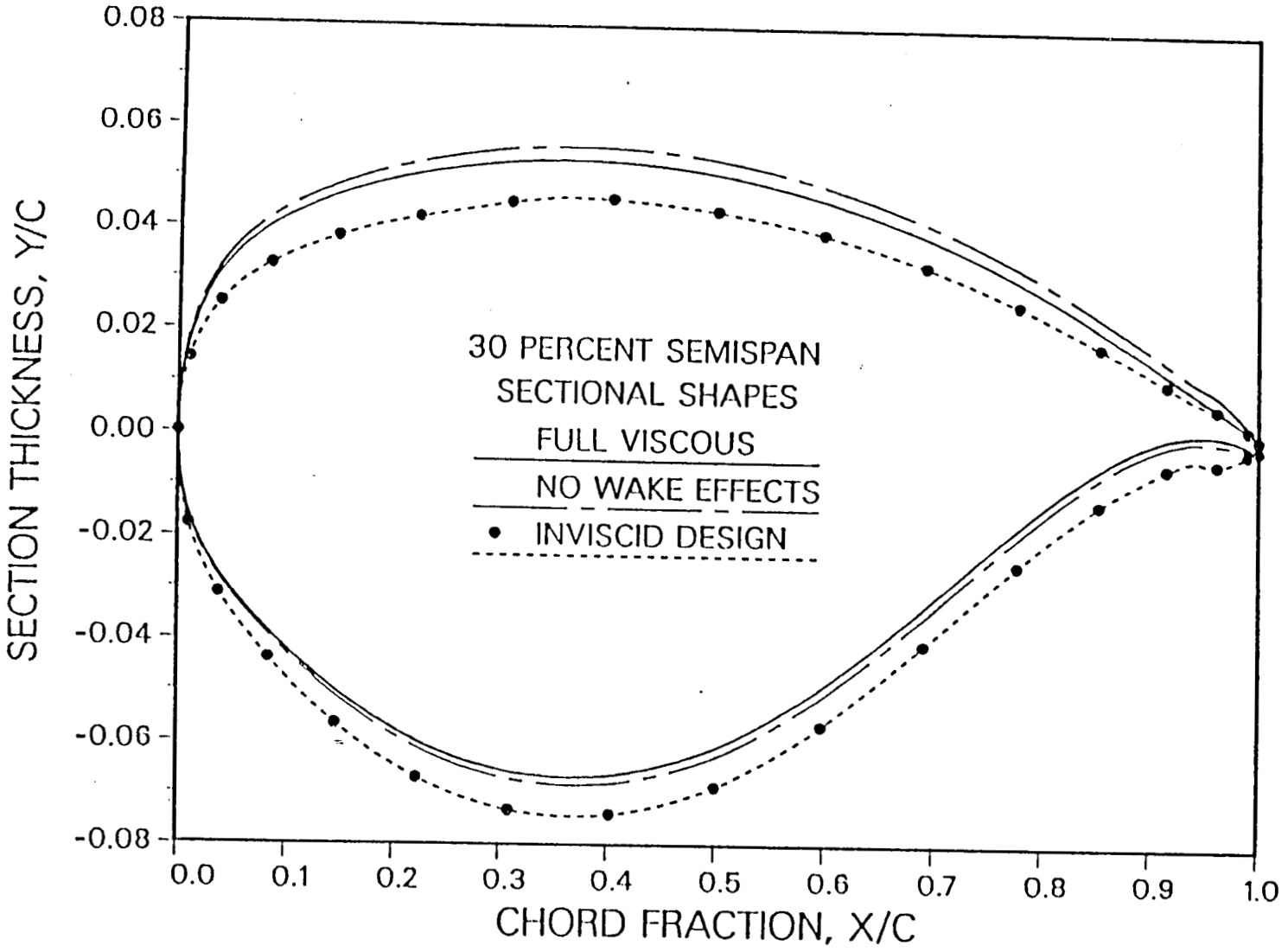

Figure 17a

Figure 17a-17c. Comparison of Sections Designed Using Different Interaction Assumptions

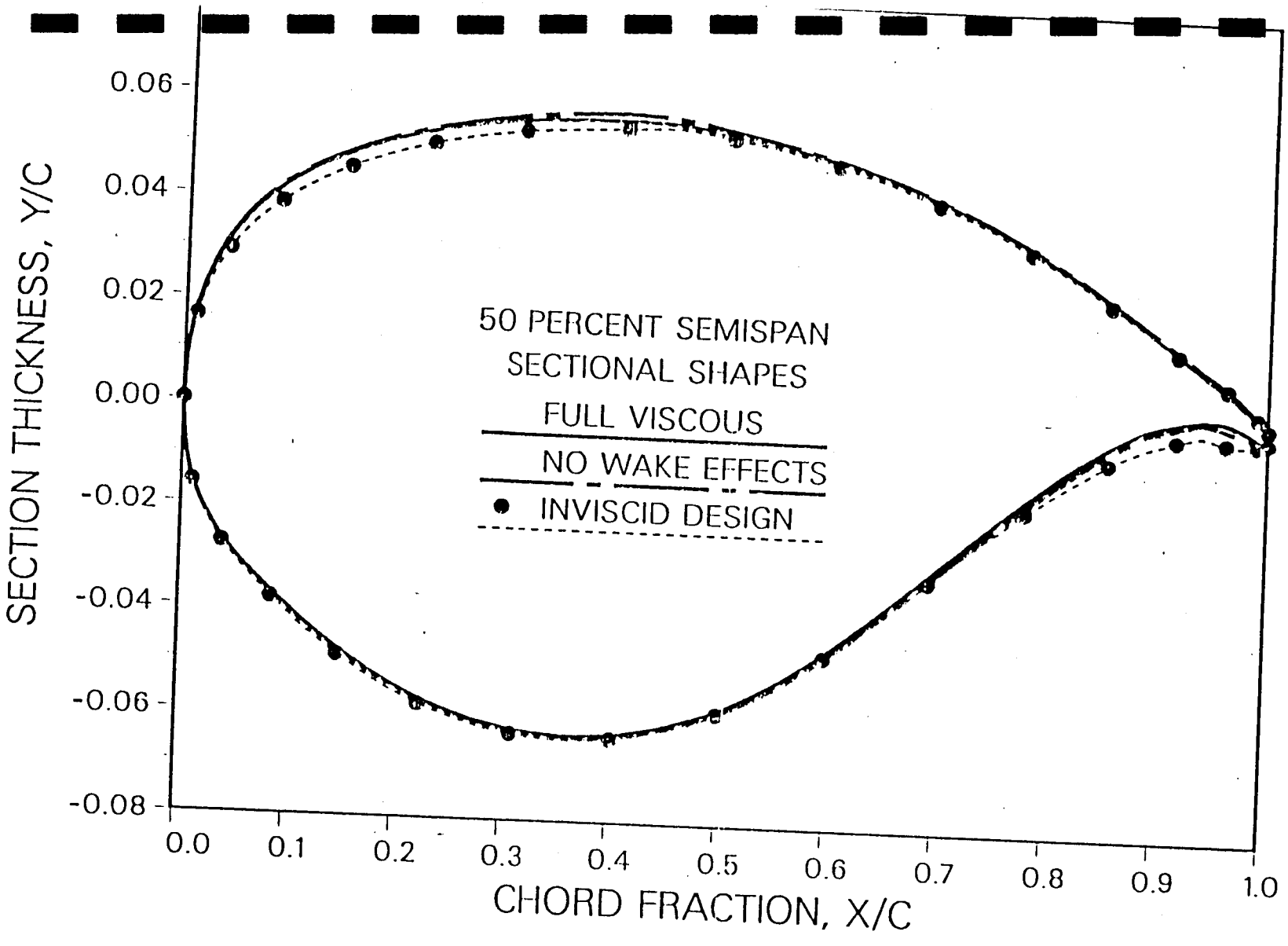
0.06
0.04
0.02
0.00
-0.02
-0.04
-0.06
-0.08
SECTION THICKNESS, Y/C
50 PERCENT SEMISPAN
SECTIONAL SHAPES
FULL VISCOUS
NO WAKE EFFECTS
INVISCID DESIGN
0.0
0.1
0.2
0.3
0.4
0.5
0.6
0.7
0.8
0.9
1.0
CHORD FRACTION, X/C

Figure 17b

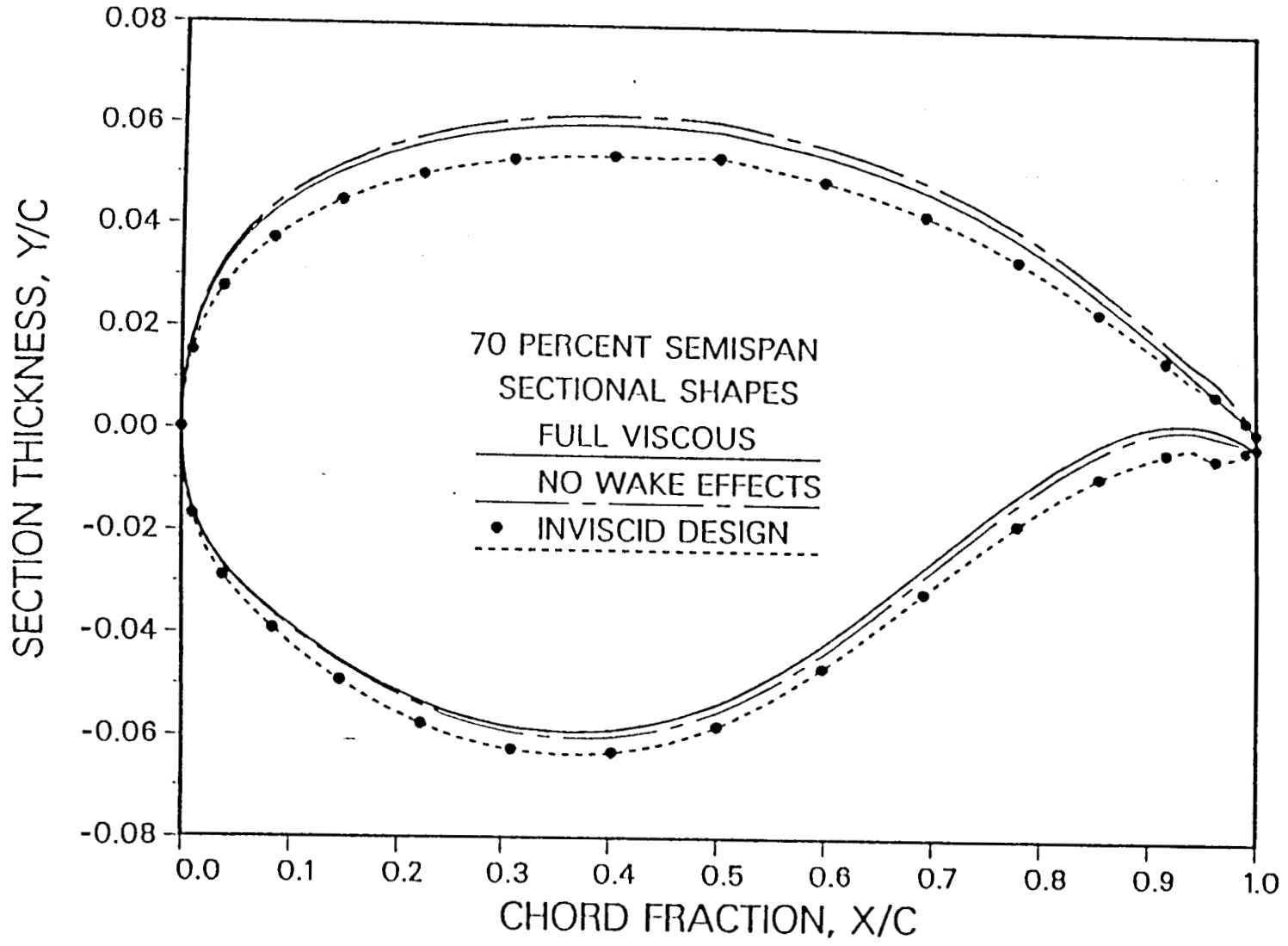
0.08
0.06
0.04
0.02
0.00
-0.02
-0.04
-0.06
-0.08
SECTION THICKNESS, Y/C
70 PERCENT SEMISPAN
SECTIONAL SHAPES
FULL VISCOUS
NO WAKE EFFECTS
INVISCID DESIGN
0.0
0.1
0.2
0.3
0.4
0.5
0.6
0.7
0.8
0.9
1.0
CHORD FRACTION, X/C

Figure 17c

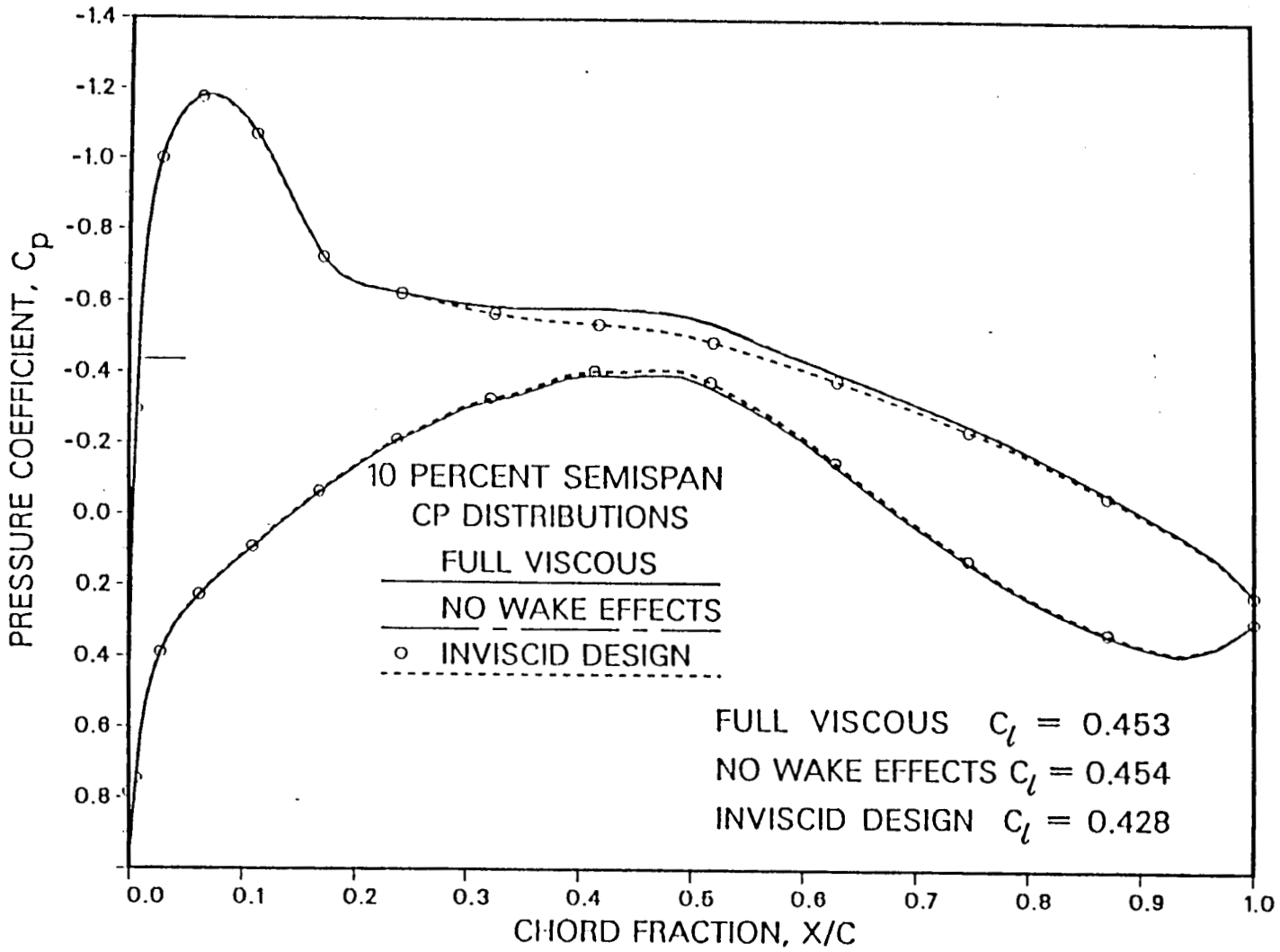

Figure 18a

Figure 18a-18c. Comparison of Pressures Obtained by a Viscous Analysis of the Wings Designed Using Different Interaction Assumptions
Lockheed Wing-A, Mach = .8, AOA = 2°, Re = 24x10^6

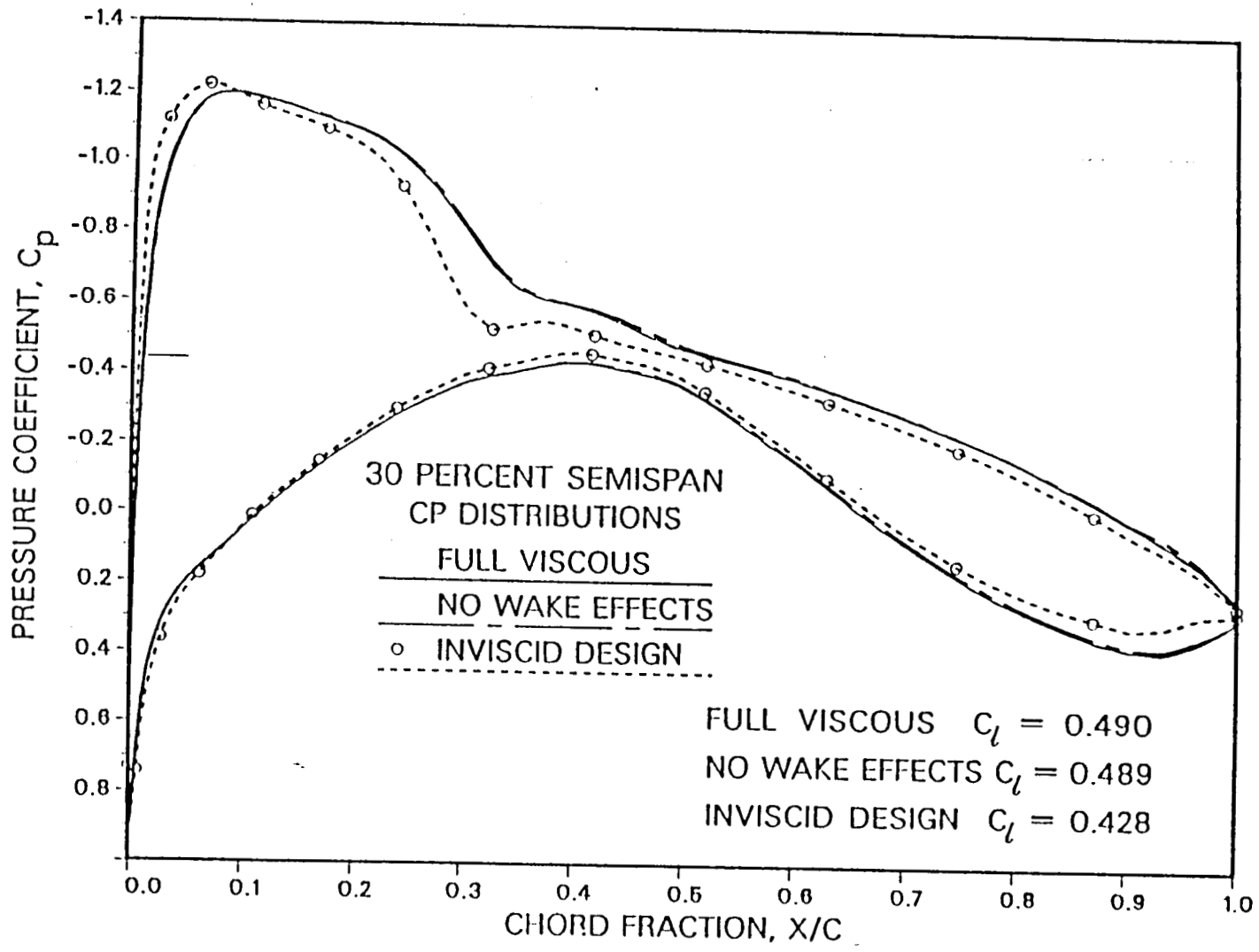
PRESSURE COEFFICIENT, C_p
-1.4
-1.2
-1.0
-0.8
-0.6
-0.4
-0.2
0.0
0.2
0.4
0.6
0.8
30 PERCENT SEMISPAN
CP DISTRIBUTIONS
FULL VISCOUS
NO WAKE EFFECTS
INVISCID DESIGN
FULL VISCOUS C_l = 0.490
NO WAKE EFFECTS C_l = 0.489
INVISCID DESIGN C_l = 0.428
0.0
0.1
0.2
0.3
0.4
0.5
0.6
0.7
0.8
0.9
1.0
CHORD FRACTION, X/C

Figure 18b

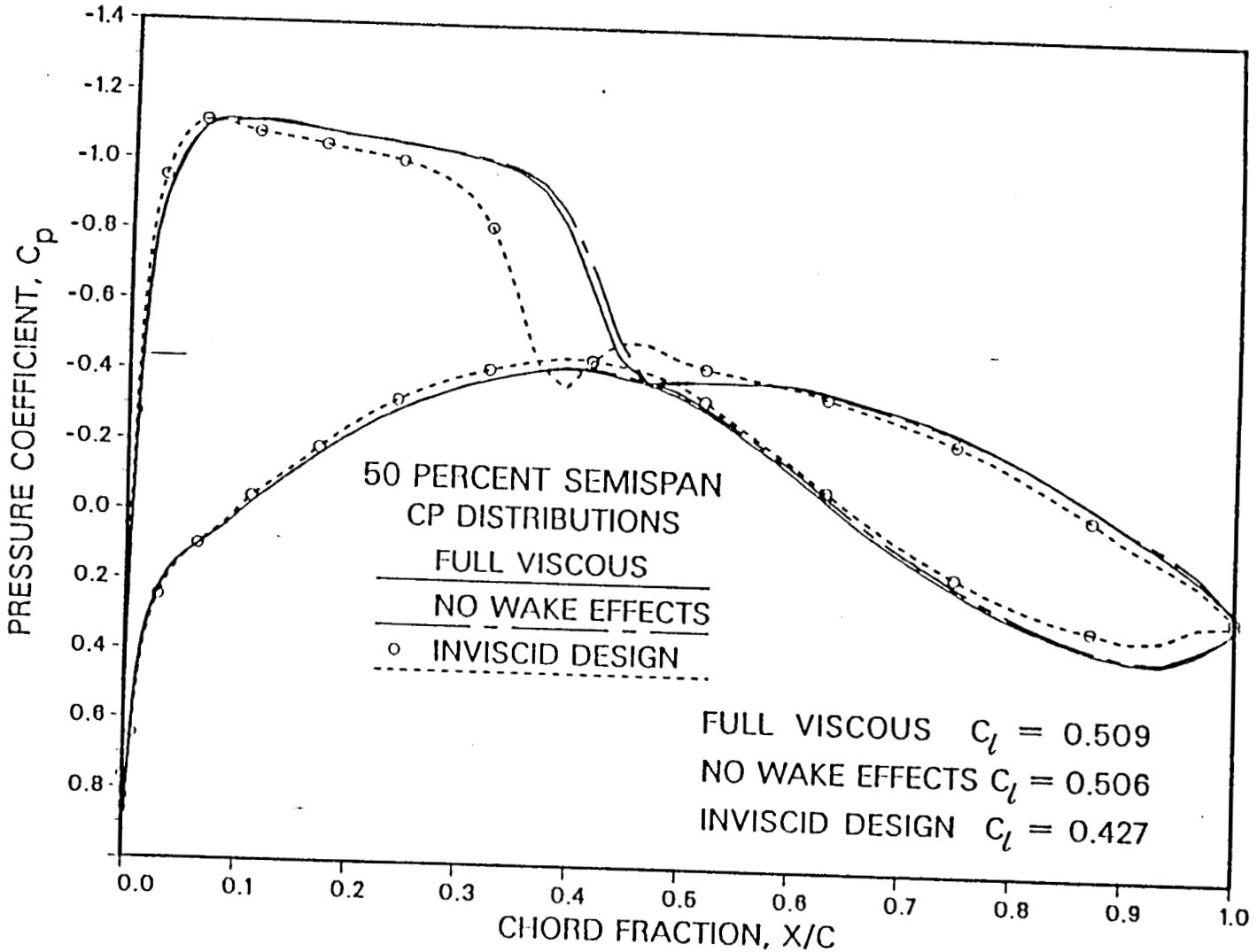
PRESSURE COEFFICIENT, C_p
-1.4
-1.2
-1.0
-0.8
-0.6
-0.4
-0.2
0.0
0.2
0.4
0.6
0.8
50 PERCENT SEMISPAN
CP DISTRIBUTIONS
FULL VISCOUS
NO WAKE EFFECTS
INVISCID DESIGN
FULL VISCOUS C_l = 0.509
NO WAKE EFFECTS C_l = 0.506
INVISCID DESIGN C_l = 0.427
0.0
0.1
0.2
0.3
0.4
0.5
0.6
0.7
0.8
0.9
1.0
CHORD FRACTION, X/C

Figure 18c

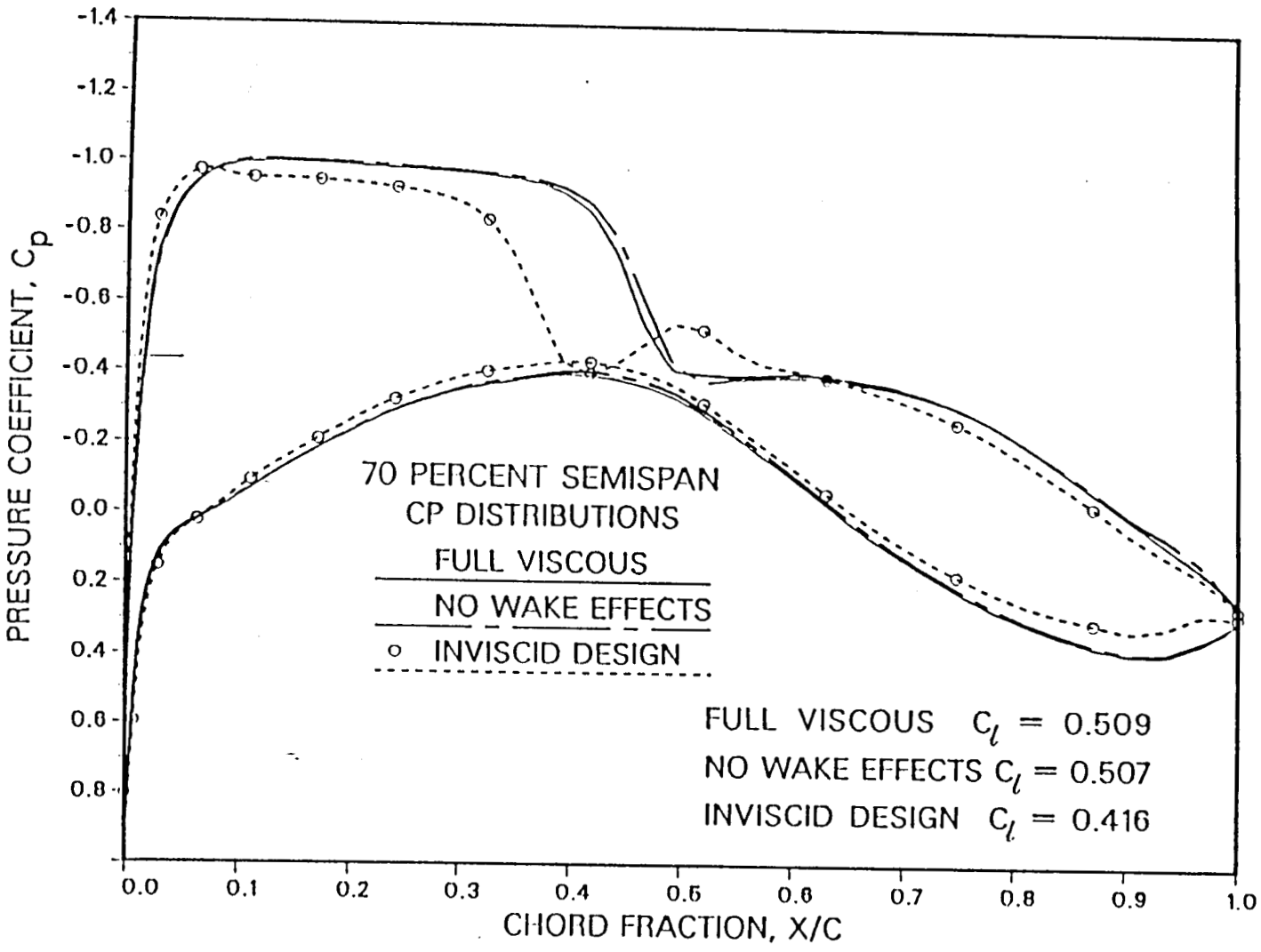
PRESSURE COEFFICIENT, C_p
-1.4
-1.2
-1.0
-0.8
-0.6
-0.4
-0.2
0.0
0.2
0.4
0.6
0.8
70 PERCENT SEMISPAN
CP DISTRIBUTIONS
FULL VISCOUS
NO WAKE EFFECTS
INVISCID DESIGN
FULL VISCOUS C_l = 0.509
NO WAKE EFFECTS C_l = 0.507
INVISCID DESIGN C_l = 0.416
0.0
0.1
0.2
0.3
0.4
0.5
0.6
0.7
0.8
0.9
1.0
CHORD FRACTION, X/C

Figure 18d

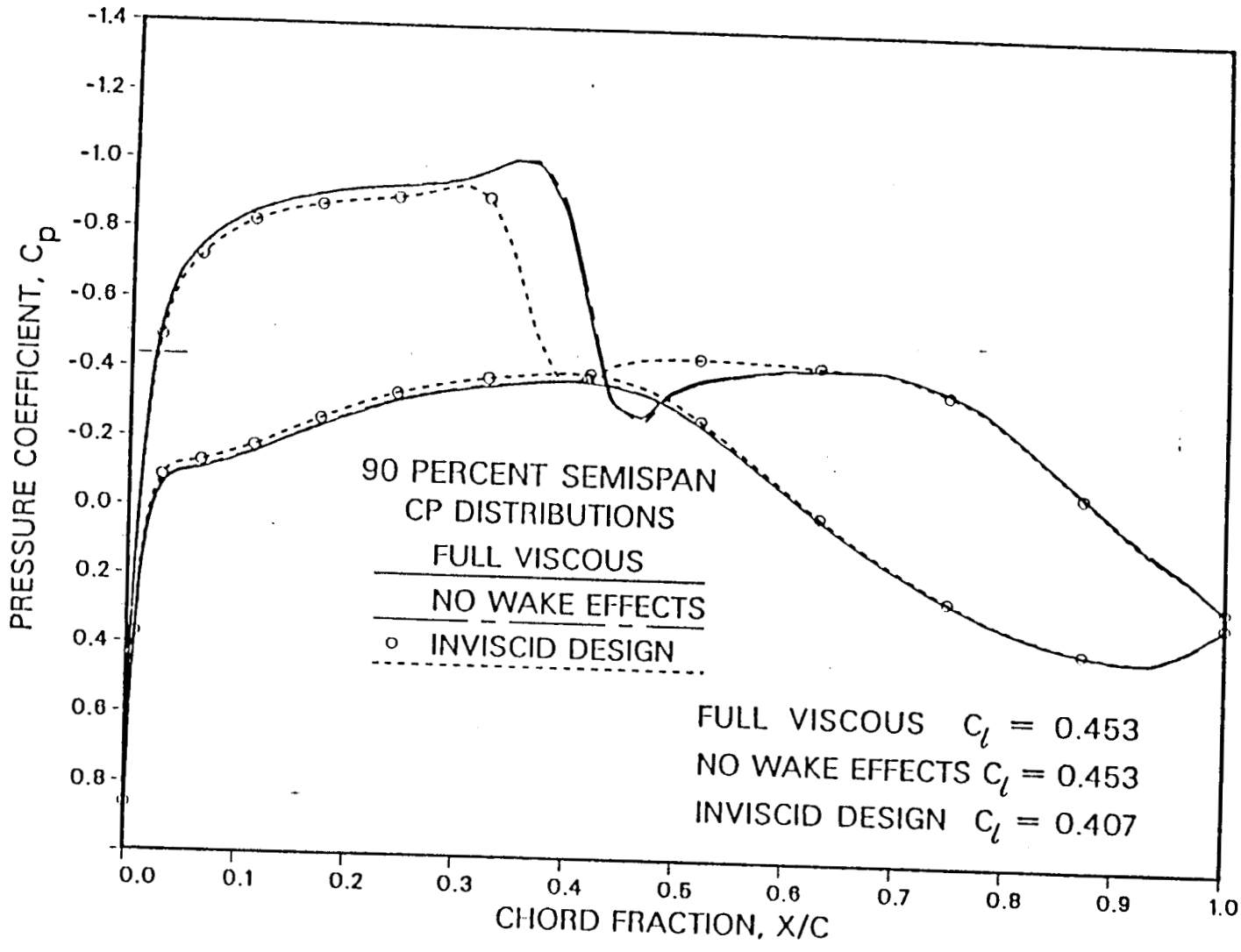
PRESSURE COEFFICIENT, C_p
-1.4
-1.2
-1.0
-0.8
-0.6
-0.4
-0.2
0.0
0.2
0.4
0.6
0.8
90 PERCENT SEMISPAN
CP DISTRIBUTIONS
FULL VISCOUS
NO WAKE EFFECTS
INVISCID DESIGN
FULL VISCOUS C_l = 0.453
NO WAKE EFFECTS C_l = 0.453
INVISCID DESIGN C_l = 0.407
0.0
0.1
0.2
0.3
0.4
0.5
0.6
0.7
0.8
0.9
1.0
CHORD FRACTION, X/C

Figure 18e

AIM

RESULTS OF THE ANALYSES OF THE DESIGNED WINGS

Lift Coefficient	Target	Full Viscous Design	No Wake Design	Inviscid Design
C_l	.514	.509	.506	.427
Wing C_L	483	.478	.477	.419

Table 1. Comparison of the Wing Lift Coefficient for the Wings designed using different Viscous Interaction Assumptions

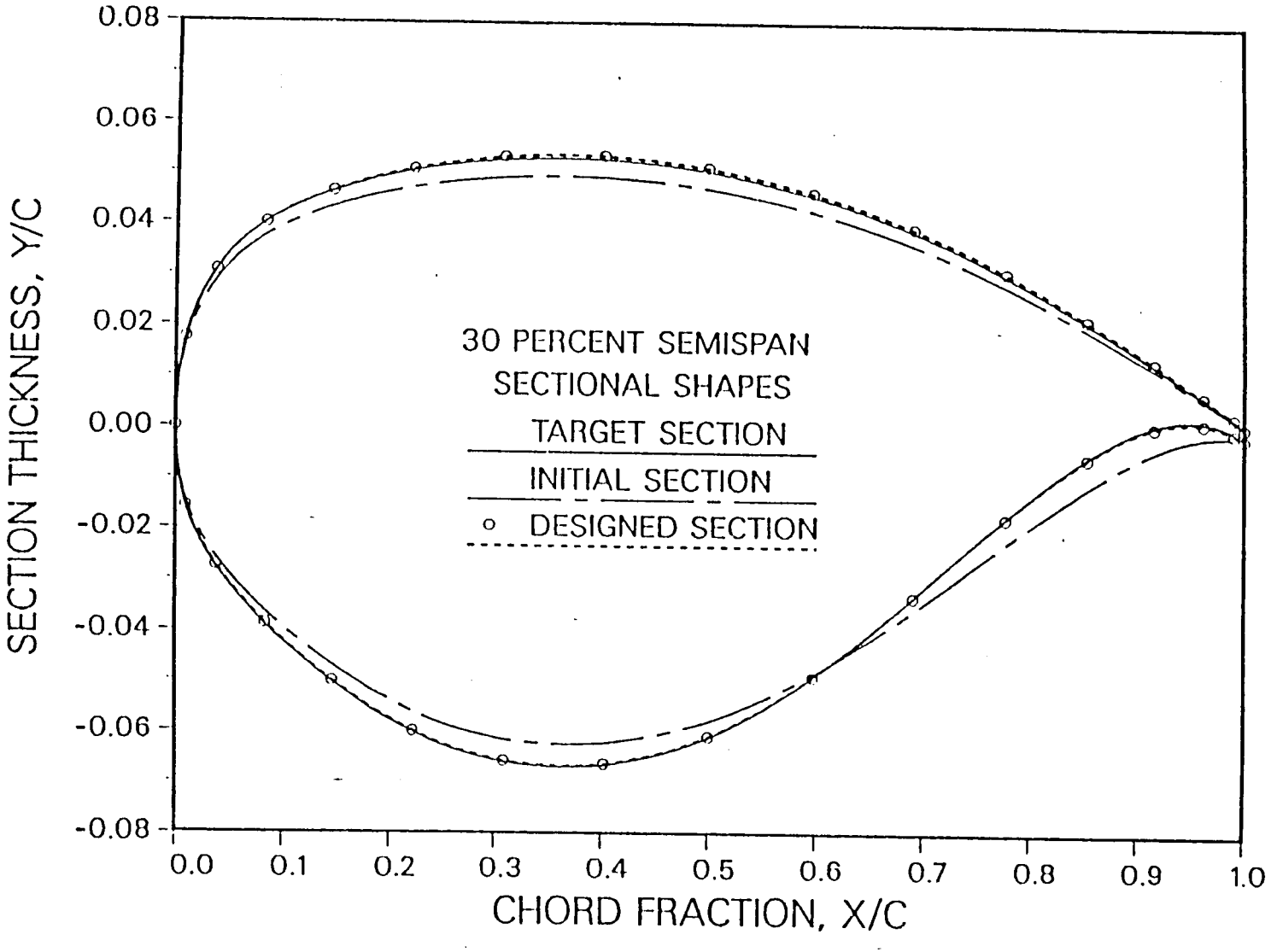

Figure 19a

Figure 19a-19c. Comparison of the Designed Section with the Target Section and the First Type of Initial Section

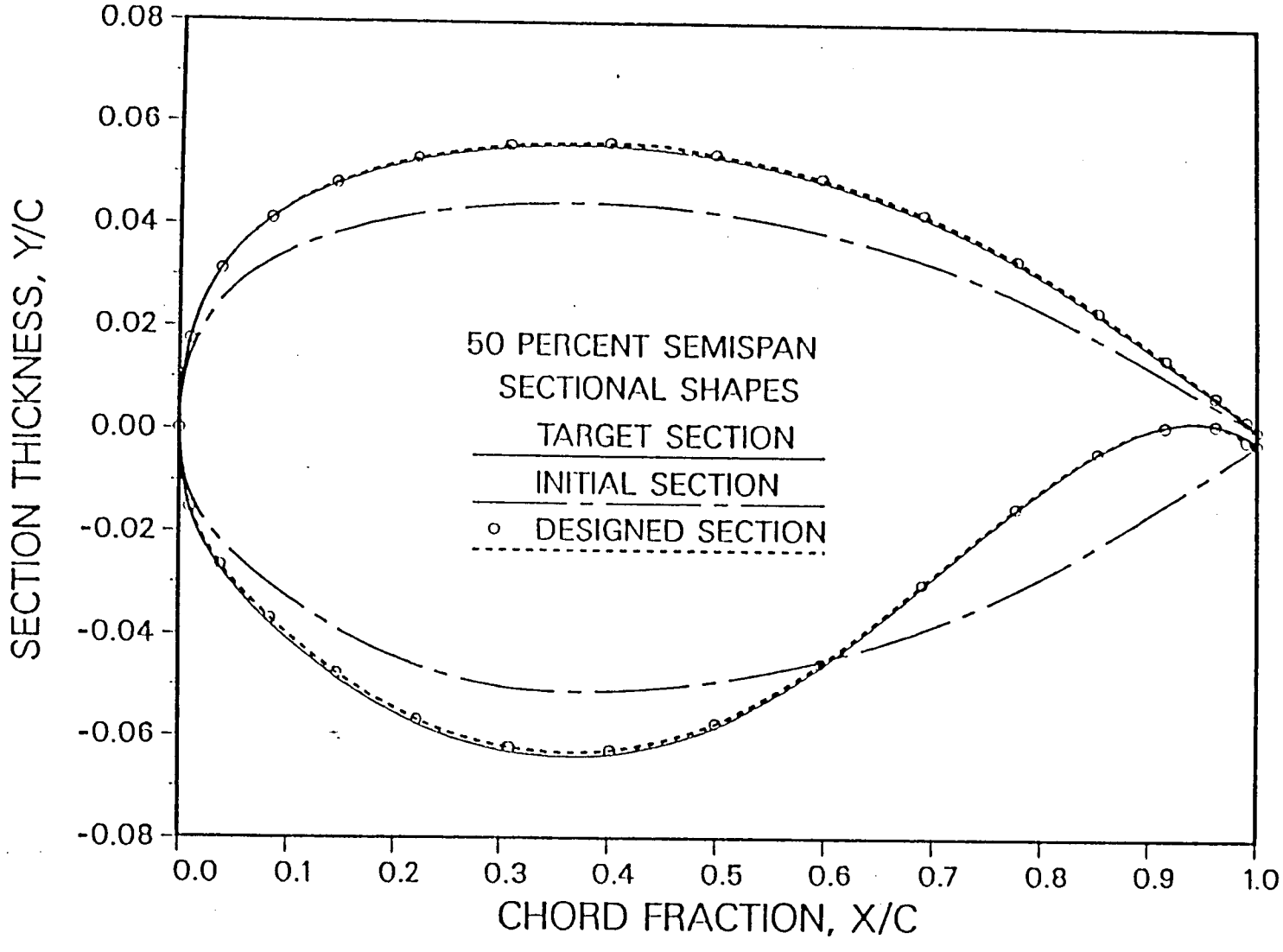
0.08
0.06
0.04
0.02
0.00
-0.02
-0.04
-0.06
-0.08
SECTION THICKNESS, Y/C
50 PERCENT SEMISPAN
SECTIONAL SHAPES
TARGET SECTION
INITIAL SECTION
DESIGNED SECTION
0.0
0.1
0.2
0.3
0.4
0.5
0.6
0.7
0.8
0.9
1.0
CHORD FRACTION, X/C

Figure 19b

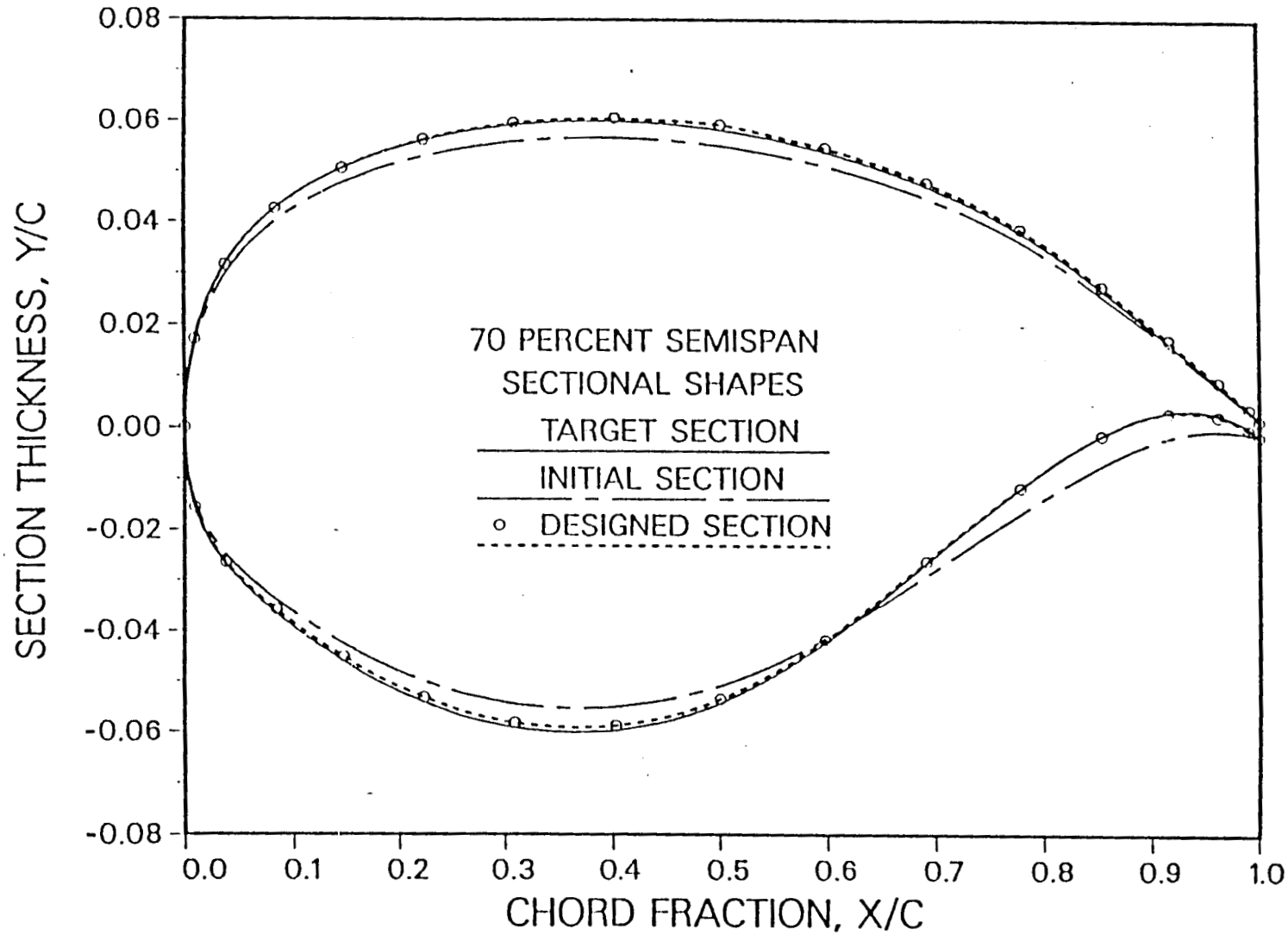
0.08
0.06
0.04
0.02
0.00
-0.02
-0.04
-0.06
-0.08
SECTION THICKNESS, Y/C
70 PERCENT SEMISPAN
SECTIONAL SHAPES
TARGET SECTION
INITIAL SECTION
DESIGNED SECTION
0.0
0.1
0.2
0.3
0.4
0.5
0.6
0.7
0.8
0.9
1.0
CHORD FRACTION, X/C

Figure 19c

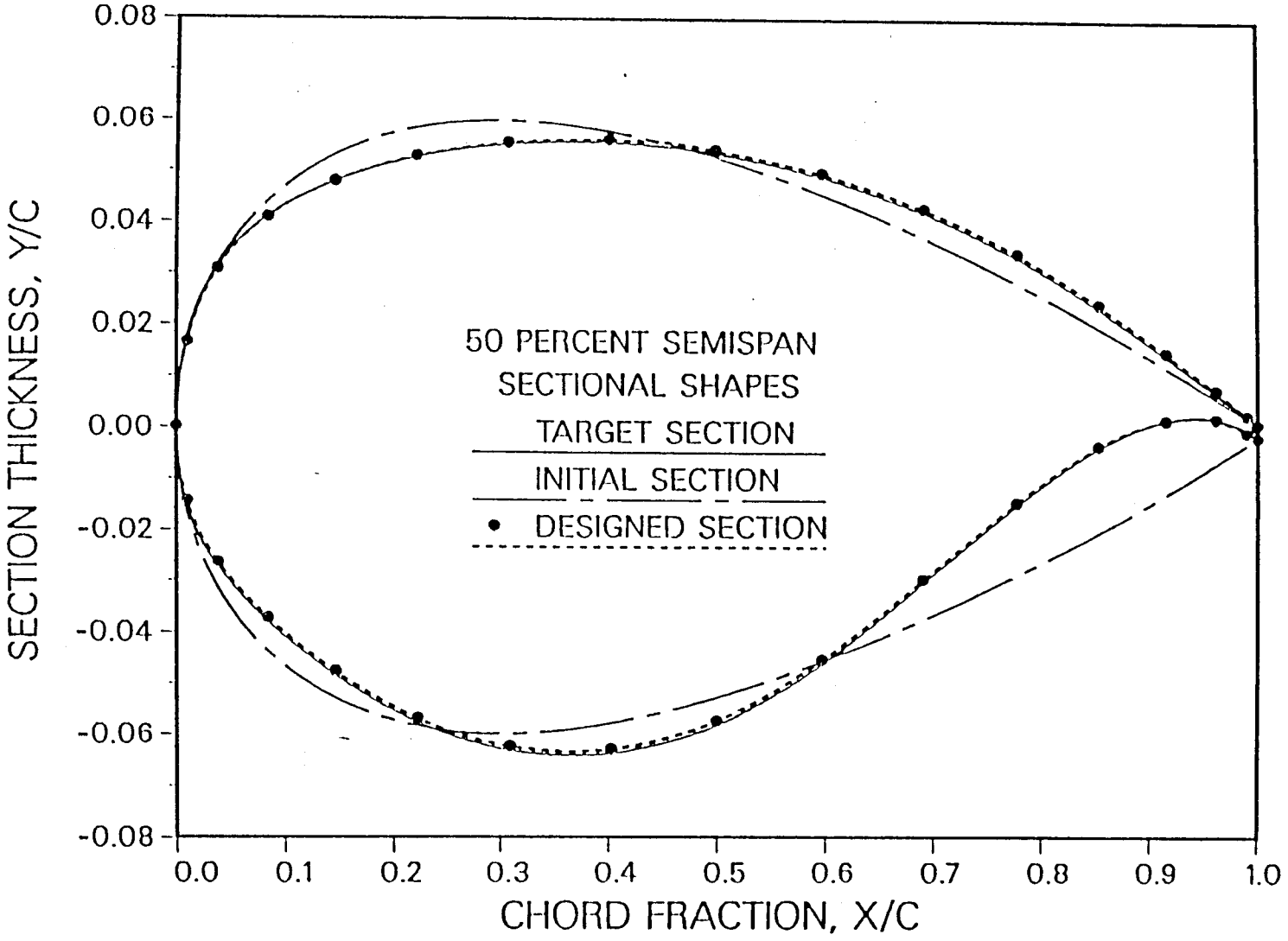

Figure 20b

Figure 20a-20c. Comparison of the Designed Section with the Target Section and the NACA 0012 Initial Section.

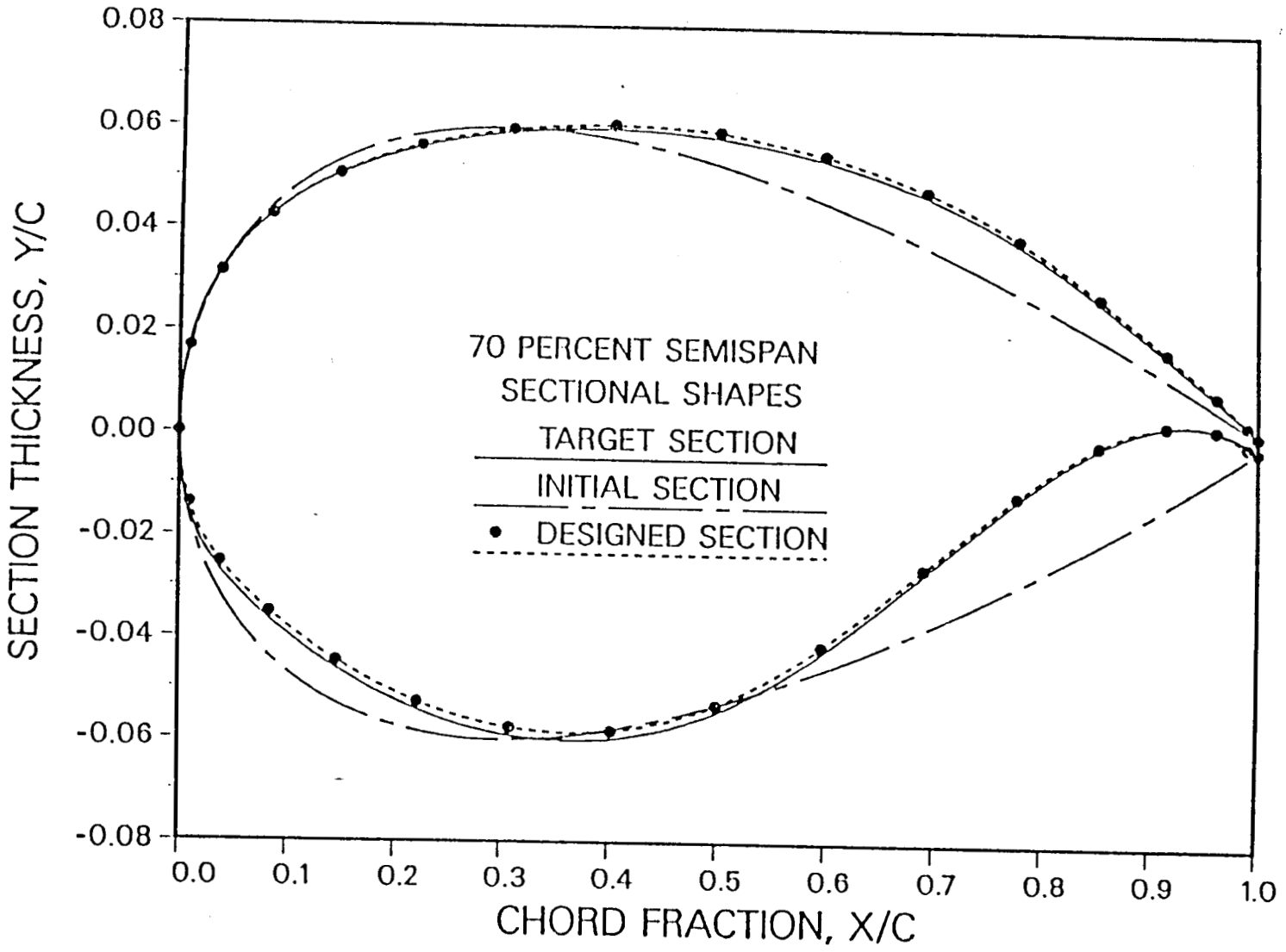
0.08
0.06
0.04
0.02
0.00
-0.02
-0.04
-0.06
-0.08
SECTION THICKNESS, Y/C
70 PERCENT SEMISPAN
SECTIONAL SHAPES
TARGET SECTION
INITIAL SECTION
DESIGNED SECTION
0.0
0.1
0.2
0.3
0.4
0.5
0.6
0.7
0.8
0.9
1.0
CHORD FRACTION, X/C

Figure 20c

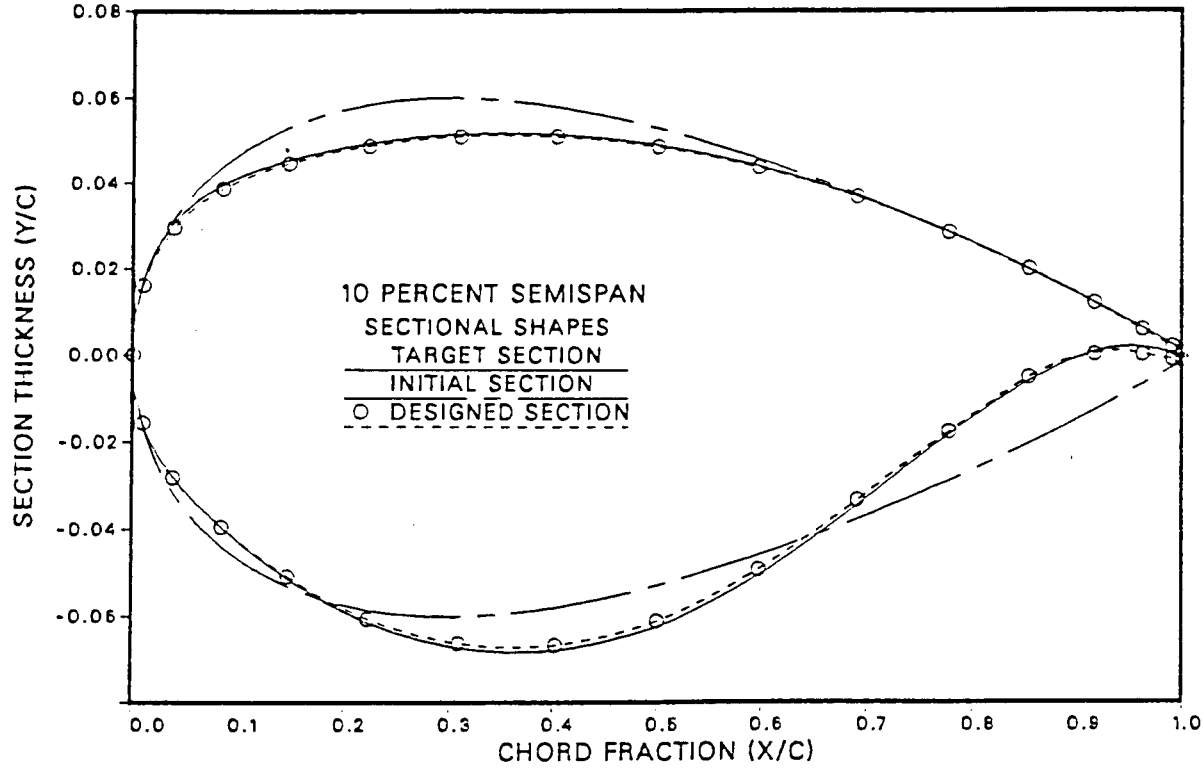

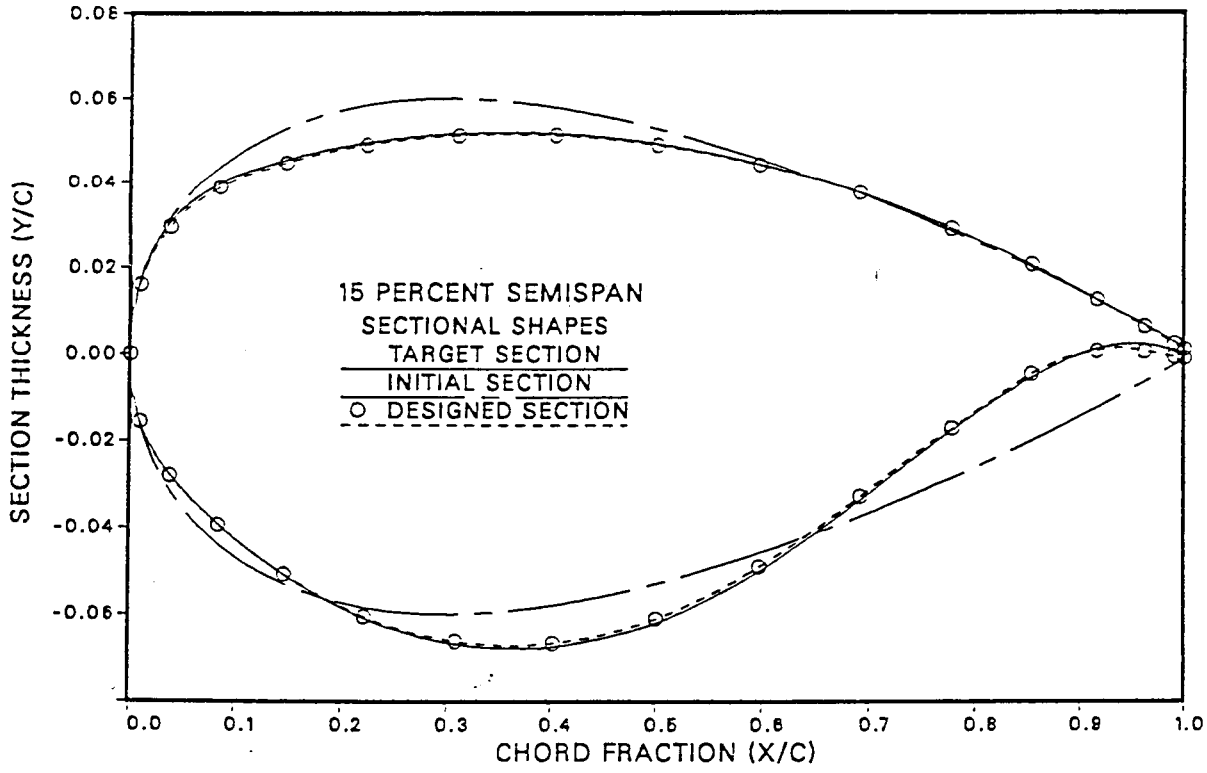

Figure 21a-21c. Comparison of the Designed Section with the Target Section and the NACA 0012 Initial Section Using a High Aspect Ratio Wing

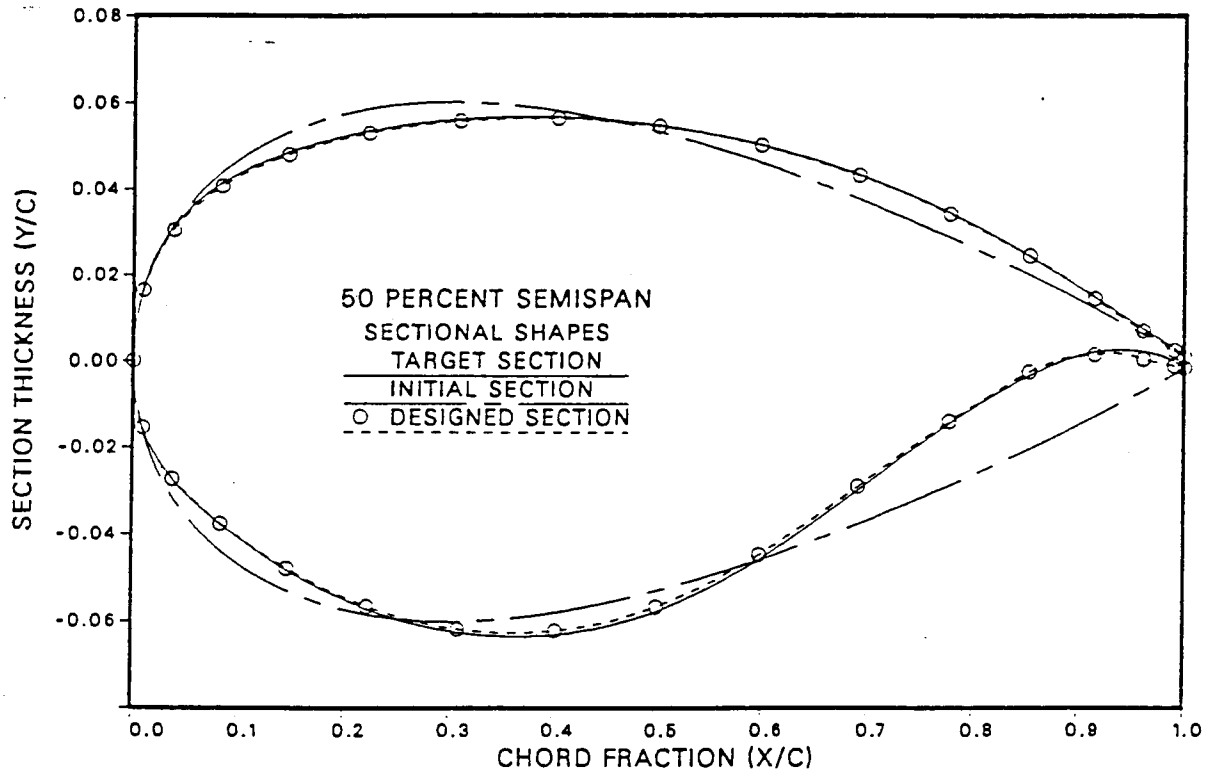
50 PERCENT SEMISPAN
SECTIONAL SHAPES
TARGET SECTION
INITIAL SECTION
DESIGNED SECTION
SECTION THICKNESS (Y/C)
CHORD FRACTION (X/C)
0.08
0.06
0.04
0.02
0.00
-0.02
-0.04
-0.06
0.0
0.1
0.2
0.3
0.4
0.5
0.6
0.7
0.8
0.9
1.0

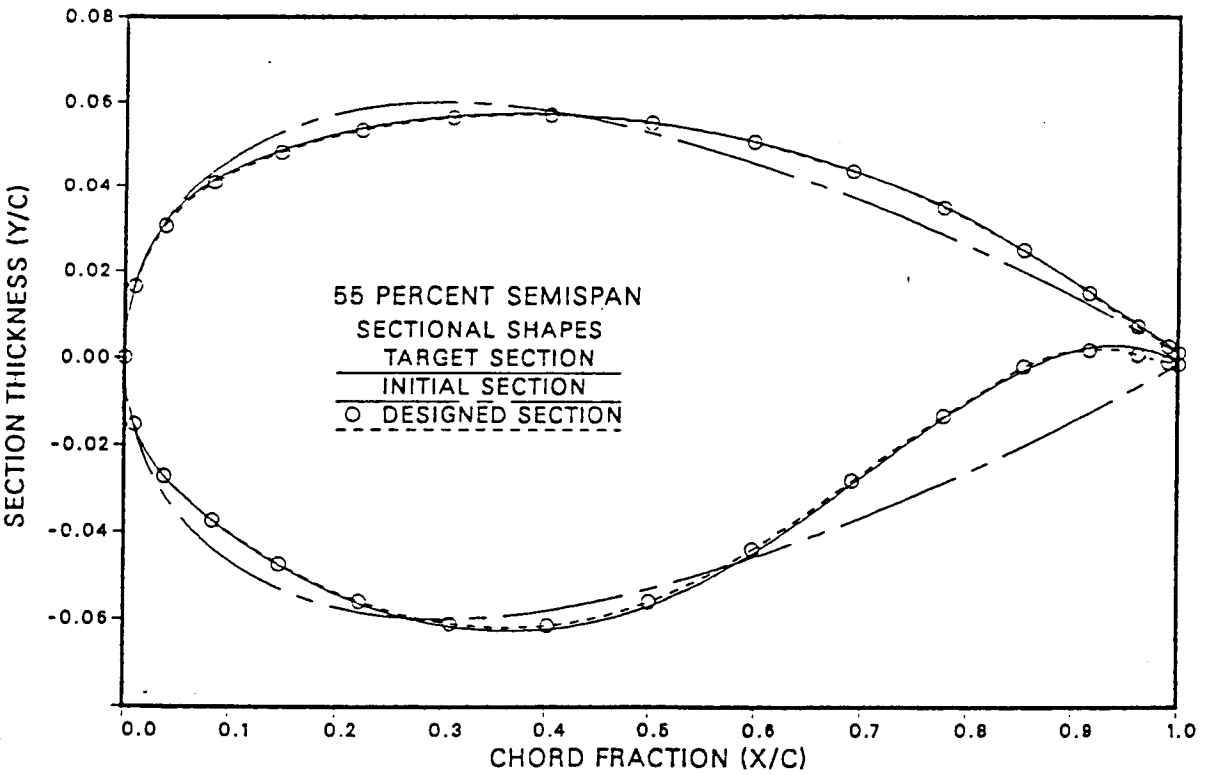
55 PERCENT SEMISPAN
SECTIONAL SHAPES
TARGET SECTION
INITIAL SECTION
DESIGNED SECTION
SECTION THICKNESS (Y/C)
CHORD FRACTION (X/C)
0.08
0.06
0.04
0.02
0.00
-0.02
-0.04
-0.06
0.0
0.1
0.2
0.3
0.4
0.5
0.6
0.7
0.8
0.9
1.0

Figure 21b

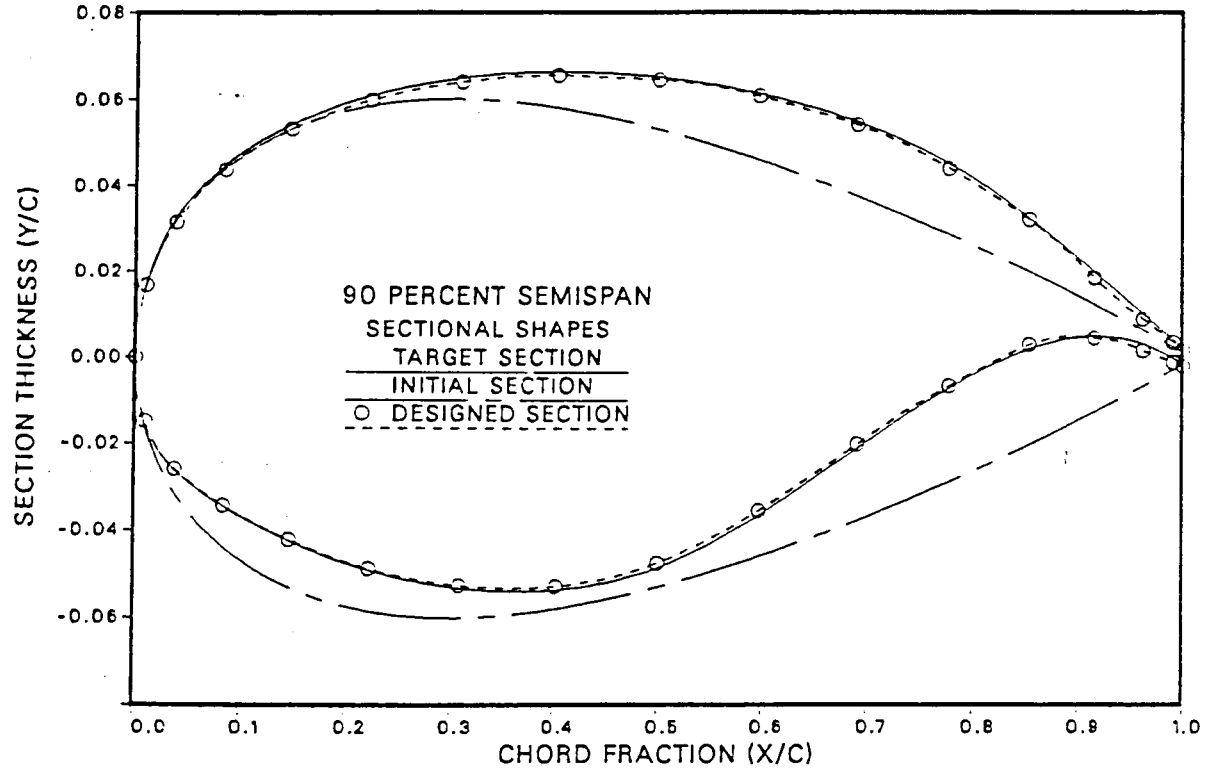
90 PERCENT SEMISPAN
SECTIONAL SHAPES
TARGET SECTION
INITIAL SECTION
O DESIGNED SECTION
SECTION THICKNESS (Y/C)
CHORD FRACTION (X/C)
0.08
0.06
0.04
0.02
0.00
-0.02
-0.04
-0.06
0.0
0.1
0.2
0.3
0.4
0.5
0.6
0.7
0.8
0.9
1.0

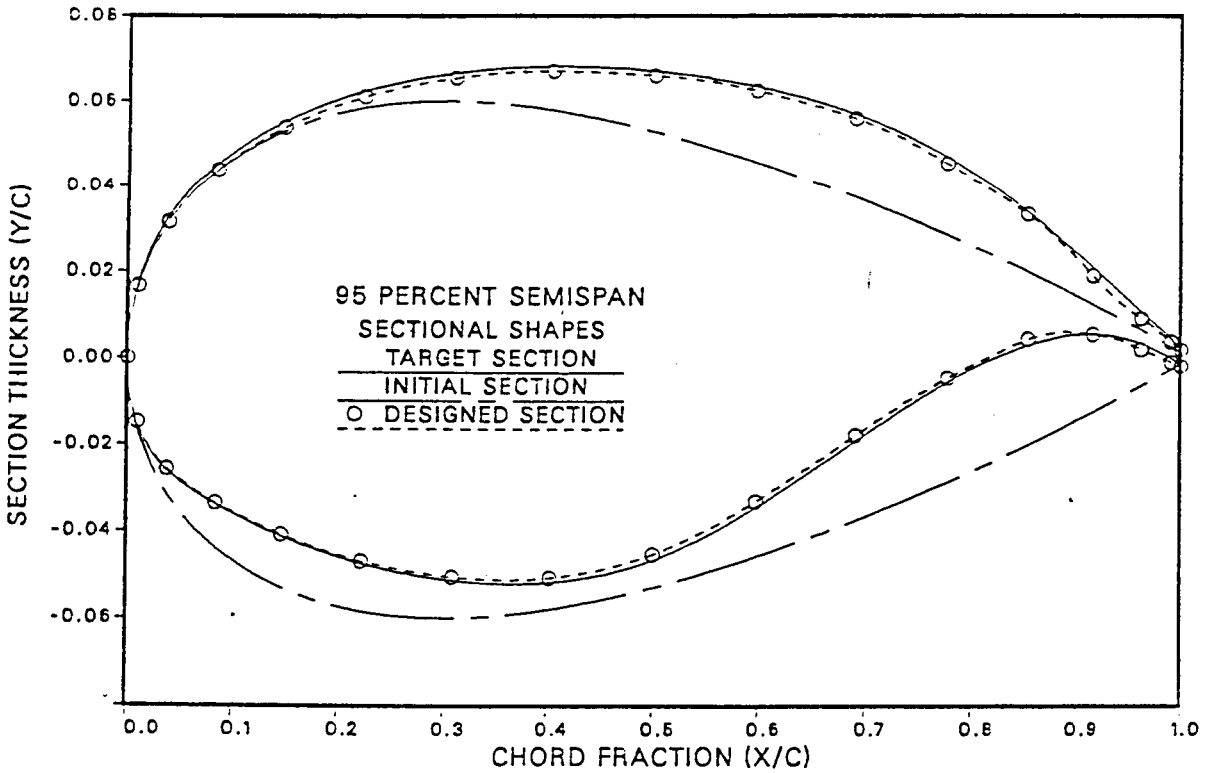
95 PERCENT SEMISPAN
SECTIONAL SHAPES
TARGET SECTION
INITIAL SECTION
O DESIGNED SECTION
SECTION THICKNESS (Y/C)
CHORD FRACTION (X/C)
0.06
0.04
0.02
0.00
-0.02
-0.04
-0.06
0.0
0.1
0.2
0.3
0.4
0.5
0.6
0.7
0.8
0.9
1.0

Figure 21c

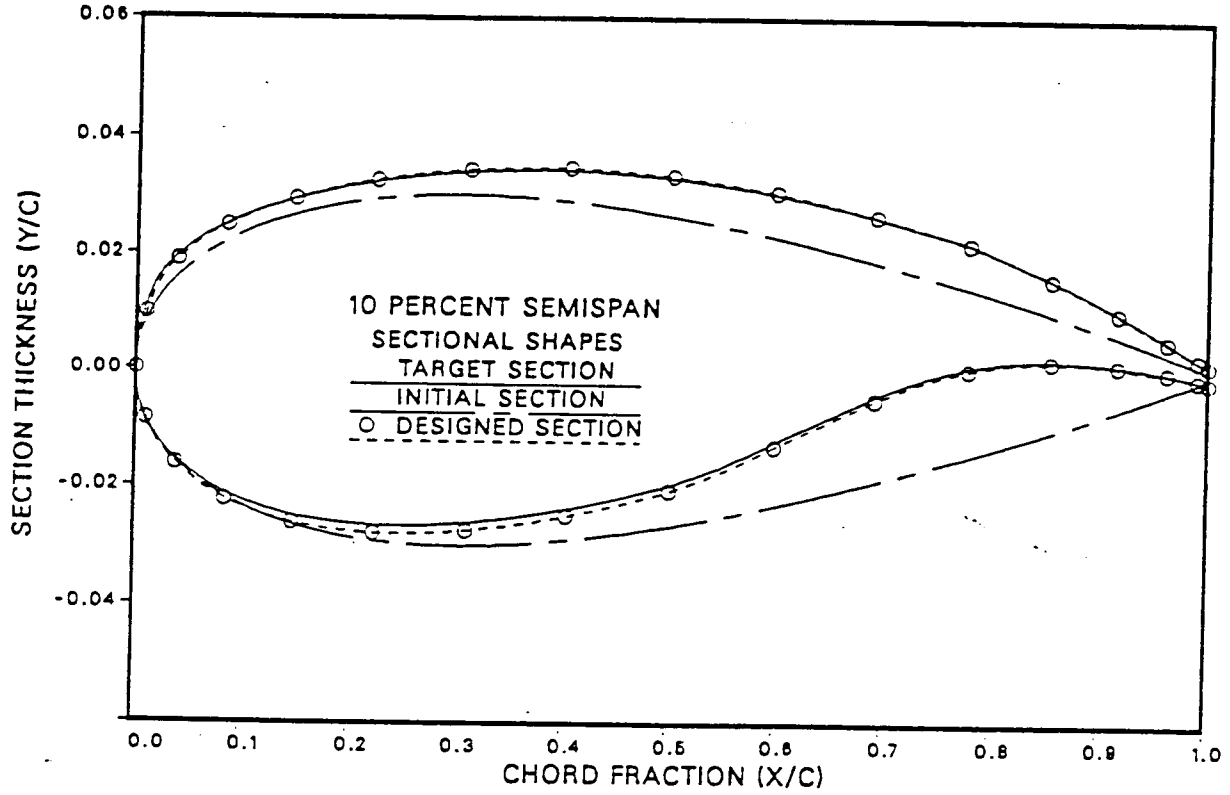

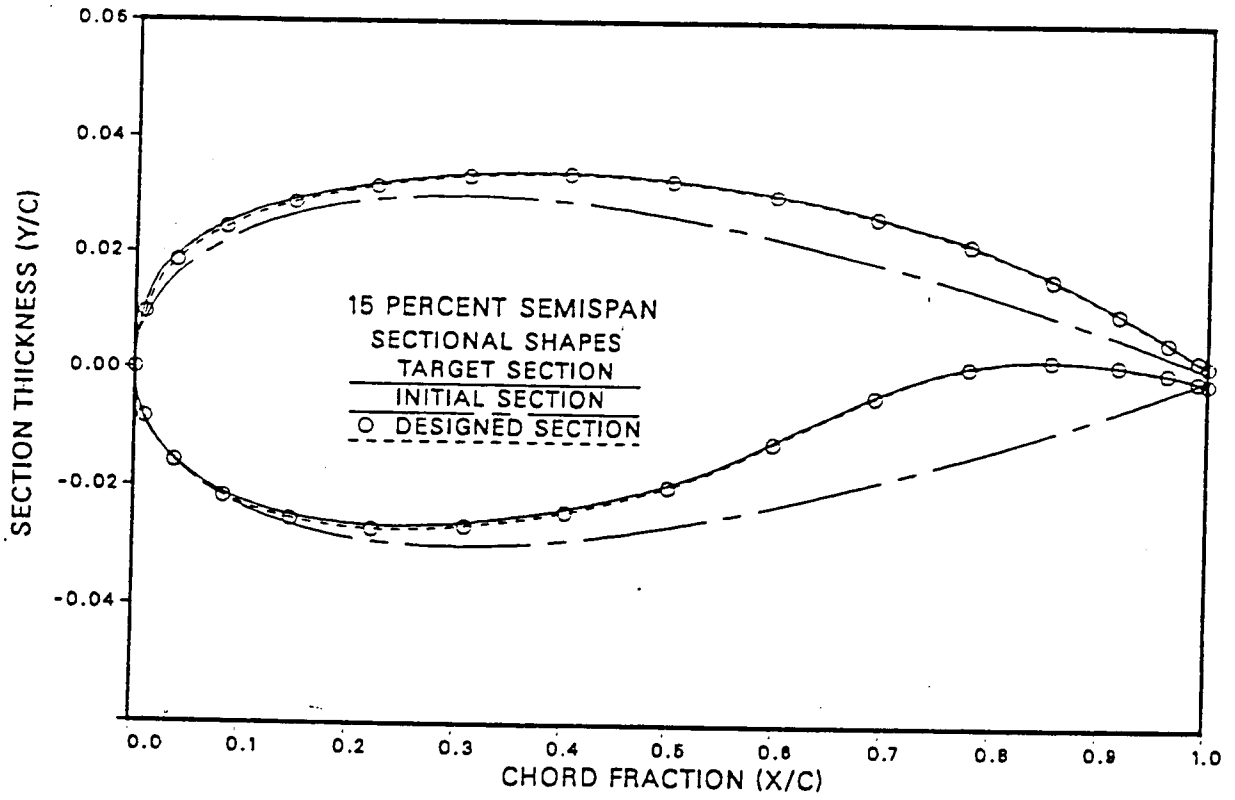

Figure 22a-22c. Comparison of the Designed Section with the Target Section and the NACA 0006 Initial Section Using a Medium Aspect Ratio Wing

ORIGINAL PAGE IS
OF POOR QUALITY

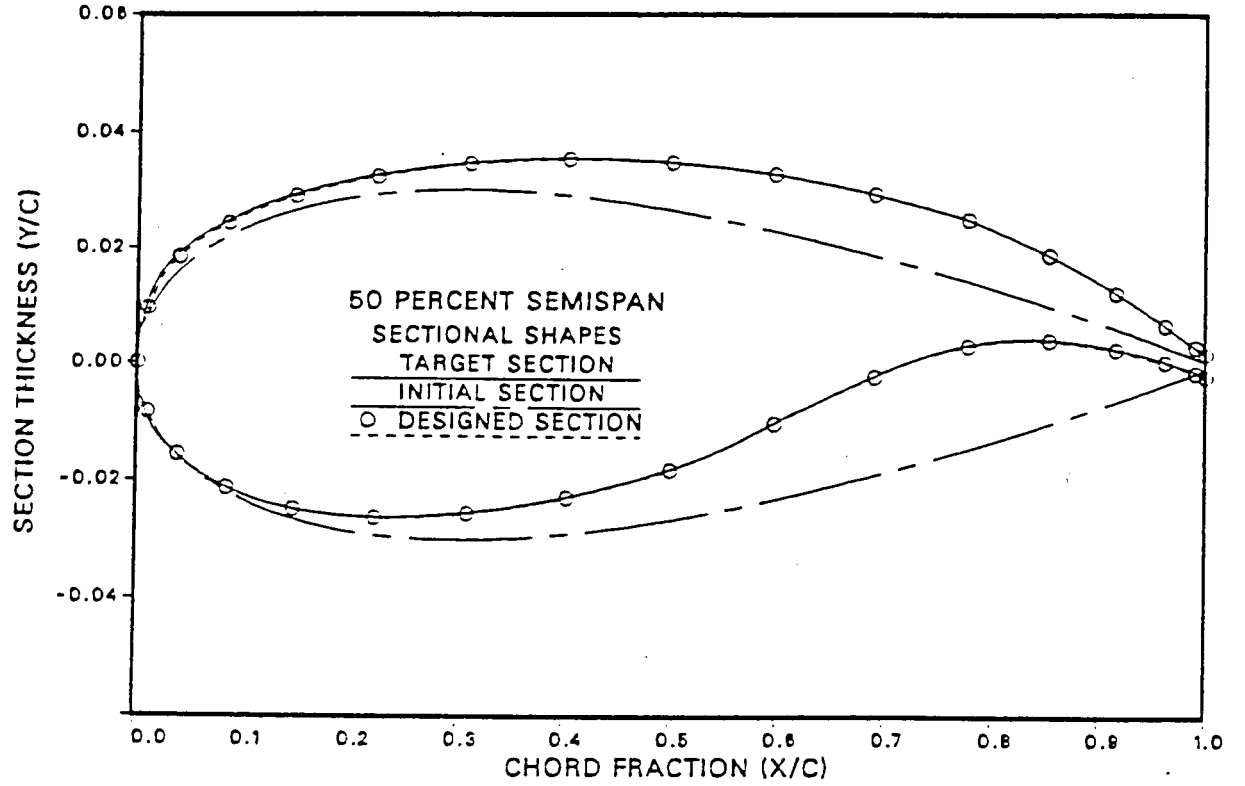

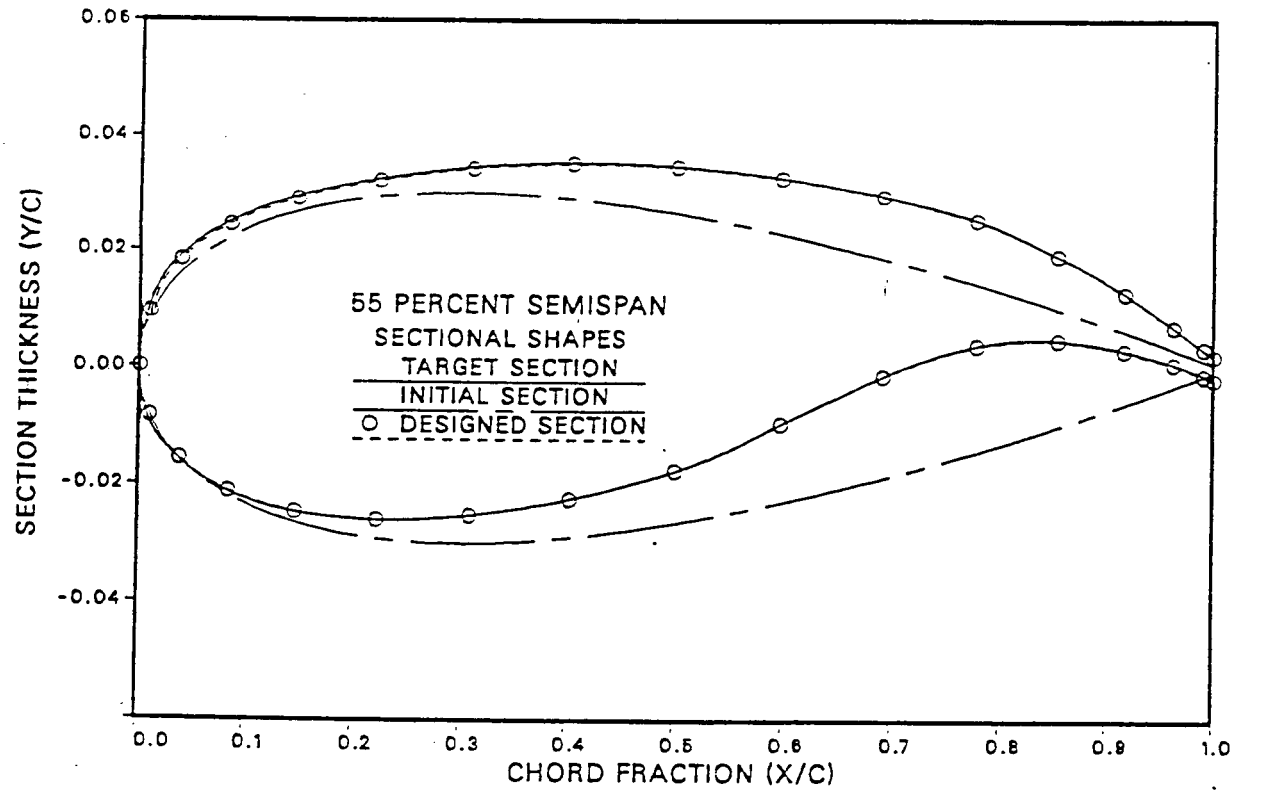

Figure 22b

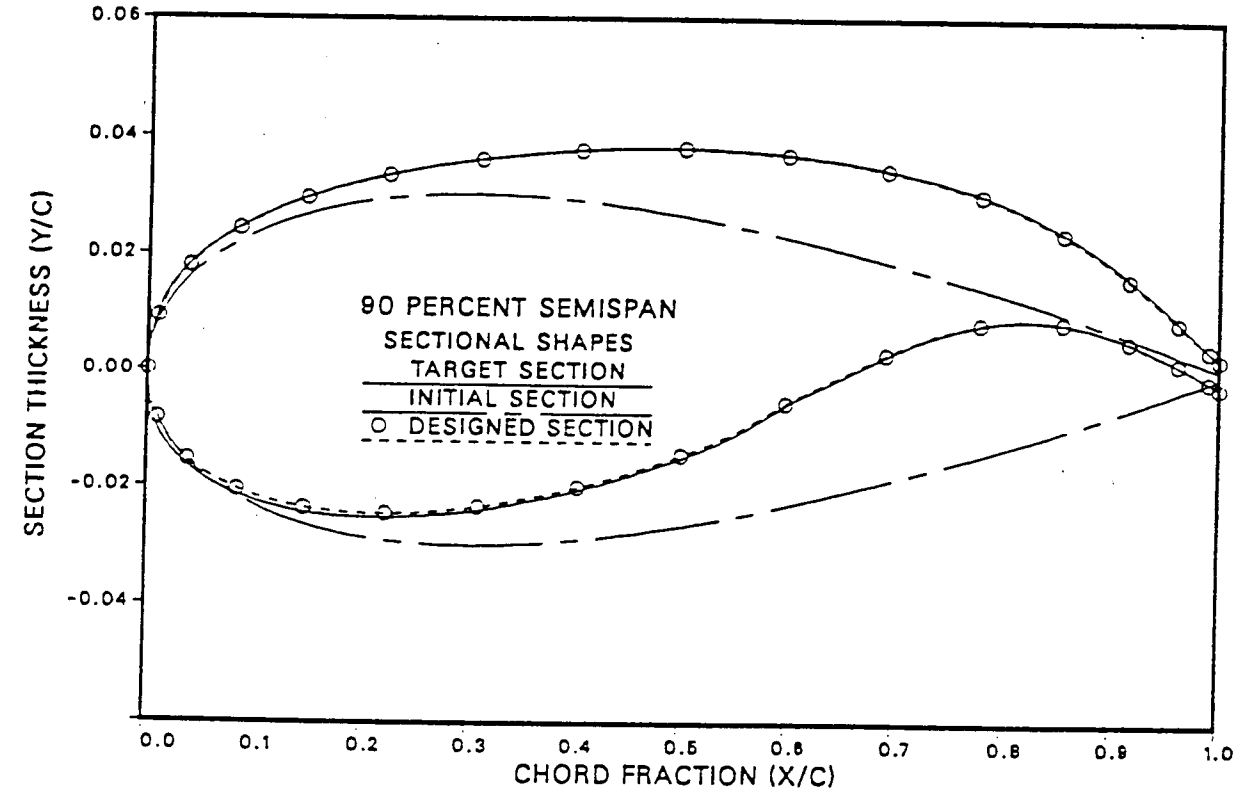
0.06
0.04
0.02
0.00
-0.02
-0.04
SECTION THICKNESS (Y/C)
90 PERCENT SEMISPAN
SECTIONAL SHAPES
TARGET SECTION
INITIAL SECTION
DESIGNED SECTION
0.0
0.1
0.2
0.3
0.4
0.5
0.6
0.7
0.8
0.9
1.0
CHORD FRACTION (X/C)

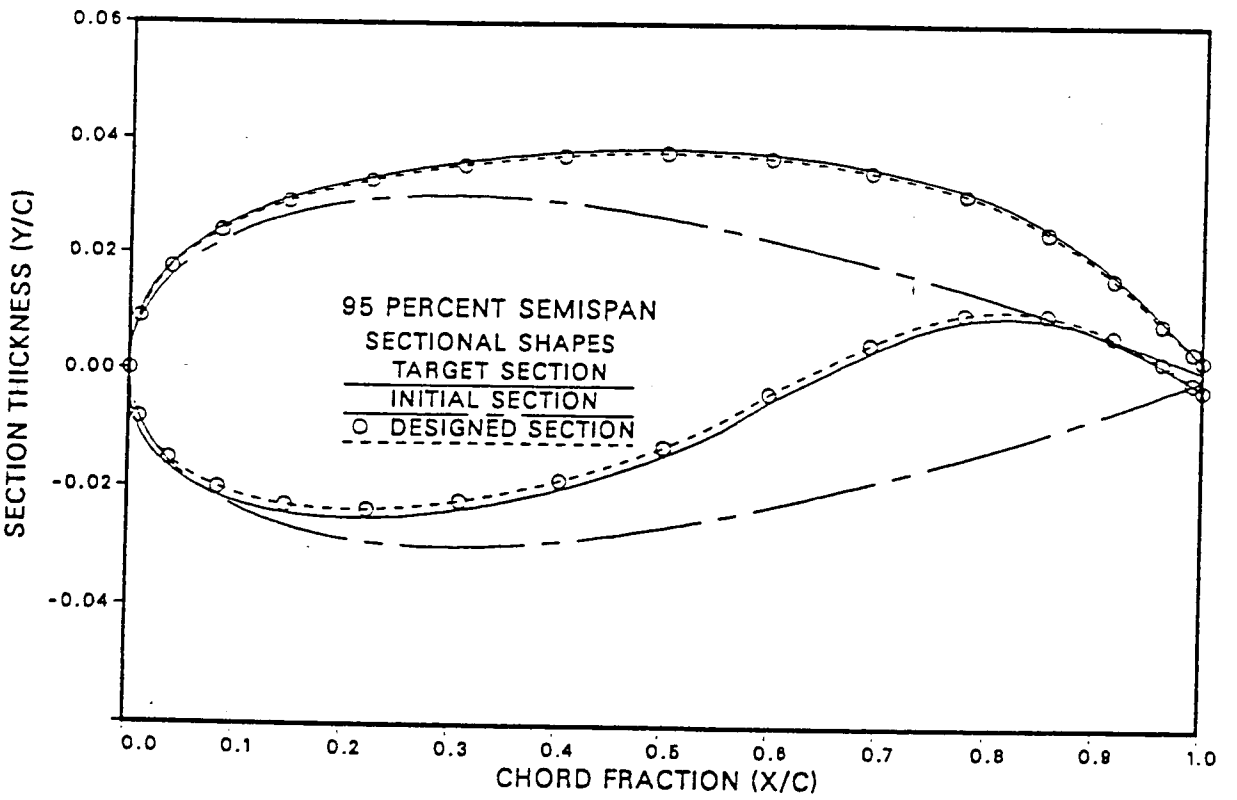
0.06
0.04
0.02
0.00
-0.02
-0.04
SECTION THICKNESS (Y/C)
95 PERCENT SEMISPAN
SECTIONAL SHAPES
TARGET SECTION
INITIAL SECTION
DESIGNED SECTION
0.0
0.1
0.2
0.3
0.4
0.5
0.6
0.7
0.8
0.9
1.0
CHORD FRACTION (X/C)

Figure 22c

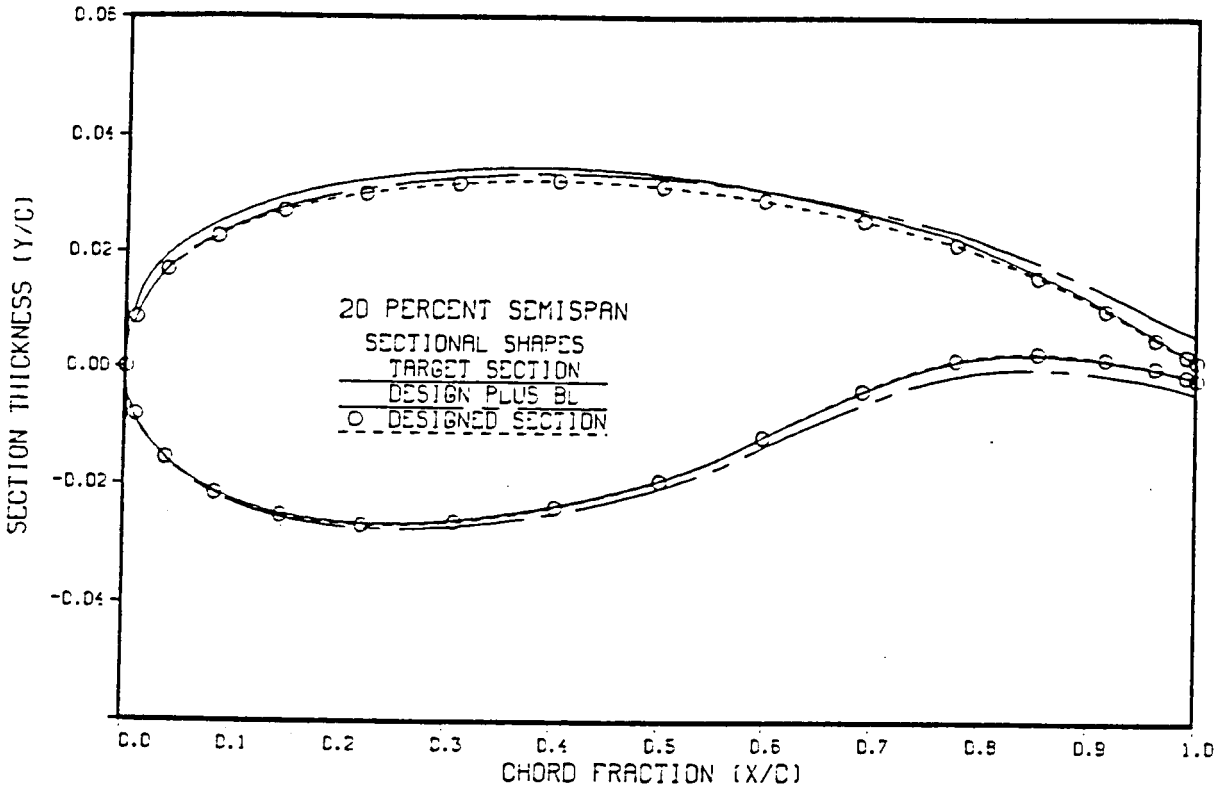

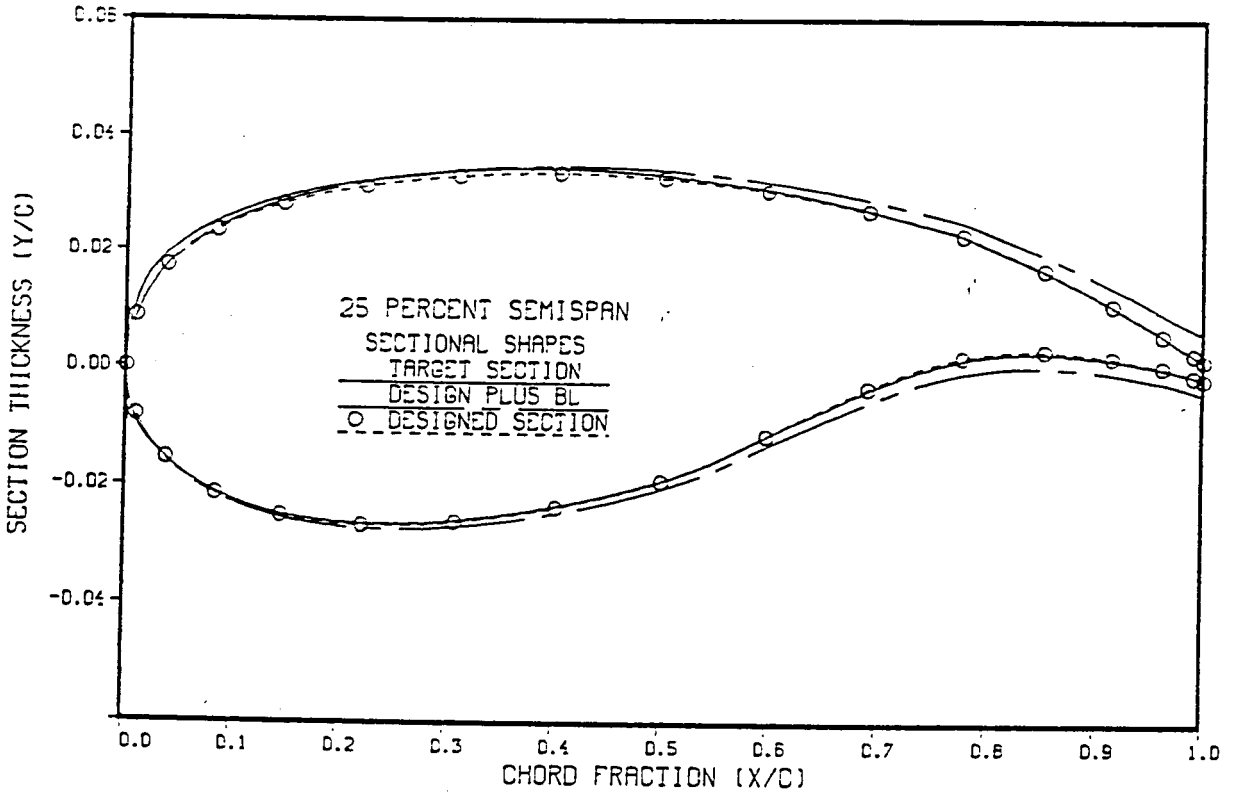

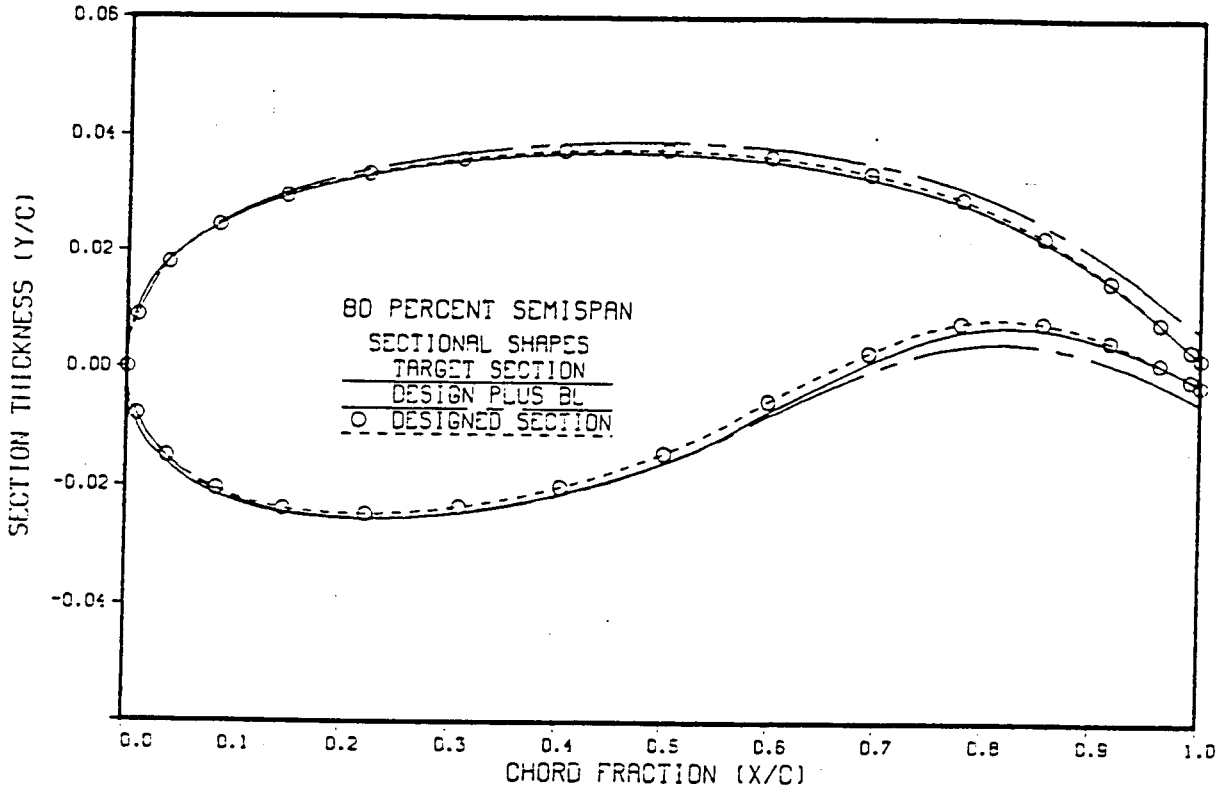
0.06
0.04
0.02
0.00
-0.02
-0.04
SECTION THICKNESS (Y/C)
80 PERCENT SEMISPAN
SECTIONAL SHAPES
TARGET SECTION
DESIGN PLUS BL
O DESIGNED SECTION
0.0
0.1
0.2
0.3
0.4
0.5
0.6
0.7
0.8
0.9
1.0
CHORD FRACTION (X/C)

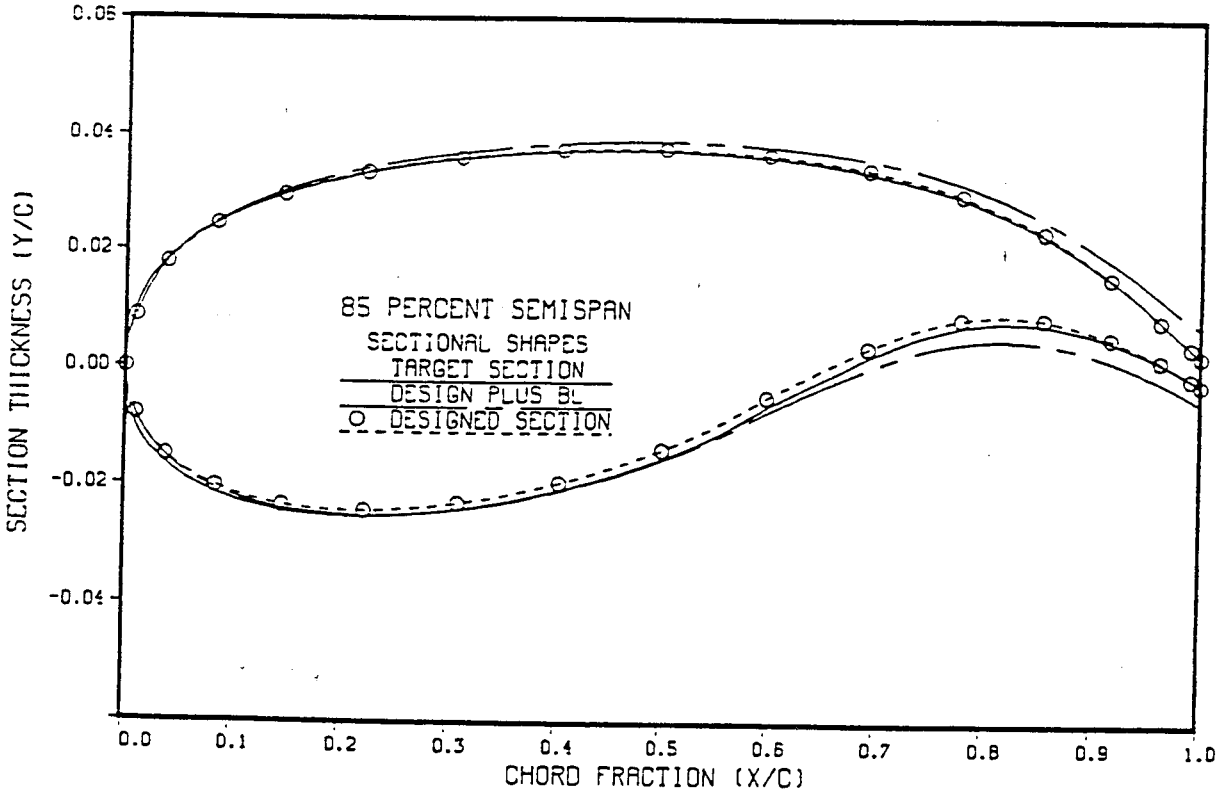
0.06
0.04
0.02
0.00
-0.02
-0.04
SECTION THICKNESS (Y/C)
85 PERCENT SEMISPAN
SECTIONAL SHAPES
TARGET SECTION
DESIGN PLUS BL
O DESIGNED SECTION
0.0
0.1
0.2
0.3
0.4
0.5
0.6
0.7
0.8
0.9
1.0
CHORD FRACTION (X/C)